ISSN 0385-2520

Rock Magnetism and Paleogeophysics

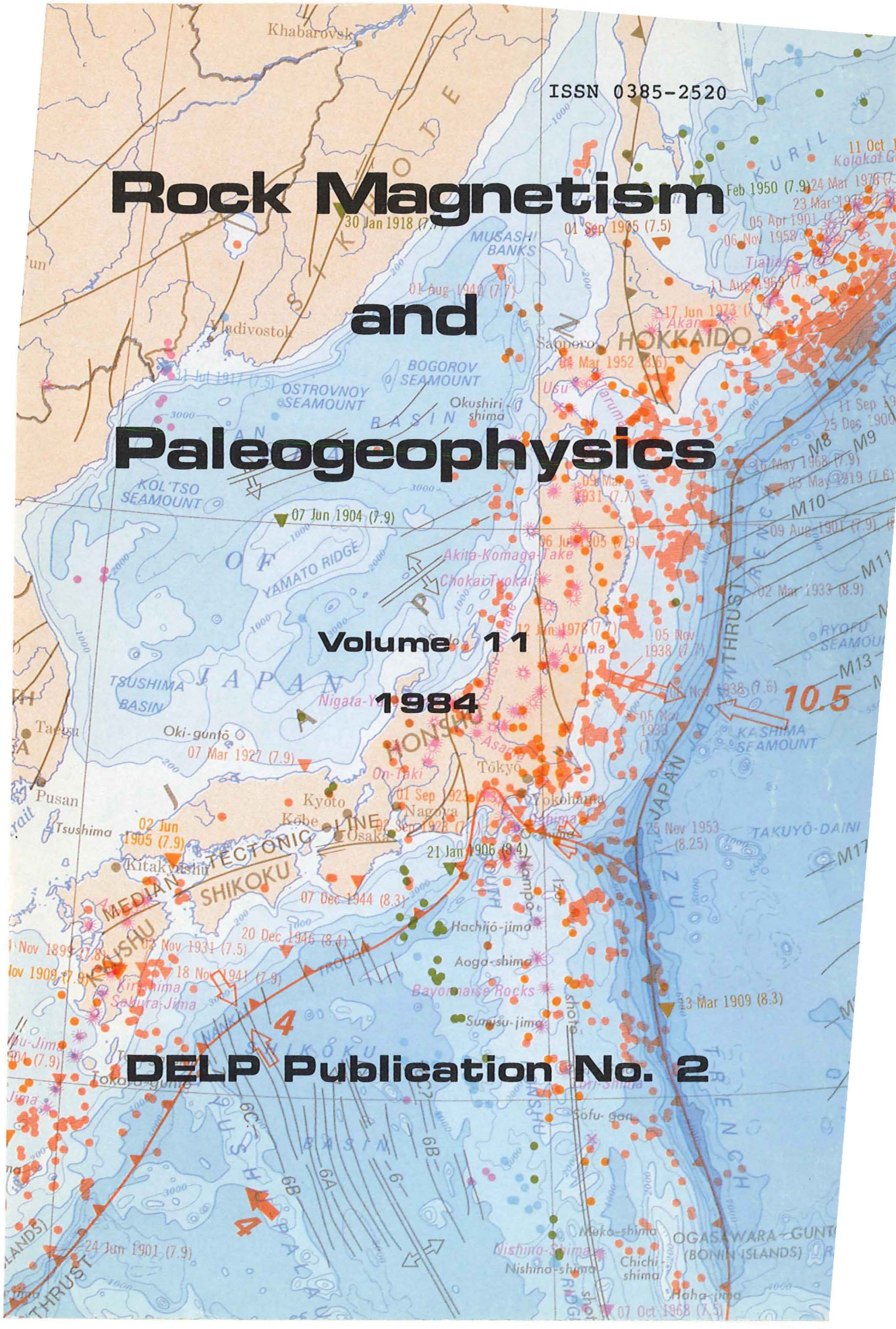

Volume 11

1984

DELP Publication No. 2

ま　え　が　き

本書は岩石磁気学・古地球物理学研究グループの1984年度の年次研究レポートであり，「国際リソスフェア探査開発計画 (DELP)」の成果報告書第2号として刊行されるものである。

岩石磁気学・古地球物理学研究グループでは，以前から Annual Report の形で英文の報文集を刊行してきた。(Annual Progress Report of the Rock Magnetism (Paleogeophysics) Research Group in Japan, 1963-1968. Rock Magnetism and Paleogeophysics, 1973-) これらの報文集は図書館などからの寄贈要請も多く，諸外国の関連分野の研究者によってかなり広く利用されている。このような経過から，この報告書も全て英文によって編集された。日本国内の研究者の方々にはいく分御迷惑をおかけすることになるが，事情を御理解いただきたい。

岩石磁気学・古地球物理学研究グループは，昭和60年度から実施されることになった DELP 計画において，特に課題5「日本列島の構造発達」の研究で大きな寄与ができるように準備を進めている。本年は7月19日から22日まで伊豆修善寺においてシンポジウムを開き，日本列島のテクトニクスに関連した多くの問題について活発な討論を行った。このシンポジウムのプログラムは目次の後に集録されている。また，本書にもその成果のいくつかが収められている。

本書の刊行および研究会の開催については，文部省科学研究費補助金「本邦周辺海盆の構造と生成機構」(代表者：秋本俊一，東大物性研）より援助を受けた。ここに記して感謝の意を表する。

1984年12月

岩石磁気学・古地球物理学研究グループ

PREFACE

This volume is an annual progress report of the Rock Magnetism and Paleogeophysics Research Group in Japan for the year 1984. As the previous reports were so, this volume contains a collection of summaries, extended abstracts or brief notes of the research works carried out in our group this year. Many of the reports contain materials which may undergo a significant revision or may be updated as the research activity continues. In this respect, the readers are warned to regard them as tentative, and are also requested to refer from a complete paper if such is published as a final result. (Names of journals appear at the end of individual articles if they are submitted, in press or in preparation of submission for some scientific journals).

After a long preparation period, the Japanese Lithosphere Project (dubbed DELP, for Dynamics and Evolution of the Lithosphere Project) finally starts from 1985 as a five-year plan. Active participation from our group is anticipated, especially in the studies of tectonic evolution of the Japanese islands and surrounding areas. A symosium on the opening of the Japan Sea is to be held at the time of the spring meeting of the Society of Terrestrial Magnetism and Electricity of Japan. We hope that this volume continues to be a useful carrier of quick information about such activities.

The publication of this volume was made possible by a grant-in-aid from Ministry of Education, Science and Culture awarded to Prof. S. Akimoto, Chairman of the DELP Committee, for "Structure and Mechanism of Formation of the Ocean Basins around Japanese Islands". We thank Prof. Akimoto and other members of the project for financial aid.

Tokyo
December 1984

Masaru Kono

Editor
Rock Magnetism and Paleogeophysics
Research Group in Japan

TABLE OF CONTENTS

PALEOMAGNETISM: MESOZOIC

ROCK MAGNETISM

MISCELLANEOUS STUDIES

Cover

Japan and its surrounding area from "Plate Tectonic Map of the Circum-Pacific Region", Northwest Quadrant.

ROCK MAGNETISM AND PALEOGEOPHYSICS SYMPOSIUM 16
19-22 July, 1984

The sixteenth Rock Magnetism and Paleogeophysics Symposium was held on 19-22 July, 1984 at Shuzenji, Izu Peninsula. In addition to the presentation of the following papers, a field excursion was organized to the Quaternary Hakone volcanoes with a guidance by Masato Koyama, Tokyo University.

19 July Evening

Session 1. Magnetometer and other instruments

1. M. Koyama (Tokyo Univ.)
   Current-regulated three-axis alternating fileld demagnetizer

2. K. Kodama (Kochi Univ.)
   A digital spinner magnetometer with ring-core fluxgate sensor

3. S. Masumoto (Osaka Univ.)
   Comment on a digital spinner magnetometer

Session 2. Remanent magnetization of sediments

4. K. Hirooka (Toyama Univ.)
   Secular variation inferred from the Holocene sediments in southwest Kanto

5. H. Morinaga, H. Inokuchi and K. Yaskawa (Kobe Univ.)
   Paleomagnetic and paleoclimatic study of cave deposit

6. F. Murata (Kobe Univ.)
   Magnetic measurement of the Rokko Island boring core (preliminaly report)

7. F. Murata (Kobe Univ.)
   Grain size dependence of SIRM and TRM, and its application to paleomagnetism

20 July Morning

Session 3. Izu Peninsula and South Fossa Magna (1)

8. M. Koyama (Tokyo Univ.)
   Stratigraphy and paleomagnetism of the northeast Izu Peninsula with special reference to local deformations along a major strike-slip fault

9. E. Kikawa (Tokyo Univ.)
   Magnetic properties of Quaternary volcanic rocks from the northern tip of the Philippine Sea Plate

10. S. Asano*(Tokyo Univ.)
    Crustal structure of the Izu Peninsula

11. T. Seno* (Building Research Institute)
    A comparative study of collisions at Taiwan and Izu Peninsula

12. K. Hirooka (Toyama Univ.)
    Northward drift of the Izu Peninsula

20 July Afternoon

13. M. Takahashi* (Ibaraki Univ.)
    Granitic magmatism in the South Fossa Magna region and its tectonic implication

14. M. Takahashi* (Ibaraki Univ.)
    Migration of the boundary between low-alkali theoleiite and high-alumina basalt zones in Izu Peninsula and its relation to recent tectonics

15. Y. Kobayashi* (Tsukuba Univ.)
    Median Tectonic Line and Itoigawa-Shiozuoka Tectonic Line

Session 4. Opening of the Japan Sea

16. M. Torii (Kyoto Univ.)
    Opening of the Japan Sea in middle Miocene

17. N. Ishikawa (Kyoto Univ.)
    Paleomagnetic study of the andesitic dykes from the lower Tanabe Group

18. A. Hayashida (Doshisha Univ.)
    Paleopostion of Southwest Japan

19. N. Niitsuma and H. Hyodo (Shizuoka Univ.)
    Paleomagnetic evidence on the rotation of Chichibu Basin in Kanto Mountains

20. T. Tosha(Tokyo Univ.)
    Tectonic inference from paleomagnetic results of the northeastern Japan

21 July Morning

Session 5. Miscellaneous Studies

21. S. Uyeda* (Tokyo Univ.)
    Report on the Japanese Lithosphere Program (DELP)

22. S. Uyeda* (Tokyo Univ.)
Recent progress in the study of subducdtion, accretion and collision

23. T. Nomura (Gunma Univ.)
Geologic structure and paleomagnetism of the southwest Iceland

21 July Afternoon

24. M. Funaki (National Institute of Polar Research)
Natural remanent magnetization of some antarctic ice and snow

Session 7. Izu Peninsula and South Fossa Magna (2)

25. T. Matsuda* (Tokyo Univ.)
Reexamination of the interpretation about South Fossa Magna based on recent data

26. T. Matsuda* (Tokyo Univ.)
Fault outcrops across the Tanna, Senya and Itoigawa-Shizuoka faults (trench study)

27. Y. Sasai* (Tokyo Univ.)
Tectonomagnetic observations in the eastern part of the Izu Peninsula (1976-1984)

Session 8. Paleomagnetism of older rocks

28. K. Hirooka (Toyama Univ.)
Accretion tectonics in the central Japan and tectonic deformation of the Circum-Hida Belt

21 July Eevening

29. M. Koyama (Tokyo Univ.)
Geology of the Izu Peninsula (guidance for the field excursion)

22 July

Field excursion in the northeast Izu Peninsula

* Speakers invited

SEVERAL ARCHEOMAGNETIC MEASUREMENTS ON BAKED EARTHS IN KYOTO PREFECTURE

Hidetoshi SHIBUYA

Department of Earth Sciencese, Callege of Integrated Arts and Sciences, The University of Osaka Prefecture, Sakai 591.

Archeomagnetic measurements on seven kilns and one fire place were carried out. All the kilns were dated as 8-th century by typological studies on excurvated Sue wears. The fireplace is where a bell for a budhist temple was casted. The age of the fireplace was also determined as about end of 9-th century or 10-th century by co-bearing Sue wears. These archeological dates were communicated by excavating archeologists.

Samples were prepared using the same procedure as described in Shibuya (1979) and Nakajima and Natsuhara (1980). Remanent magnetizations were measured using astatic magnetometer situated in Fukui University for the samples from the kilns and SQUID magnetometer of Kyoto University for those from the fireplace.

Directions of natural remanent magnetization (NRM) of the samples from the kilns were illustrated in Fig. 1. The characteristics of most of the sites are that the magnetic directions consists of two groups; One is relatively tightly clustered ones and the other is scattered exteriors. The kilns were constructed on pebly

Table 1 Archeomagnetic directions of several baked earth sites in Kyoto prefecture.

No.	N	Dm	Im	k	A_{95}	archeological age
Kitanohaiji kilns (35°01'26"N, 135°44'02"E)						
1	8	-19.8	59.0	77.2	6.3	8c
7	7	-22.7	60.9	438.8	2.9	early 8c
9	9	-13.0	59.1	104.8	5.1	middle 8c
Mamushidani kiln (34°47'50"N, 135°46'22"E)						
	12	-3.2	63.9	210.6	3.0	early 8c
Shuzan kilns (35°08'48"N, 135°38'06"E)						
1	8	-8.1	53.7	518.3	2.4	early 8c
2	6	-4.5	54.2	102.9	6.6	early 8c
3	9	-11.3	55.2	1034.1	1.6	early 8c
Casting-bell site in Kyoto Univ. (SK-257) a.f. 20mT (35°01'11"N, 135°46'55"E)						
	13	-13.2	45.9	90.2	4.4	end of 9c or 10c

N: number of samples. Dm and Im: mean declination and inclination, respectively, in degree. k: precision parameter. A_{95}: radius of confidence circle in degree. Archeological ages are personal communication by excavating archeologists.

gravel strata. The pebles would be easy to move when the kiln was destroyed or excuvated, or while the sample preparation procedure. The scattered magnetic directions would be due to such a movement of material. Therefore, we excluded the exteriors (triangles in the figures) when getting site mean directions, which is summarized in table 1. The directions agreed well with the archeomagnetic secular variation curve presented in Shibuya (1979).

NRM of the samples from the fireplace of the casting-bell site was not stable. Large part of the NRM was decayed when the samples were put in magnetic field-free space in the SQUID magnetometer. Therefore, alternating field (a.f.) demagnetization was applied to these samples. A pilot sample was demagnetized progressively upto a peak field strength of 30 mT. Change of magnetic direction was smallest from 15 to 20 mT Therefore, we treated remaining samples on peak a.f. of 15 and 20 mT and employed the values after a treatment at 20 mT, because they gave larger precision parameter than those after a treatment at 15 mT. NRM directions before and after demagnetization were presented in Fig. 1. The mean directions are shown in table 1. The site mean after the demagnetization is also agree with the archeomagetic secular variation curve (Shibuya, 1979).

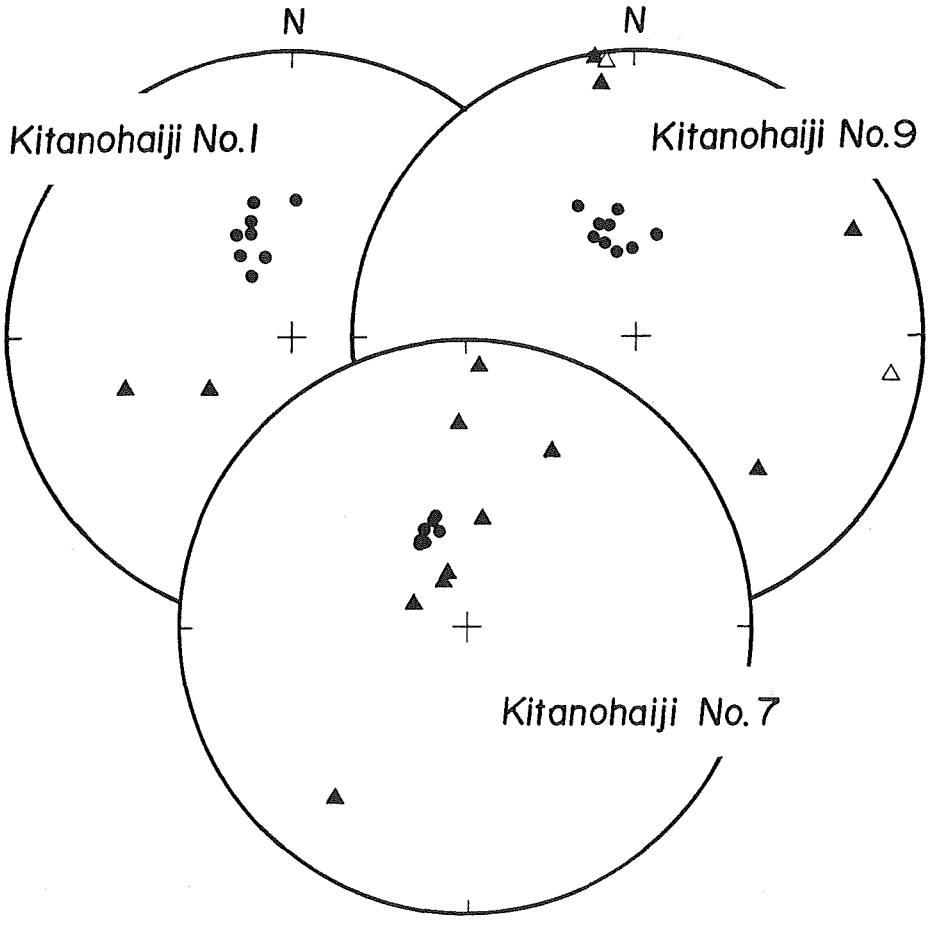

Fig. 1 Schmidt equal area projection of archeomagnetic directions of several baked earth sites in Kyoto prefecture.

Reference

Shibuya,H. (1979) M.E. Thesis, Faculty of Engineering Science, Osaka University.
Nakajima,T. and Natsuhara,N. (1980) "Koukochijiki Nendai Ketteihou" (Archeomagnetic Dating), New Science, Tokyo. (in Japanese)

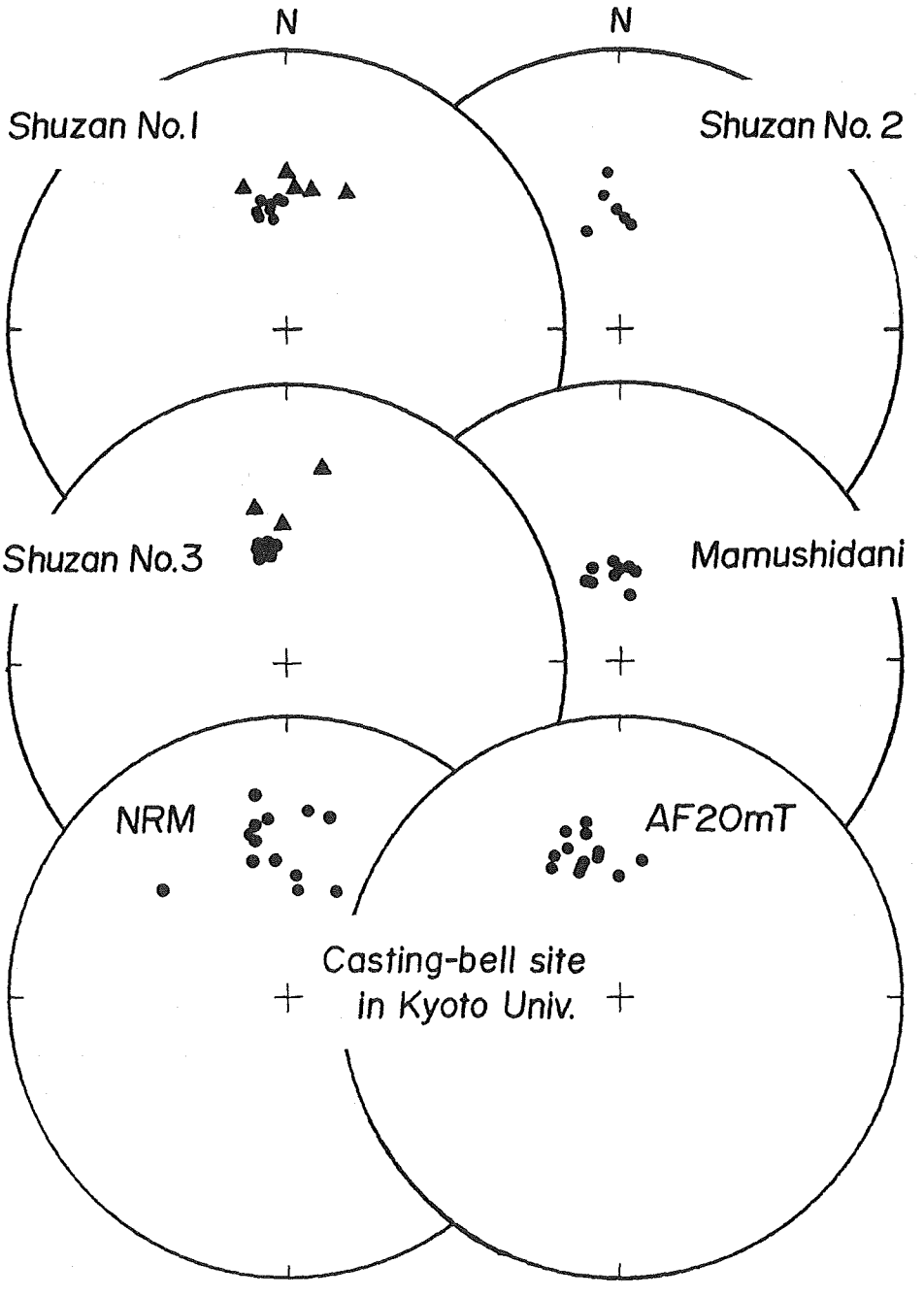

Fig. 1 (Continued)

PALEOMAGNETISM OF A CORE-SEDIMENT FROM THE INLAND SEA, JAPAN (SETO NAIKAI) I

Masayuki HYODO* and Katsumi YASKAWA**

* Cryogenic Center, Kobe University, Nada, Kobe 657, Japan
** Department of Earth Sciences, Faculty of Science, Kobe University, Nada, Kobe 657, Japan

1. Introduction

Magnetic stratigraphy of the geomagnetic field reversals established by remanent magnetization of igneous rocks (Cox et al., 1963 ; Cox et al., 1964) was confirmed by stable remanence of ocean bottom sediments. After that, many paleomagnetists tried to trace back more detailed behaviour of the geomagnetic field in the past with unconsolidated sediments rapidly deposited in lake bottom. As a result, a number of events and excursions of different ages were discovered in many places (Clark & Kennett, 1973 ; Yaskawa et al, 1973 ; Denham, 1974). In recent years, sedimentary paleomagnetism has been extended to an investigation of the geomagnetic secular variation in the Holocene time (Creer et al., 1972 ; Creer et al., 1976 ; Hyodo & Yaskawa, 1980). Such a study of a secular variation requires much higher precision and resolution in records of the geomagnetic field than that for polarity changes alone. Fundamental data on remanent magnetization of sediments are insufficient to meet the requirement of geophysicists engaged in research on the geomagnetism, especially on its secular variations. We must strive to increase the number of such data on the past geomagnetic field to determine the probable secular variation curve of the past geomagnetic field by stacking them. This study is one of our serial paleomagnetic works on sediments in south-western Japan (Hyodo & Yaskawa, 1980 ; Hyodo et al, 1984 ; Hyodo & Yaskawa, 1984a ; Hyodo and Yaskawa, 1984b).

Sampling of a core sediment was made at Mizushima-Nada in the middle of the Inland Sea, Japan (Fig.1). A core sample of sediment 20 cm in diameter and 7.38 m long was taken from a water depth of 11.6 m at 4 km off the coast. The core sediment (core MZ1) mainly consists of silty clay except for a basal interval of about 50 cm. An age 5430 years B.P. was observed by ^{14}C-dating using shells at a depth of 2.98 m. Top section of 38 cm was not used for measurement of magnetization because of its coring disturbance. The remaining 7 m was carried to our laboratory, after separation into seven 1m-segments. Each 1m-segment was split into two portions cut along core axis. Columnar specimens of 2.5 cm in both diameter and height were collected from the 1m-segments in such a way that the axis of each specimen was perpendicular to the cut-surface. A total of 926 specimens were taken and they cover over 225 horizontal levels of every ca. 3 cm in the core.

Natural remanent magnetization (NRM) was measured for all the specimens and saturation isothermal remanent magnetization (SIRM) given in a steady field of 3000 Oe was measured for one specimen per depth level, using a

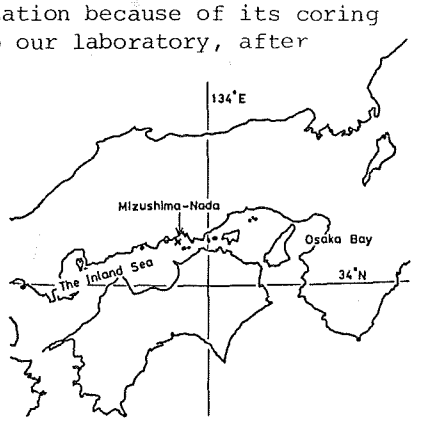

Fig.1 Location map of Mizushima-Nada, the Inland Sea (Seto Naikai). Core station is shown by a cross.

cryogenic magnetometer. We present here characteristic features of the magnetization-record in the core-sediment, and discuss a magnetizing process of the sediment and the change of the past depositional environment deducible from the characteristics of its magnetization.

2. Experimental results and discussion

It was found that there was a clear correlation between directional dispersion and intensity of remanence of the core sediment, whose dispersion was obtainable at each contemporaneous depth level (Hyodo et al., 1983). The directional dispersion of the present core calculated at each depth level have the same relation to remanent intensity as mentioned above. The curve (a) in Fig.2 shows depth dependency of the remanent intensity normalized by the SIRM intensity, and the curve (b) shows that of the precision parameter (K), inversely proportional to the square of dispersion. They exhibit closely similar change, being coincident in general trend and even in small changes. They show that the dispersion becomes small as the intensity of magnetization increases.

The above fact can be explained using a model that magnetization of sediment is a resultant of a convolution integral of the geomagnetic field variation and a moment fixing function (Hyodo, 1984). The formulated model predicts the existence of intensity reduction due to cancellation of magnetic moments aligned in various directions. It has been verified by the remanence of both deep-sea and shallow water sediments that the intensity component due to cancellation is predominant in the NRM intensity (Hyodo, 1984). We calculated such intensity reduction using the declination and inclination data of the present core. An exponential function, which is determined by half fixing depth $Z_{1/2}$, was used for the moment fixing function (Hyodo, 1984). As a result of calculation repeated by varing $Z_{1/2}$ successively, we obtained the curve at $Z_{1/2}$= 3.6 cm, which is a depth-dependency curve of intensity due to cancellation fitting best to both the depth-dependency curves of NRM/SIRM intensity and of precision parameter (K). The curve is shown in Fig.2(c), representing highly correlative change with the above two curves, especially in short wavelength changes.

It substantiates that both change curves of remanent intensity and directional dispersion reflect the resultant effect of magnetic moments aligned in various directions resulting from the integration of field variation. The value of $Z_{1/2}$= 3.6 cm, with which most correlative intensity is calculated, may be the mean half fixing depth throughout the

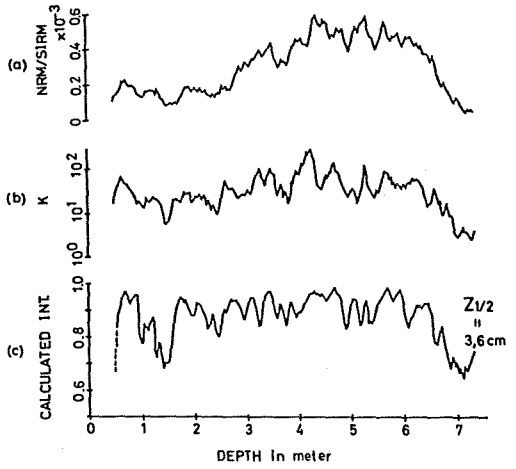

Fig.2 Intensity of NRM/SIRM, precission parameter K in each depth and intensity reduction due to cancellation of moments aligned in various direction calculated with declination and inclination data. Each curve is smoothed by an opperation of 5-points running mean.

length of the core. Then, filtering effect by moment fixing function is negligible with such a small $Z_{1/2}$(Hyodo, 1984). We can regard the change of the magnetic declination and inclination recorded in the core MZ1 as the geomagnetic secular variation without any amplitude attenuation and phase shift.

Relative declination and inclination of the present core (MZ1) is shown in Fig.3, eliminating the uppermost portion 1.4 m considered to be unreliable because of twisting. The declination has a large discrepancy at a depth of 6.9 m, which coincides with the depth where material of sediment sharply changes from the basal sand to upper clay. Inclination curve has the large gap at the depth 6.9 m, too. A major characteristic feature of the entire declination change is found in a long wavelength change ; the declination swings most westerly at 6.9 m, graduallly shifts eastward going upwards, and turns westwards again after passing the extremum around 2.5 m.

Now, we correlate the declination and inclination curves of the core MZ1 with those obtained from Osaka Bay 150 km west of the present core station in order to recognize the reliability of the curves as the secular variation of the geomagnetic field. The secular variation over the past 11000 years was studied in unconsolidated marine clay sampled at the mouth of the River Samondo, situated at the northern coast of Osaka Bay (Muroi & Yaskawa, 1977). The sampling was carried out in a caisson for the construction of a bridge pier. Sediment samples were taken directly from the cutting surface of stratum under the water over the depth from 8 to 25 m below the sea level. Data of the magnetization of the sediment have the following advantages : (1) Samples were azimuthally oriented. (2) Samples of more than 5 were taken in a contemporaneous horizon to analyze the data of magnetization statistically. (3) Detailed depth-age relation was determined at fifteen depth levels of the sequence of the sediment by ^{14}C-dating. The declination and inclination of the mean magnetization vector in each horizon is plotted to the age axis in Fig.3, correlated with the depth-dependency curves of declination and inclination of MZ1. The declination and inclination from Samondo (SD1) displays very similar change with the variation curves of MZ1, possessing the same general trend and the same swings and fluctuations. The high degree correspondence between the two declination and inclination records from the different sites indicates that their remanent magnetization has been acquired under the control of the same geomagnetic field.

Corresponding features in the two variation curves before about 5500 years ago are linked in consideration of not only shape of the curves but also absolute values of the declination and the inclination (Fig.3). The age at each depth in core MZ1 was determined by the curve correlation as listed in Table 1. The declination of SD1 from about 6000 years B.P. back to about 8000 years B.P. changes in the range of about 60° from 50°W to 10° E, and that of MZ1 for the same period changes within about 60°, too. Based on this fact, we provided an azimuth of the true north on the relative scale of the axis of declination as the origin of the absolute declination of MZ1, as shown with a broken line in Fig.3. The secular variation of the geomagnetic field from about 8000 to 5430 years B.P. is as follows : Declination largely swings westerly before 6600 years B.P.. The most westerly declination is about 50°W. Inclination has a minimum of 30° at 5500 years B.P., and a maximum over 70° at about 6500 years B.P.. Declination simultaneously has an easterly peak at about 6500 years B.P.. Although we have any definite ages by neither ^{14}C-dating nor magnetic one in the basal portion of 50 cm in MZ1, the age of the portion appears to be older than 11000 years B.P. according to the correlation of the declination and the inclination curves with those of SD1. The unconformity at depth 6.9 m may indicate a hiatus in sedimentation more

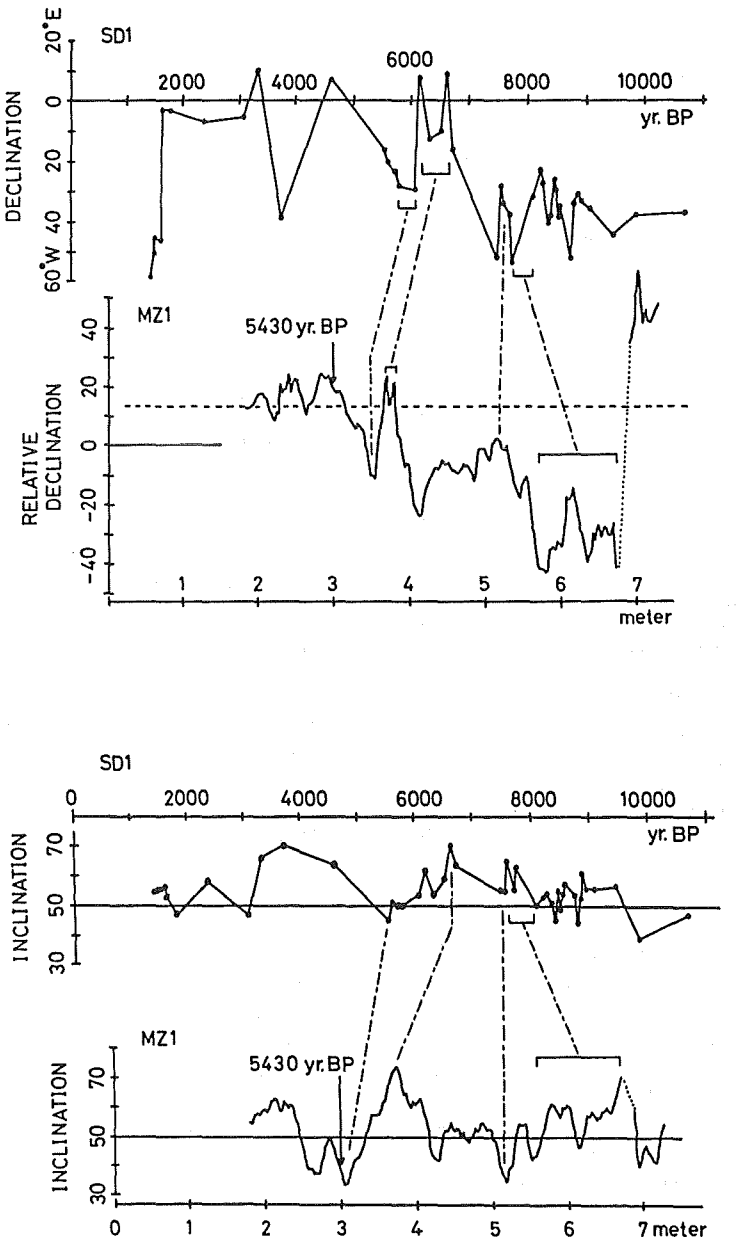

Fig.3 Correlation of declination and inclination from the River Samondo (SD1), Osaka Bay and Mizushima-nada (MZ1). Declination and inclination of MZ1 are smoothed by an opperation of 5-points running mean. Directions of mean magnetic vectors in each depth of SD1 are plotted to age axis and those for MZ1 to depth axis. Zero declination of SD1 points to the true north and that of MZ1 the mean declination throughout the length. A horizontal broken line in declination of MZ1 shows the north estimated from the comparison with declination of SD1.

Depth (cm)	Age (yr. B.P.)	curves
350	5900 - 6000	dec.
375	6600	inc.
375 - 385	6100 - 6600	dec.
520	7500	inc. & dec.
575 - 675	7600 - 8000	inc. & dec.

Table 1 Magnetic ages in core MZ1, estimated from curve correlation of declination and inclination between SD1 and MZ1.

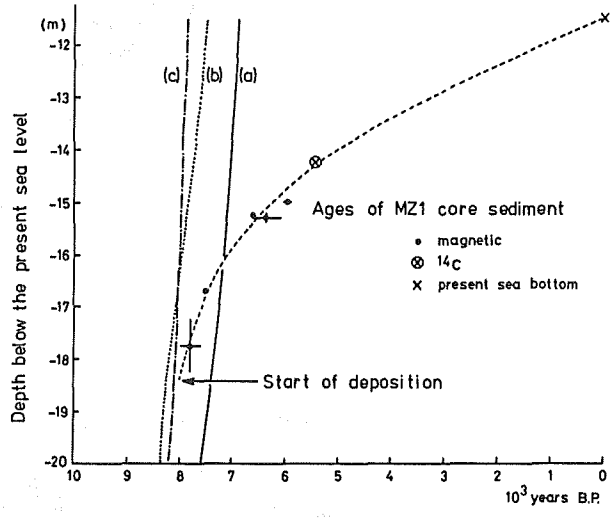

Fig.4 Plots of ages in the present core (MZ1). A broken line approximates the depth-age relation. Three curves (a,b,c) show the sea level changes by geological estimation : curve (a) from Osaka Bay (after Maeda, 1976), curve (b) from Tokyo Bay (after Kaizuka et al., 1977), and curve (c) from southern Kanto region (after Sugimura & Naruse, 1955).

than 3000 years if there is no weathering.

The hiatus at depth 6.9 m may be explained by the sea level change due to the Holocene transgression. Ages of the sediment of the core MZ1 are plotted to depth beneath the present sea level in Fig.4. The relation between age and depth is approximated by a freehand smooth curve of a broken line, in Fig.4. The curve shows that deposition started at about 8000 years ago and has continued through up to the present. It further shows that the rate of deposition was higher in the beginning and has been gradually decreasing. Many geologists have estimated the sea level change in the Holocene times using marine terraces or marine shell fossils in tidal zones (Sugimura, 1977). Three curves of sea level change from different places in Japan are represented in Fig.4 on the basis of their estimation. These three curves are not perfectly consistent with each other. The inconsistency may be caused by difference in methods of estimation of the past sea levels rather than by difference in places. Anyway, some uncertainty as shown by these three curves should be considered in geological estimation of the past sea level. The sediment of the core MZ1 started to be accumulated at the present water depth 18.4 m 8000 years ago after some break of deposition. It means that the sea level has risen at least 18.4 m during the last 8000 years, being consistent with the geological estimations of the sea level change within the uncertainty mentioned above. It is further infered that the sea level change causes a change in rate of deposition ; the sea level has continued

to rise at so high rate around and after 8000 years B.P. that the coast had receded toward north, to the place of core MZ1, sedimentary supply of coarse grains had almost ceased, and depositional rate had rapidly decreased because supply of material to our boring place had been getting poorer. It is thus verified that the discrepancy of magnetization curve at depth 18.4 m shows the lower limit of the sea level about 8000 years ago.

3. Conclusion

Paleomagnetism of the present core sediment provides following information. 1) Intensity and directional dispersion of the remanence show correlative changes. This fact is explained as the resultant effect of magnetic moments alighned in various directions resulting from the integration of field variation. 2) The geomagnetic field in south-western Japan had kept westerly declination from about 6700 years B.P. through back to at least 11000 years B.P.. 3) The lower limit of the sea level at 8000 years B.P. was 18.4 m beneath the present sea level.

References

Clark, H.C. and J.P. Kennett (1973) Earth planet. Sci. Lett., 19, 267.
Cox, A., R.R. Doell and G.B. Dalrymple (1963) Nature, 198, 1049.
Cox, A., R.R. Doell and G.B. Dalrymple (1964) Science, 144, 1537.
Creer, K.M., F.H. Mackereth, L. Molyneux and R. Thompson (1972) Earth planet. Sci. Lett., 14, 115.
Creer, K.M., D.L. Gross and J.A. Lineback (1976) Bull. Soc., Am., 87, 531.
Denham, C.R. (1974) J. Geomag. Geoelectr., 26, 487.
Hyodo, M. and K. Yaskawa (1980) J. Geomag. Geoelectr., 32, 581.
Hyodo, M., S. Onishi and K. Yaskawa (1983) Rock Mag. Paleogeophys., 10, 29
Hyodo, M. (1984) J. Geomag. Geoelectr., 36, 45.
Hyodo, M., H. Morinaga, H. Nishimura, H. Inokuchi and K. Yaskawa (1984) Submitted to J. Geomag. Geoelectr..
Hyodo, M. and K. Yaskawa (1984a) Submitted to J. Geomag. Geoelectr..
Hyodo, M. and K. Yaskawa (1984b) To be submitted to J. Geomag. Geoelectr..
Kaizuka, S., Y. Naruse and I. Matsuda (1977) Quaternary Research, 8, 32.
Maeda, Y. (1976) Jour. Geosci. Osaka City Univ., 20, 43.
Muroi, I. and K. Yaskawa (1977) Rock Mag. Paleogeophys., 4, 76.
Sugimura, A. and Y. Naruse (1955) J. Geol. Geogr., 24., 101.
Sugimura, A (1977) Kagaku (Science), 47, 749 (in Japanese).
Yaskawa, K., T. Nakajima, M. Torii and N. Kawai (1973) J. Geomag. Geoelectr., 25, 447.

(Submitted to Geophys. J. R. astr. Soc.)

PALEOMAGNETISM OF A CORE FROM THE INLAND SEA, JAPAN (SETO NAIKAI) II
: A SECULAR VARIATION RECORDED IN SILTY SEDIMENTS

Masayuki HYODO* and Katsumi YASKAWA**

* Cryogenic Center, Kobe University, Nada, Kobe 657, Japan
** Department of Earth Sciences, Faculty of Science,
Kobe University, Nada, Kobe 657, Japan

1. Introduction

A few core samples of shallow water sediment were taken from the Inland Sea, Japan (Seto Naikai). Paleomagnetic experiments with one of the core samples resulted in discovery of some characteristic features on remanence direction, which have never recognized yet in remanence of other sediments. We try to clarify the intrinsic process of magnetization buried in the sediment of this core, and discuss the methods to deduce a secular variation of the geomagnetic field from magnetization of such a sediment as will be mentioned below.

2. Sampling and experiments

Sampling of a core sediment was made in Harima-Nada in the west of the Inland Sea (Fig.1). A core sample of sediment 20 cm in diameter and 865 cm in length was taken from the bottom of depth 34 m at 11 km off the western coast of Awaji island, using a percussion corer with a 500 kg-hammer on its head. The sediment is composed of silt throughout the length, including sandy silt with coarser grains at some portions. Ages of the sediment were obtained in three depths by radio-carbon dating of shells in the core. These ages are as follows :

290.0 ± 2.5 cm	2470 ± 125 yr
526.4 ± 2.5 cm	5320 ± 190 yr
875.0 ± 5.0 cm	8120 ± 220 yr

Topmost portion 65 cm was not used for experiments because of its looseness. The rest part of 8 m was divided into eight 1m-segments on board and carried to our laboratory. Each 1m-segment was further sliced into round sections 5 cm thick. Five cylindrical specimens of 1 inch diameter and 1 inch height were collected from each sliced round section. Topmost loose 1m-segment was freezed in a refrigerator before being sliced and dissolved before preparing specimens of 1 inch size. Total number of specimens is 885 over 177 slices.

Natural remanent magnetization (NRM) of all specimens were measured with a super conducting magnetometer, whose sensitivity was 10^{-8} emu. Results are shown in Fig.2. They are notably characterized by small amplitudes of depth-variational curves compared with finer sediments like mud or ooze. Declination and inclination curves are almost flat. Mean inclination over all depth levels in the core is 51.6°, which is closer to the inclination of the axial dipole field, 54.0° than that of the present field, 47.0° at the sampling site.

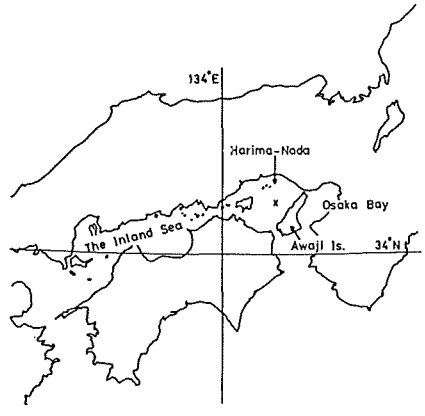

Fig.1 Location map of a sampling site.

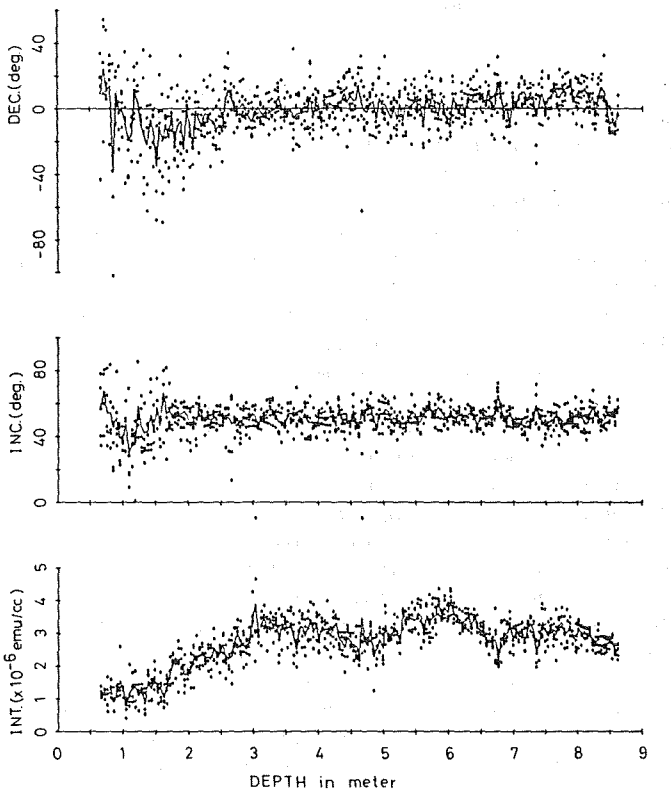

Fig.2 Declination, inclination and intensity of NRM. Solid circles show all data points. Solid curves are drawn on horizon means.

Partial demagnetization test with an alternating field (AF) was carried out on eight sets of pilot specimens which were selected from every 1m-segment and belonged to the same depth level, using a demagnetizer with a field rotating system (Matsuda et al., 1981). Results on two levels of depths 217 cm (HR711) and 517 cm (HR411) are shown in Fig.3(a). Most of specimens have their MDF between 100 and 150 Oe. Being subjected to the stepwise AF-demagnetization the specimens belonging to the both depth levels changed the direction of their remanent magnetization, but the pattern of the change is characteristic in each depth level, i.e. the change in case of the depth level HR711 shows a clockwise vortex pattern and that of HR411 shows a straight line pattern from the left to the right as seen in Fig.3(a). In these cases the directions of their remanence do not converge as a peak field increases, but the directions of the specimens from the same depth-level shift in the same pattern. Let us call this "parallel shift" of direction of the magnetization. Most of specimens from other depth levels also have characteristic pattern of changing the direction of their remanence under alternating fields. Some of them have so stable remanence that its direction remains almost unchanged. Some have so unstable remanence that the direction of their remanence radially disperses as peak field is increased.

Next, the 79 specimens, selected from every other horizon except that in top loose section of 165 cm, were stepwise-demagnetized in alternating fields of 50, 100 and 150 Oe. Results are shown in Fig.3(b). As was clearly seen in Fig.3(b), the amplitudes of quasi-periodic depth-variation in both declination and inclination of the magnetization gradually increase as the peak field of alternative demagnetization increases. This phenomenum together with the parallel shifting of remanence direction may be reflected an essential mechanism of magnetizing in sediments.

3. Discussion and conclusion

Concerning to the large shift of remanent direction of a pilot specimen through stepwise AF-demagnetization, first, it is considered to be caused by removal of soft components due to viscous remanent magnetization (VRM). However, the systematic shifting of magnetic direction after demagnetization can be hardly explained by removal of VRM only. Another possible explanation is that each magnetic particle of different coercivity or mobility in the sediments has been fixed at different ages, and therefore magnetic directions of individual particles should align along various directions of the geomagnetic field in different ages. Stepwise AF-demagnetization separates each component of the field corresponding to different ages. We must note that the disappearence of partial magnetization through AF-demagnetization may be caused by either vanishing of remanence of magnetic grains or cancellation of randomized magnetic-vectors due to grain rotation.

The growth of swings in declination and inclination curves, being accompanied with increment of the peak field intensity of AF-demagnetization, appears to be subjected to the similar phenomenon to deconvolution of magnetization data using a linear system model of magnetizing process (Hyodo, 1984). The model is formulated as :

$$\mathbf{m}(\zeta) = \int_{-\infty}^{\infty} \mathbf{f}(z)\ r(z-\zeta)\ dz \qquad (1)$$

where $\mathbf{m}$, $\mathbf{f}$ and r are magnetization, a field variation and a moment fixing function, respectively. The moment fixing function $r(z)$ is determined by a half fixing depth $Z_{1/2}$, at which a half of magnetic moments in a unit sediments is locked in. We consider fixing of magnetic grains of different coercivity or mobility in connection with the linear system model. Two types of fixing magnetization in the sediment can be expected:

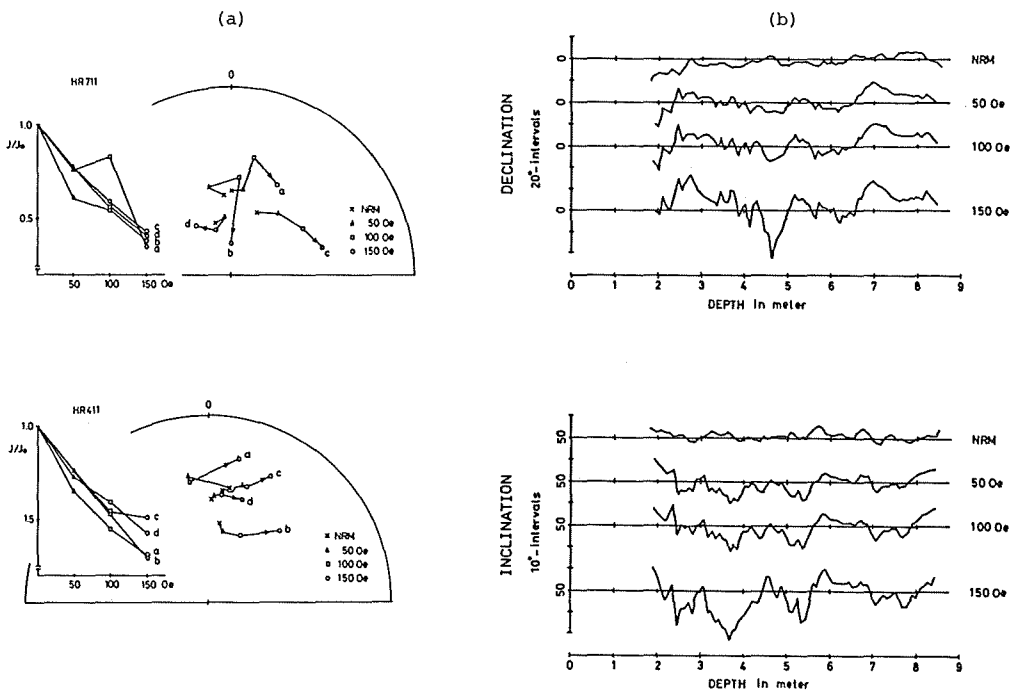

Fig.3 Results of stepwise AF-demagnetization at fileds of 50, 100 and 150 Oe. (a) Results on two sets of pilot specimens from depth-levels of 217 cm (HR711) and 517 cm (HR411). (b) Gradual change of declination and inclination curves after demagnetization. The directional curve is that of remanence of a serial samples every 10 cm. It is smoothed by an operation of 5-points of running mean.

Fig.4 A schematic view of the model showing that magnetization of sediment sheet of age τ is a resultant of convolution integral of a field variation f(t) and a moment fixing function r(t). Two types of moment fixing are shown in r(t). Individual magnetization components by type I fixing integrate the field variation of different time spans as shown by broken lines. All components by type II fixing integrate the same field variation.

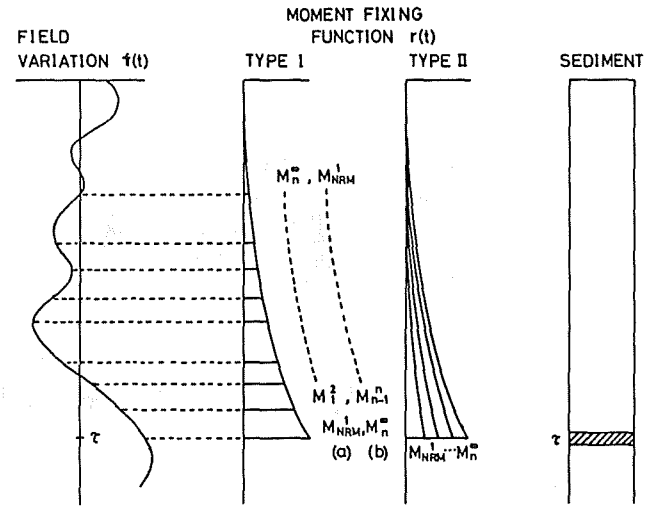

M_i^{i+1} ; Magnetization component removed by the operation of AF-demagnetization with the i-th to (i+1)-th peak field.

(I) magnetic grains are successively fixed in the order of the magnitude of their coercivity or immobility, and (II) fixing of magnetization in the sediments is independent of coercivity or immobility of magnetic particles. The two models of fixing are represented by showing how distribute magnetic components of different coercivity or immobility in a moment fixing function, in Fig.4. The two models can be distinguished by a result of stepwise AF-demagnetization. The magnetization as the result of fixing of type II will not change its direction by AF-demagnetization, since all components are magnetized in the same direction integrating the same geomagnetic field variation. If magnetization is acquired by the fixing of type I, each component is aligned along the direction of the field in the different age to the others because of the different time of its fixation to the others, and therefore partial demagnetization brings shifting of remanence direction. Experimental results of the present core sediment can be explained using the model of type I.

The fixation of magnetization of type I is further divided into two cases ; fixing begins with (a) softer components and (b) harders (Fig.4). The pilot set of specimens from the horizon HR411 at depth 517 cm, where the directional change curve of NRM shows that the declination goes eastward and the inclination becomes shallow as depth goes up, shows the eastward and upward shift of remanence direction through the stepwise AF-demagnetization in Fig.3(a). This fact may imply the possibility of the fixing of type I(b). There is a result of experiment by redeposition which supports the type I(b) : harder components are fixed at the first stage of compaction and softers at the last (Payne & Verosub, 1982).

It is considered that the small amplitude of the depth-dependency curve of change in declination and inclination of the present core is caused by filtering effect (Hyodo, 1984), i.e. the curve of directional change of magnetization vs. depth is smoothed out by superposition of magnetic components aligned along the various direction of the geomagnetic field over some time span long enough to bury the characteristics. The operation of partial demagnetization has the effect of reducing the time span of the field variation covered by remanences of individual specimens, and as the result the magnetization curve after demagnetization approaches to the field variation without amplitude attenuation. The two phenomena to AF-demagnetization, the directional parallel shifting and the

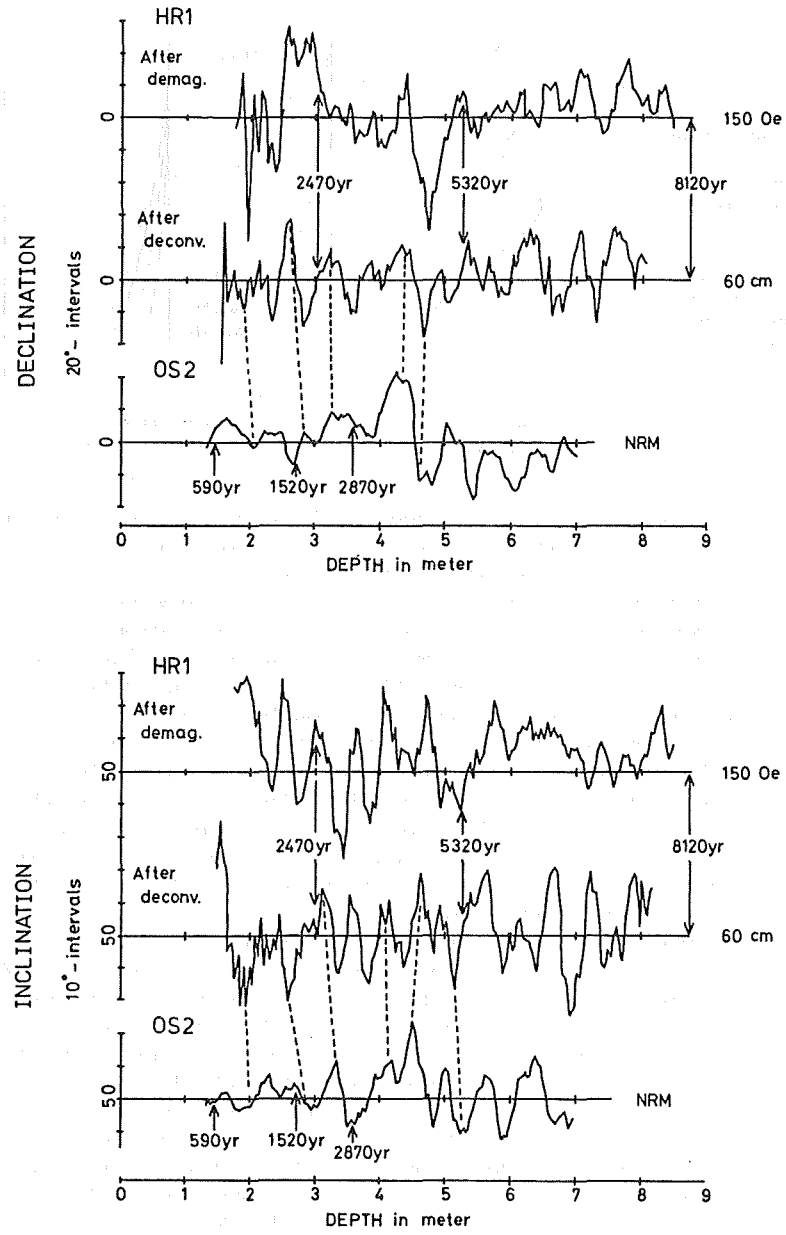

Fig.5 Correlations among directional curves of magnetization in core HR1 after two kinds of operation and a standard curve of the geomagnetic secular variation from core OS2 : curves after demagnetization in a field of 150 Oe (top) and after deconvolution with $Z_{1/2}$= 60 cm (middle) for HR1, and directional curve of NRM for OS2 (bottom). Each curve is smoothed by an operation of 5-points running mean.

growning-up of swings in directional curves, are thus explained by the model described in Fig.4.

It is revealed that the operation of AF-demagnetization is equivalent to the deconvolution based on Eq.(1). Then we compare directional curves subjected to AF-demagnetization with those after deconvolution. The 79 specimens selected from every other depth-level had been already demagnetized. We further demagnetized 78 specimens from the remaining depth-levels, from which no specimen had been taken in the previous operation of demagnetization, at a peak-field of 150 Oe. Declination- and inclination-curves of the demagnetized magnetizations every 5 cm are shown in Fig.5, comparing with those after deconvolution with $Z_{1/2}$ = 60 cm. They show very similar changes in both curves of declination and inclination. High frequency changes, which are especially remarkable in inclination and could be even regarded as being excessively amplified by deconvolution, coexist correspondingly in the two curves. Only part showing large difference in the two curves is between 6 and 7.5 m, where amplitude of changes in curves after deconvolution is much larger than that of curves after demagnetization. This part coincides with that of low bulk density and finer grains. The fact may indicate that the exact half fixing depth for the part from 6 to 7.5 m is smaller than that of the other part, so that the operation of deconvolution using the $Z_{1/2}$ of 60 cm, which is too large for the part, produce out extraordinarily high amplitude changes. With respect to phase, the curves after demagnetization are slightly delayed to those after deconvolution, but there are some swings which are just in phase or out of phase in the opposite sense. The phase shift of the curves is generally small and negligible.

The declination and inclination curves after deconvolution with $Z_{1/2}$= 60 cm are well correlated with those of core OS2 from Osaka Bay (Hyodo & Yaskawa, 1980)(Fig.5), which are inferred, from large amplitude in its swings, to be subjected to only small effect of filtering because of small $Z_{1/2}$. The sediment of the core OS2 consists of very fine clay throughout length and the remanence is very stable against AF-demagnetization. As shown with broken lines in Fig.5, these two cores show high correspondence in both declination and inclination, especially over the time span from about 1000 years B.P. to 5000 years B.P.. Considering that the part for the last 2000 years in the declination and the inclination curves of OS2 are well consistent with the archeomagnetic ones (Hyodo & Yaskawa, 1980), it is correct to regard the depth-dependency curve deduced from the magnetization of core HR1 by deconvolution with $Z_{1/2}$ = 60 cm as the geomagnetic secular variation.

In conclusion, a deconvolution method is an useful technique to deduce a secular variation of the geomagnetic field from magnetization of sediments whose directional changes are smoothed out, and AF-demagnetization can replace the deconvolution as an experimantal deconvolution.

References

Hyodo, M. (1984) J. Geomag. Geoelectr., 36, 45.

Hyodo, M. and K. Yaskawa (1980) J. Geomag. Geoelectr., 32, 581.

Matsuda, J., M. Hyodo, H. Inokuchi, N. Isezaki and K. Yaskawa (1981) J. Geomag. Geoelectr., 33, 161.

Payne, M.A. and K. L. Verosub (1982) Geophys. J. R. astr. Soc., 68, 625.

(Submitted to J. Geomag. Geoelectr.)

PALEOMAGNETIC AND PALEOCLIMATIC STUDY WITH A STALAGMITE

Hayao MORINAGA[1], Hiroo INOKUCHI[2] and Katsumi YASKAWA[1]

1) Division of Environmental Science, The Graduate School of Science and Technology, 2) Faculty of Science, Kobe University, Rokkodai, Kobe 657, Japan

Various sediments have been studied to find the correlation between the geomagnetic field variations and the climatic changes in the past (Wollin et al., 1971a and 1971b; Kawai, 1972; Bucha, 1980). The geomagnetic record in argillaceous sediments tends to have been fixed behind the time of deposition as a post depositional remanent magnetization (PDRM) through such realignment processes as a bioturbation (Irving, 1957; Irving and Major, 1964; Kent, 1973). The recording process tends to be subject to the amplitude attenuation and phase lag of the directional change of magnetization, and to the intensity reduction due to cancellation effect of magnetic moments (Hyodo, 1984). On the other hand, the climatic record, which we can decipher with the oxygen isotopic ratio of organic materials in sediments or merely with the abundance of organic materials in each depth level, tends to be an information before deposition, because it seems to take a long time to deposit after death of the organisms. Time lag between these two records puzzles us to find the true correlation between them.

A few paleomagnetic studies (Latham et al., 1979; Inokuchi et al., 1981) clarified that speleothems had weak but stable natural remanent magnetization (NRM) unaffected by surface conditions such as roughness, dripping or crystal growth. On the other hand, some isotopic studies (Hendy and Wilson, 1968; Fornaca-Rinaldi et al., 1968; Duplessy et al., 1970; Emiliani, 1971) indicated the possibility of obtaining a paleotemperature through the analysis of carbon or oxygen isotope in a speleothem. We have studied the remanent magnetization and the oxygen isotopic ratio of a stalagmite deposit collected from Komori-Ana, a cave in Akiyoshi plateau, Yamaguchi Prefecture, west Japan, for the purpose of tracing back both geomagnetic and climatic records upon the past continuously and of finding the true correlation between both records.

We collected eleven core samples 1 inch diameter and 5 to 18 cm long

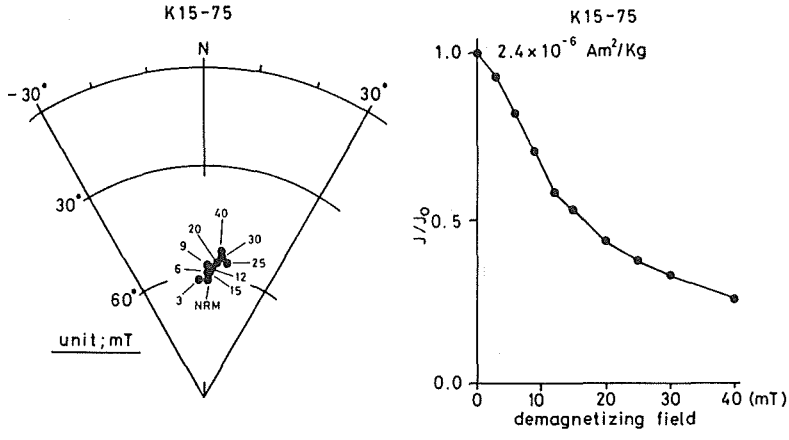

Fig.1 An example of direction change and intensity decay of a stalagmite specimen (K15-75) by progressive AF demagnetization

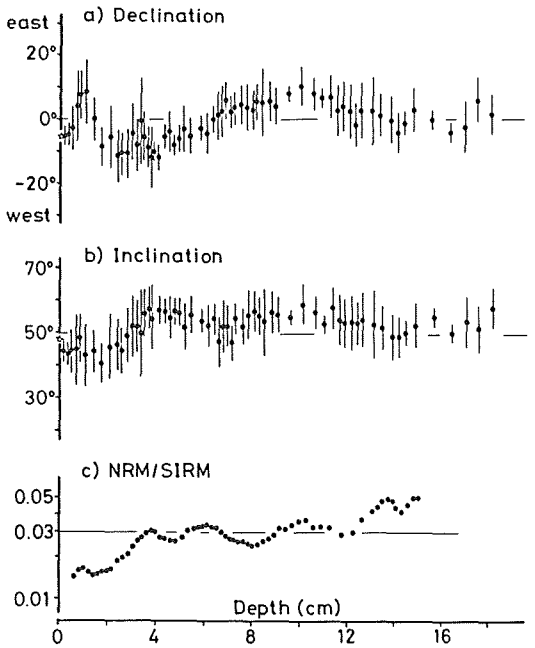

Fig.2 Depth variations in declination, inclination and intensity ratio of NRM to SIRM of stalagmite specimens

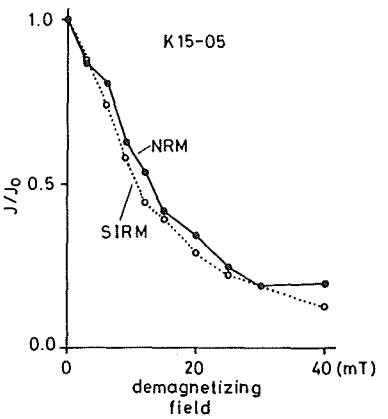

Fig.3 An example of intensity decay of NRM and SIRM of a stalagmite specimen (K15-75) by progressive AF demagnetization

from a stalagmite deposit and oriented them in situ. After bringing them to the laboratory, we sliced them into disks of 1.5 mm thick perpendicularly to their axis.

We measured NRM of these disk specimens with a cryogenic magnetometer whose sensitivity is 10^{-11} Am^2, and made progressive alternating-field (AF) demagnetization on all the specimens. We also measured saturation isothermal remanent magnetization (SIRM) given to the specimens sliced from a core sample (K15) in the uniform field of 450 mT.

The NRM intensity is of the order of 10^{-5} to 10^{-7} Am /Kg before AF demagnetization. The median destructive field (MDF) is between 5 and 15 mT for most specimens, showing that they hold quite stable NRM. Actually their direction of magnetization did not change against demagnetizing field up to 3 to 20 mT. Fig.1 shows the progressive AF demagnetization of Specimen K15-75; the MDF was about 15 mT and the direction of magnetization moved only slightly around a point, declination 2° and inclination 58°. Fig.2 shows variation of declination, inclination and intensity ratio of NRM to SIRM as a function of depth. Each dot in Fig.2-(a) and -(b) indicates the sequential five-point average of individual measured values from the top downward. The length of vertical line across the dot indicates the error angle corresponding to the radius of Fisher's 95 per cent circle of confidence (α_{95}). Each dot in Fig.2-(c) indicates the five-point moving average of the ratio of NRM to SIRM. In order to deal statistically with the data obtained from all the core samples, we normalized the depth level of all the samples with that of core sample K15, being based on the common growth layers' pattern and the depth dependency pattern of NRM intensity, since these patterns are to be equivalent in all the samples each other, because we collected them from a stalagmite, i.e. they were chemically from the same parent water.

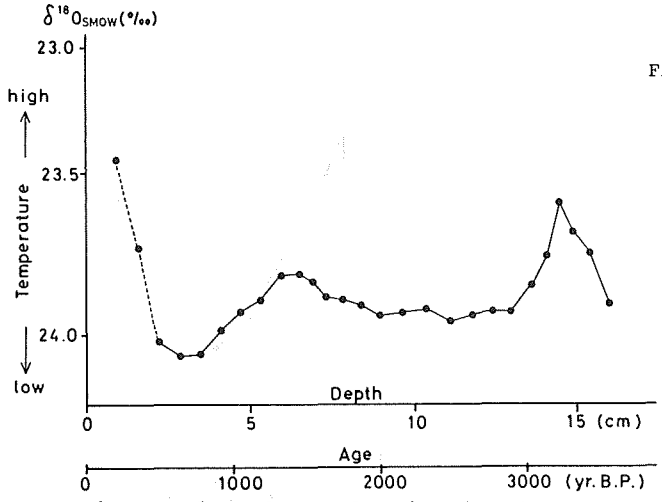

Fig.4 Depth variationin oxygen isotopic ratio of stalagmite specimens

As the result, the stalagmite is clearly a sure recorder of the geomagnetic field direction. The younger part of the specimens, taken near the upper surface of the stalagmite, keeps the NRM of the same direction as the present geomagnetic field at the sampling place, the declination -6.4° and the inclination 48.3° of which are indicated with stars in Fig.2. The directional variation of the NRM is consistent with the archeomagnetic result in southwest Japan (Hirooka, 1971). The depth level of 9 cm in the stalagmite samples corresponds to the age of 2000 years B.P. in the archeomagnetic result. Assuming the linear deposition rate, we tentatively estimated that the age of older specimens at the depth of about 18 cm is 4000 years B.P..

The intensity ratio of NRM to SIRM may give relative intensity of the past geomagnetic field. Because both remanences have very similar AF demagnetization curves (Fig.3), indicating that the SIRM intensity change compensates for depth variations of the content of magnetic particles which carried the NRM (Levi and Banerjee, 1976). Thus, we can conclude that the geomagnetic field intensity decreases gradually from 3500 years B.P. to the present, based on the fact that the ratio of NRM to SIRM decreases for this period.

We measured stable isotopic ratio of oxygen of twenty-nine specimens sliced from the identical sample used in the SIRM measurement. We reacted 30 mg of each specimen with 100 per cent phosphoric acid at 25°C in an evacuated glass reaction vessel. We purified carbon dioxide yielded by the reaction and compared the ratios of mass 45 to (mass 44 + mass 46) and mass 46 to (mass 44 + mass 45) with a standard sample of carbon dioxide using a mass spectrometer. We describe the $^{18}O/^{16}O$ ratio in this report as $\delta^{18}O$ with respect to the international standard SMOW (Standard Mean Ocean Water) (Craig, 1961), where

$$\delta^{18}O(\text{per mil}) = \frac{^{18}O/^{16}O(\text{sample}) - ^{18}O/^{16}O(\text{standard})}{^{18}O/^{16}O(\text{standard})} \times 1000$$

Fig.4 shows the results of isotopic measurement with the $\delta^{18}O_{SMOW}$ values. Each dot indicates three-point moving average of the values obtained from the measurements. The curve connecting the dots gives a relative change of paleotemperature for the past 3500 years. Higher $\delta^{18}O_{SMOW}$ values mean lower temperatures. Hendy and Wilson (1968) estimated the paleotemperature change from the oxygen isotopic composition for two speleothems in Waitomo, New Zealand. Emiliani (1971) demonstrated that the oxygen isotopic trend of the speleothems from both southern France (Duplessy et al., 1969) and New Zealand (Hendy and Wilson, 1968) parallels

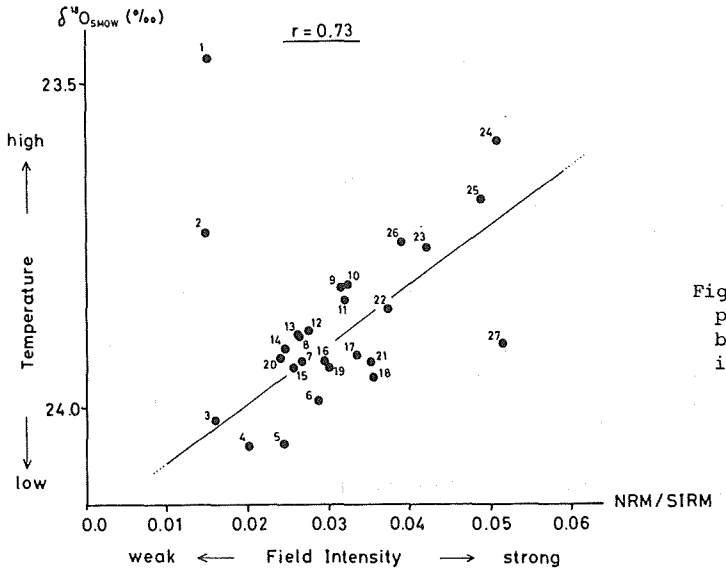

Fig.5 Diagram indicating positive correlation between the geomagnetic intensity and temperature

closely that of the generalized paleotemperature curve obtained from the deep-sea cores.

The intensity ratios of NRM to SIRM were averaged in every identical period, in which $\delta^{18}O_{SMOW}$ values were averaged. We gave a consecutive number (1,2,•••,27) to each period in an ascending order. The point corresponding to a pair of averaged values, NRM/SIRM and $\delta^{18}O_{SMOW}$, in every period was plotted in Fig.5.

Correlation between the intensities of the geomagnetic field estimated from the NRM/SIRM ratios and the temperatures estimated from the $\delta^{18}O_{SMOW}$ value is apparently positive and the correlation coefficient is 0.73 for all the points excluding two points, no.1 and no.2. Deviation of these two points from positive correlation is due to anomalous $\delta^{18}O_{SMOW}$ values of two original specimens, K15-01 and K15-04, (23.195 and 23.222 per mil, respectively). These two specimens were taken near the upper surface of a sample and their $\delta^{18}O_{SMOW}$ appears to be subject to the influence of some other factors than the temperature at the time of deposition. The factors are not investigated for the present.

On the basis of the result reported here we conclude the existence of correlation between the geomagnetic field intensity and the temperature for the past 3500 years: the stronger the intensity was, the warmer the climate was and the weaker the intensity was, the colder the climate was. In the case of sediments, estimation of time lag for fixation of the geomagnetic field and of the climatic record is usually quite difficult and it is not easy to find the true correlation between them. Contrary, in case of speleothems, acquisition of both records must have been at the same time with deposition.

References

Bucha, V. (1980) J. Geomag. Geoelectr., 32, 217.
Craig, H. (1961) Science, 133, 1833.
Duplessy, J. C., J. Labeyrie, C. Lalou and H. V. Nguyen (1969) Nature, 226, 631.
Emiliani, C. (1971) Science, 171, 571.
Fornaca-Rinaldi, G., C. Panichi and E. Tongiorgi (1968) Earth Planet. Sci. Lett., 4, 321.
Hendy, C. H. and A. T. Wilson (1968) Nature, 219, 48.

Hirooka, K. (1971) Mem. Fac. Sci. Kyoto Univ., 38, 167.
Hyodo, M. (1984) J. Geomag. Geoelectr., 36, 45.
Inokuchi, H., H. Morinaga and K. Yaskawa (1981) J. Geomag. Geoelectr., 33, 325.
Irving, E. (1957) Philos. Trans. R. Soc. Lond., A250, 100.
Irving, E. and A. Major (1964) Sedimentology, 3, 135.
Kawai, N. (1972) Proc. Japan Acad., 48, 687.
Kent, D. V. (1973) Nature, 246, 32.
Latham, A. G., H. P. Schwarcz, D. C. Ford and G. W. Pearce (1979) Nature, 280, 383.
Levi, S. and S. K. Banerjee (1976) Earth Planet. Sci. Lett., 29, 219.
Wollin, G., D. B. Ericson and W. B. F. Ryan (1971a) Nature, 232, 549.
Wollin, G., D. B. Ericson, W. B. F. Ryan and J. H. Foster (1971b) Earth Planet. Sci. Lett., 12, 175.

(Submitted to J. Geomag. Geoelectr.)

PALEOMAGNETISM AND FISSION-TRACK AGES OF KIMBŌ VOLCANO, SOUTHWEST JAPAN

Masao TAKAI*, Mutsumi MIYACHI** and Isamu HIRANO***

* Department of Geology, Faculty of Science, Kyushu University, Fukuoka, 812 Japan.
** Laboratory of Earth Science, College of General Education, Kyushu University, Fukuoka, 810 Japan.
*** Geology Division, Geology and Chemistry Department, Public Works Research Institute, Ministry of Construction, Ibaraki, 305 Japan.

Introduction

Kimbō volcano is situated in the western part of central Kyushu, Japan. This volcano consists mainly of six volcanic edifices (Matsuo, Old Kimbō, Sannotake, Ninotake, Hantaka-yama, and Ichinotake), which are aligned in north to south direction. This volcano has been studied by several authors (Yoshii, 1955; Kurasawa and Takahashi, 1963; Matsumoto, 1963, 1979). However, the geology and growth history of this volcano have not been fully clarified. Therefore, paleomagnetic and fission-track ages measurements were carried out on volcanic rocks erupted from this volcano, together with geological investigation.

Outline of geology

The volcanic sequence and the geologic sketch map of Kimbō volcano are shown in Table 1 and Fig. 1, respectively. Lavas and pyroclastic rocks erupted from this volcano are divided into 38 stratigraphic units, and are classified broadly into two stages, the older and the younger. The rocks are composed mainly of andesites, but some basalts and rhyolites are also intercalated.

In the older stage, the eruptions of Matsuo volcanic rocks (M1-M9) occured first, which formed a small volcanic cone in the southern part. After this activity, the eruptions of Old Kimbō volcanic rocks (K1-K11) took place, resulting in the formation of the main stratovolcano (Old Kimbō volcano). The vent of Old Kimbō volcano is considered to be situated at the base of Ichinotake (Mt. Kimbō). After this activity, Ishigami-yama volcanic rocks, which consist of three small lava domes

Table 1. Volcanic sequence of Kimbō volcano.

Kimbō volcanic rocks	Younger stage	Ichinotake volcanic rock	(lava dome)
		Ninotake volcanic rocks	(N1-N7)
		Sannotake volcanic rocks	(S1-S9)
	Older stage	Ishigami-yama volcanic rocks	(lava domes)
		Old Kimbō volcanic rocks	(K1-K11)
		Matsuo volcanic rocks	(M1-M9)

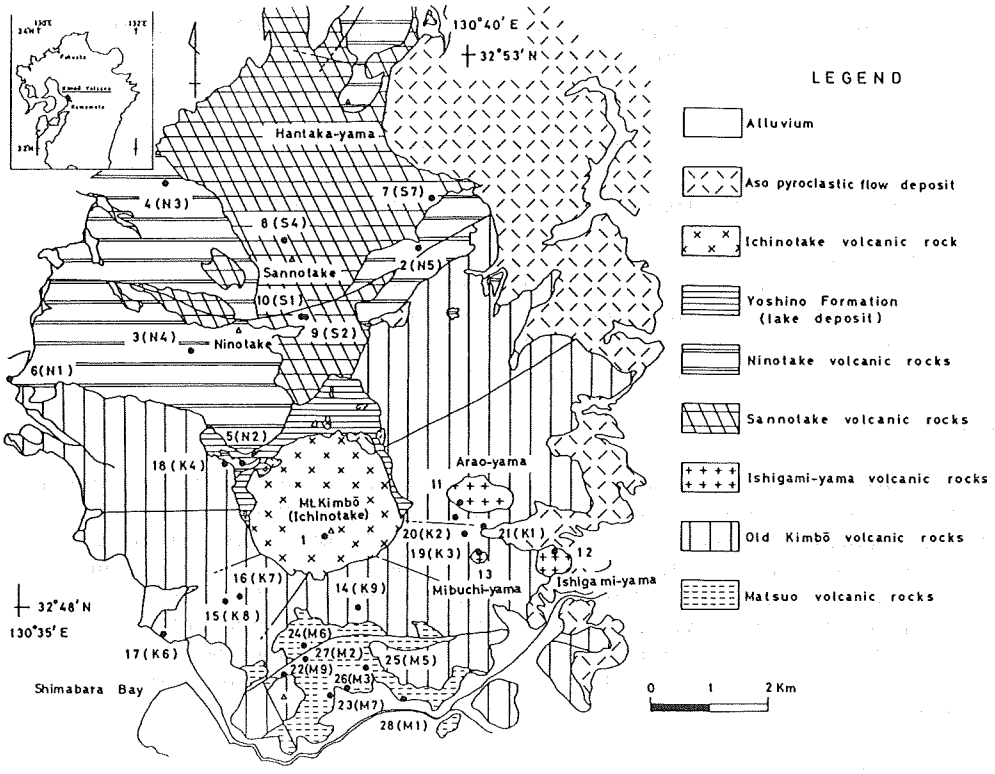

Fig.1. Geologic sketch map of Kimbō volcano and sampling sites. Numerals indicate Site No.

(Arao-yama, Ishigami-yama, and Mibuchi-yama), erupted on the eastern flank of Old Kimbō volcano.

After a long period of erosion, the volcanic activity of the younger stage took place. This stage is divided into the following substages; Sannotake volcanic rocks (S1-S9), Ninotake volcanic rocks (N1-N7), and Ichinotake volcanic rock in order of eruption. The eruptions of Sannotake volcanic rocks formed a Sannotake volcanic cone. The eruptions of Ninotake volcanic rocks formed two volcanic cones, Ninotake and Hantaka-yama. Finally, Ichinotake volcanic rock erupted from the same vent as that of Old Kimbō volcano, and formed a lava dome (Ichinotake).

Paleomagnetism

Paleomagnetic measurements were made on lavas collected from Kimbō volcanic rocks. Natural remanent magnetization (NRM) of specimens was measured with an astatic magnetometer. One or two pilot specimens from each site were progressively demagnetized in alternating field (AF) up to a maximum field of 600 Oe. The examples of change in direction and relative intensity of remanent magnetization in the course of progressive AF demagnetization are shown in Fig.2. 169 specimens collected from 28 sites were allowed to be possessed of stable and reliable polarity directions. The results of paleomagnetic measurement are summarized in Table 2. Mean directions of remanent magnetization for each sampling site are also shown in Fig.3. Lavas of the older stage, except for a Matsuo volcanic rock(M3), have the reversed magnetizations. M3 has the intermediate direction of

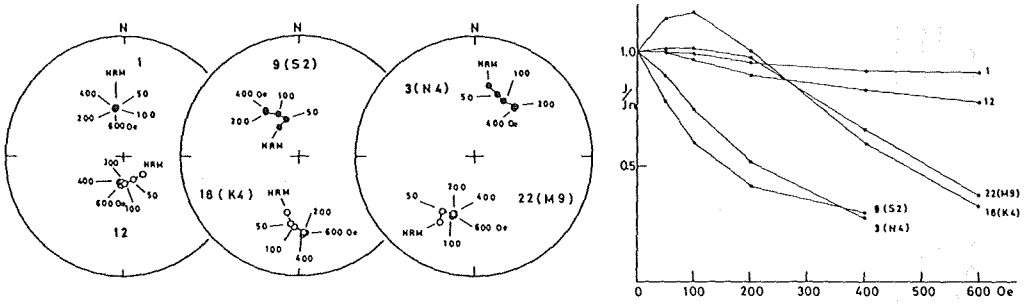

Fig.2. Change in direction and relative intensity of remanent magnetization in the course of progressive AF demagnetization. Projection is the Schmidt's equal area. open circle: upper hemisphere, solid circle: lower hemisphere. Numerals indicate Site No.

Table 2. Results of paleomagnetic measurement.

Site No.	Rock Unit		N	D (°E)	I (°)	K	α_{95}	V.G.P. Lat.	V.G.P. Long.	$Jn \times 10^{-4}$ (emu/g)
1	Ichinotake volcanic rock		5	353	+57	177.4	5.8°	83°N	82°E	13.40
2	Ninotake volcanic rocks	N5 *	6	330	+26	272.7	4.1°	57°N	13°E	4.58
3		N4 **	7	37	+45	522.7	2.6°	57°N	138°W	5.85
4		N3 **	6	23	+26	344.1	3.6°	62°N	102°W	4.59
5		N2 **	7	27	+31	190.0	4.4°	61°N	112°W	3.56
6		N1 **	6	32	+24	144.1	5.6°	54°N	112°W	3.69
7	Sannotake volcanic rocks	S7 *	6	332	+30	255.0	4.2°	60°N	14°E	4.54
8		S4 **	2	344	+43	638.8	9.9°	74°N	15°E	1.50
9		S2 **	5	320	+53	306.8	4.4°	57°N	53°E	5.37
10		S1 **	9	309	+57	103.6	5.1°	49°N	62°E	4.61
11	Ishigami-yama volcanic rocks	**	5	165	- 7	170.4	5.9°	58°S	159°E	5.44
12		*	10	175	-69	150.6	3.9°	70°S	58°W	9.86
13		*	5	180	-74	306.1	4.4°	63°S	49°W	4.06
14	Old Kimbō volcanic rocks	K9 **	6	173	-21	93.9	6.9°	67°S	149°E	1.92
15		K8 **	6	183	-43	78.6	7.6°	82°S	111°E	3.41
16		K7 *	7	187	-47	535.2	2.6°	82°S	76°E	3.98
17		K6	6	200	-38	1575.1	1.7°	69°S	68°E	14.76
18		K4 **	5	174	-37	1313.1	2.1°	77°S	156°E	6.49
19		K3 *	6	195	-34	307.9	3.8°	70°S	84°E	8.21
20		K2 **	5	208	-44	129.4	6.8°	65°S	49°E	2.72
21		K1 *	5	191	-35	94.1	7.9°	73°S	92°E	20.80
22	Matsuo volcanic rocks	M9 *	3	194	-47	234.0	8.1°	77°S	58°E	8.52
23		M7 **	6	178	-66	59.6	8.7°	74°S	54°W	1.94
24		M6 *	6	160	-41	319.3	3.8°	70°S	162°W	7.79
25		M5 **	6	219	-12	46.9	9.9°	45°S	68°E	2.20
26		M3 **	7	48	-56	35.6	10.3°	7°N	86°W	2.63
27		M2 *	7	196	-36	123.4	5.5°	71°S	79°E	7.65
28		M1 *	9	198	-53	480.2	2.4°	75°S	33°E	11.87
	Mean values †		27	4	+43	11.8	8.4°	81°N	74°W	

N: number of samples measured, D and I: mean declination and inclination of remanent magnetization, K: Fisher's precision parameter, $\alpha 95$: semi-angle of cone of 95% confidence for the mean direction, V.G.P.: virtual geomagnetic pole, Jn: intensity of NRM, * and **: direction of remanent magnetization after AF demagnetization of 100 and 200 Oe.

† Calculation for mean values excludes a Matsuo volcanic rock(M3) with the intermediate direction of NRM.

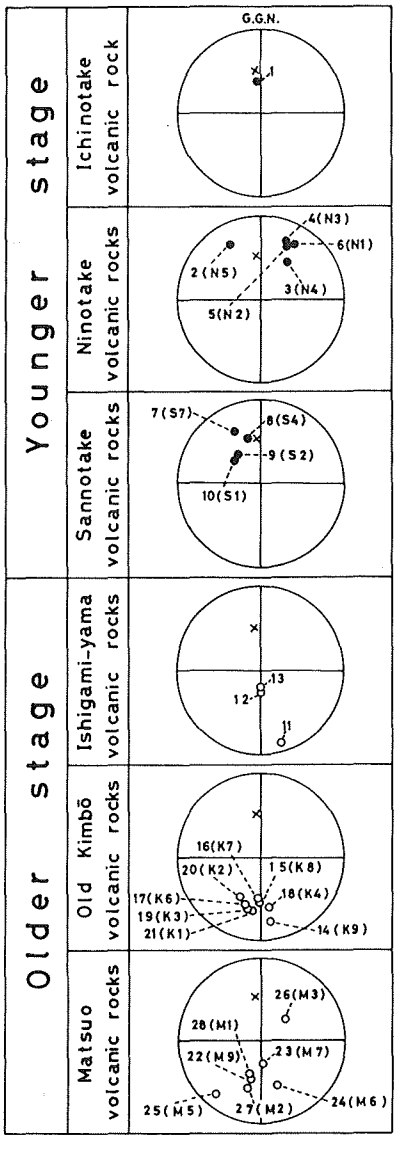

Fig.3.Mean direction of remanent magnetization for each sampling site. Projection is the Schmidt's equal area. Numerals indicate Site No. open circle: upper hemisphere, solid circle:lower hemisphere, cross: direction of the present geomagnetic field in this area, G.G.N.:geographic north.

NRM. Specimens of M3 were collected at a quarry where any local crustal movement after the emplacement of the lava was not recognized in the field. Accordingly, it is considered that the intermediate direction of M3 was acquired in a field of transitional dipole. Lavas of the younger stage have the normal magnetizations. The directions of remanent magnetization of Sannotake volcanic rocks are northwesterly, and Ninotake volcanic rocks, except for N5, are northeasterly. Thus, Sannotake and Ninotake volcanic rocks were characterized by the directions of remanent magnetization. N5 is restricted in distribution. Therefore, the vent and eruption age of N5 may be different from those of other volcanic rocks of Ninotake.

Fission-track age

Fission-track ages of zircons from four lava domes (Ishigami-yama and Ichinotake volcanic rocks) have been determined by the external detector method (Naeser,1976). Several hundred grains were mounted in teflon and polished to expose an internal surface. The polished mount was etched in a eutectic melt of NaOH+KOH at 220°C for 28 to 68 hours for optimum fossil track development. The mount was covered with muscovite and irradiated in the TRIGA reactor at the U. S. Geological Survey, Denver, Colorado. The neutron dose was determined by counting the tracks present in a muscovite detector placed next to National Bureau of Standards SRM 962 during the irradiation The NBS copper flux value was used for the calibration (Carpenter and Reimer, 1974). After irradiation the muscovite detector was etched (14 min. with 48% HF at 25°C) to develop the induced fission tracks. The analytical uncertainty of the age was calculated using the method of Johnson et al. (1979). Samples of four lava domes were collected from the same site as that of paleomagnetic measurement. The ages of four lava domes are as follows: Arao-yama, 0.94 ± 0.15 m.y.; Ishigami-yama, 1.12 ± 0.20 m.y.; Mibuchi-yama, 1.01 ± 0.09 m.y.; Ichinotake, 0.15 ± 0.05 m.y. (Table 3).

Table 3. Zircon fission-track ages of four lava domes.

Site No.	Locality	Number of grains	Number of fossil counts	ρ_s $\times 10^6$ t/cm^2	Number of induced counts	ρ_i $\times 10^6$ t/cm^2	ϕ $\times 10^{15}$ n/cm^2	U (ppm)	Age (m.y.)	$\pm 2\sigma$ (m.y.)	r
1	Ichinotake	31	32	0.028	5452	9.505	0.875	344	0.15	0.05	0.42
11	Arao-yama	45	105	0.086	2926	4.820	0.875	175	0.94	0.15	0.76
12	Ishigami-yama	32	97	0.085	2276	3.776	0.875	137	1.12	0.20	0.83
13	Mibuchi-yama	18	270	1.234	1009	9.220	0.127	2301	1.01	0.09	0.90

$\lambda_F = 7.03\times10^{-17}\,yr^{-1}$; $^{235}U/^{238}U = 7.252\times10^{-3}$; $\sigma_f = 580\times10^{-24}\,cm^2$; r=correlation between ρ_s and ρ_i

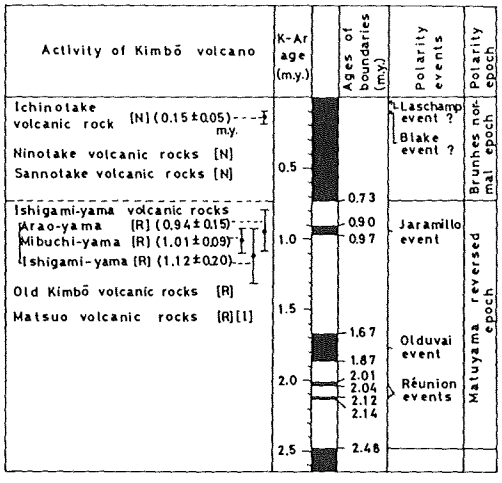

Fig.4. A possible correlation of volcanic rocks of the present study to the geomagnetic polarity time scale (Mankinen and Dalrymple, 1979). [N]:normal polarity, [R]: reversed polarity,[I]: intermediate polarity.

Activity of Ishigami-yama volcanic rocks was previously considered to be of final stage of Kimbō volcano as that of Ichinotake volcanic rock (Kurasawa and Takahashi, 1963; Matsumoto, 1963,1979). However, the ages obtained on four lava domes indicate that the activity of Ishigami-yama volcanic rocks is quite different from that of Ichinotake volcanic rock in age. This fact is in harmony with that of the paleomagnetic data.

Summary

Comparing the fission-track ages and paleomagnetic data with the geomagnetic polarity time scale(Mankinen and Dalrymple,1979), it is considered that the volcanic activity of the older stage occured during the Matuyama reversed epoch,while the younger stage occured during the Brunhes normal epoch (Fig. 4).

Mean virtual geomagnetic pole (VGP) position (74°W,81°N) calculated from the mean direction of NRM of Kimbō volcanic rocks lies nearly close to that of Plio-Pleistocene (56°W, 85°N) of southwest Japan compiled by Yasukawa and Nakajima (1974).

Reference

Carpenter, B.S. and G.M. Reimer (1974) NBS special publication, 260.
Johnson, M.N., V.E. McGee and C.W. Naeser (1979) Nuclear tracks,3-3, 93.
Kurasawa, H. and K. Takahashi (1963) Bull. Geol. Surv. Japan, 14, 80.
Mankinen, E.A. and G.B. Dalrymple (1979) J. Geophys. Res., 84, 615.
Matsumoto, Y. (1963) Report of Research Institute of Industrial Science, Kyushu Univ., 34, 1.
——————— (1979) Chikyu Kagaku (Earth Sci.), 33, 192.
Naeser, C.W. (1976) U. S. Geological Survey, Open-file report, 76.
Yasukawa, K. and T. Nakajima (1974) J. Geol. Soc. Japan, 80, 215.
Yoshii, M. (1955) Mem. Fac. Educ., Kumamoto Univ., 3, 135.

PALEOMAGNETISM OF THE FUDESHIMA DIKE SWARM, OSHIMA ISLAND, CENTRAL JAPAN

Eiichi KIKAWA

Earthquake Research Institute, University of Tokyo
Tokyo 113, Japan

1. Introduction

It is rather difficult to decipher the precise history of paleosecular variations of some data sets. Generally, the paleomagnetic information about ancient secular variation may be described by a single parameter;the angular standard deviation(ASD) of virtual geomagnetic poles (VGP) from their mean. It is useful to calculate the angular dispersion of VGPs of some paleomagnetic data set such as those of successive lava flows of a stratovolcano and a dike swarm in deducing the amount of the ancient geomagnetic secular variation(paleo secular variation, PSV). Because the activity duration of a stratovolcano is over $10^{4\sim5}$ years and that of a dike swarm is regarded as almost similarto a stratovolcano(Nakamura, 1977), both successive lava flows of a stratovolcano and a dike swarm may record the paleosecular variation of the geomagnetic field during a time span long enough to average the secular variation. There have been several estimates of PSV (Ozima and Aoki,1972; Heki and Tsunakawa, 1981; Tsunakawa, 1982; Tsunakawa and Hamano, 1982; Heki, 1983) for the Japanese region. Heki(1983) concluded that 1) the ASD of the VGPs caused by the PSV is around 14 for Japanese region and this value agrees well with that expected from the global trend of ASD. 2) the time span of more than a few times 10^4years is needed to obtain meaningful estimates of PSV.

A paleomagnetic study on the Fudeshima dike swarm, the Pleistocene dike system exposed on the southeast cliff of Oshima Island situated to the east of the Izu Peninsula has been carried out for the purpose of adding and examining a PSV data set for Japanese region during Brunhes epoch. Consideration about the tectonic movement of Fudeshima region is also presented.

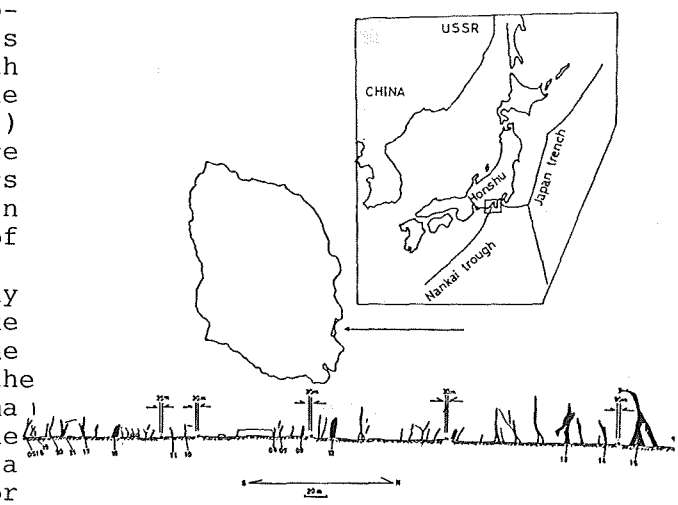

Fig. 1. Detailed paleomagnetic sampling localities in Fudeshima dike swarm (opposite side of Fudeshima, OS07-21; near nejinohana, OS24-29). Sketch of dike swarm is simplified from Inamoto (1974).

2. Geology and Measurement

Fudeshima volcano situated on the southeastern coast of the Oshima Island(Fig. 1) consists of lavas and pyroclastic rocks of pyroxene olivine basalt and olivine basalt which are cut by explosion breccia and numerous dikes of the same petrographic character as that of the lavas. The dikes strike in the north-north-west direction, which coincides with the direction of the maximum compressional stress inferred from shallow earthquake mechanisms and the trend of the zone of flank volcanoes of Oshima Island(Inamoto,1974;Nakamura,1980). Because of low K content and comparatively young age,only older limit of K-Ar age of 2.4 Ma is obtained(Kaneoka et al., 1970). The age of the volcano, however, is best estimated to be in the Pleistocene(Kaneoka et al., 1970), as will be discussed later.

Ninety-two separate hand samples oriented by magnetic compass were collected from twenty-one dikes. Measurements of remanent magnetization were made on a Shonstedt spinner magnetometer at the Ocean Research Institute, University of Tokyo. Specimens from each dike were then progressively demagnetized in peak alternating field up to 800Oe.The cleaning level yielding the smallest alpha 95 was chosen to represent the unit. Magnetic susceptibilities were measured on at least three specimens per site using

Table 1. Summary of Magnetic Properties of Samples

Site	K	Jn	Qn	MDF	TC1	TC2	Jo	Jh/Jo
OS07	2.1	0.6	1.7	350	540	530	1.1	1.0
08	2.4	1.9	3.5	175				
09	2.6	0.4	1.1	175	560	530	0.6	0.6
10	2.3	2.3	5.1	375	530	480	1.3	0.7
11	1.8	0.3	0.9	225				
12	2.4	1.0	2.3	225				
13	2.0	1.0	3.1	250	490	460	2.1	1.1
14	2.0	1.1	3.7	250	560	520	1.2	0.8
15	2.0	0.9	2.5	200				
16	2.8	0.9	1.7	175	550	520	1.0	0.9
17	4.6	1.7	2.7	225				
18	2.4	5.8	12.6	375				
19	3.5	7.9	13.0	300				
20	2.6	5.9	14.7	475	560	540	2.4	0.8
21	2.9	3.1	6.3	225				
24	2.3	1.5	4.2	200	480	440	1.5	1.2
25	2.1	0.7	2.2	275				
26	2.3	2.5	6.8	150				
27	1.9	1.8	5.6	200	320	340	1.1	1.1
28	2.3	2.0	6.4	375				
29	2.0	1.1	3.3	250	520	470	1.3	0.9

K, magnetic susceptibility(10^{-3} emu/cc Oe); Jn, intensity of natural remanent magnetization(10^{-3} emu/gr); Qn, Kenigsberger ratio; MDF, median demagnetizing field(Oe); TC1, Curie temperature of heating process(°C); TC2, Curie temperature of cooling process(°C); Jo, saturation magnezation before heating(emu/gr); Jh, saturation magnetization after thermal treatment(emu/gr).

Bison Instruments Magnetic Susceptibility Model 3101A and then Koenigsberger(Qn) ratios were calculated.

3. Magnetic Properties

The average intensity of NRM(Jn), median demagnetizing field (MDF),magnetic susceptibility(K) and Koenigsberger(Qn) ratios are given in Table 1. The representative alternating field demagnetization curves are shown in Fig. 2. The MDF varies from about 150 to 475 Oe. NRM directions were tightly grouped and changed little after the partial demagnetization. NRM intensities ranged from 0.3 to 7.9 x 10^{-3}emu/gr with the average value of 2.1 x 10^{-3} emu/gr. Fig.3 shows the relation between Jn, K and Qn. Saturation magnetization and its temperature dependence curves have been run on ten samples by an automatic torque balance in a field of 4.5 KOe in vaccum of 10^{-5}~$^{-6}$torr. In each, almost thermally reverssible type curves were obtained. This suggests an unoxidized titanomagnetite is a main carrier of remanent magnetization. Several polished thin sections studied indicate that the opaque minerals contained are predominantly fresh titanomagnetite, which is consistent with the result of thermomagnetic analysis.

4. Paleomanetic Results and Discussion

Table 2 gives paleomagnetic results from this study. The mean field directions and VGPs are summarized in Fig. 4. The mean paleomagnetic vector calculated is I(inclination)= 51.9, D(declination)= 2.4 with 95% confidence(A_{95}) of 6.6. This mean field direction is consistent with the geomagnetic field direction of the geocentric axial dipole(I= 54.3). The remanent magnetization of normal polarity and the older limit of K-Ar age of 2.4Ma allow one to infer several possible correlations to the general magnetic stratigraphy(Harland et al., 1982). Reviewing ages of other

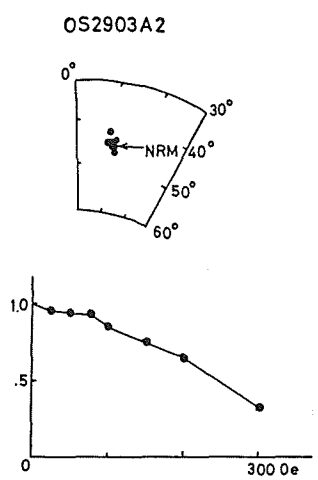

Fig. 2. Typical example of change of magnetic vectors and normalized NRM intensity as a function of demagnetizing field intensity.

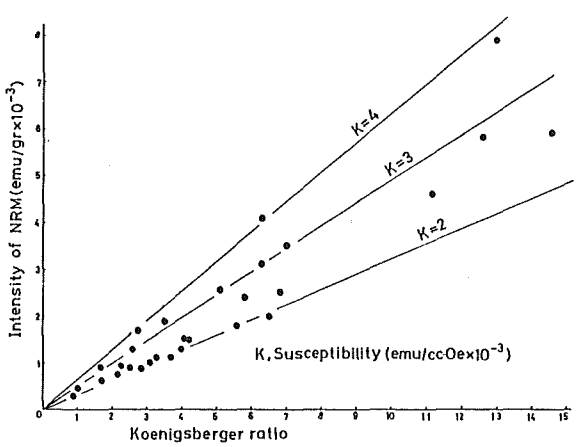

Fig. 3. Intensity of NRM versus Koenigsberger ratio and corresponding magnetic susceptibility.

Table 2. Directions of Remanent Magnetism and Paleomagnetic Pole Positions.

SITE	N	ODF	INCL	DECL	K	A_{95}	VGPLAT	VGPLONG
OS07	3	NRM	76.5	298.6	125	11.1	43.1 N	108.6 E
08	4	NRM	54.7	354.2	40	14.8	85.2 N	57.4 E
09	3	NRM	65.1	304.9	750	4.5	47.5 N	83.8 E
10	4	75	58.8	356.9	77	10 5	84.6 N	113.1 E
11	5	NRM	57.8	9.0	503	3.4	81.9 N	199.4 E
12	5	100	42.6	27.6	47	11.3	64.1 N	244.7 E
13	4	NRM	58.0	37.4	86	9.9	60.0 N	210.8 E
14	4	NRM	40.7	11.0	230	6.1	75.1 N	276.6 E
15	5	NRM	58.4	357.7	160	6.1	85.2 N	117.4 E
16	4	NRM	50.0	356.9	399	4.6	85.3 N	354.0 E
17	4	NRM	52.4	351.0	469	4.3	82.3 N	39.1 E
18	4	NRM	43.9	350.8	697	3.5	78.0 N	3.3 E
19	5	NRM	56.4	346.9	143	6.4	79.2 N	65.3 E
20	4	NRM	52.5	345.9	273	5.6	78.2 N	45.6 E
21	4	100	55.3	356.2	81	10.3	86.7 N	70.6 E
24	5	100	39.9	16.0	84	8.4	71.6 N	265.9 E
25	7	NRM	48.7	8.8	203	4.2	81.0 N	261.3 E
26	5	NRM	43.5	358.9	825	2.7	80.6 N	325.6 E
27	5	100	25.2	24.6	113	7.3	59.1 N	267.4 E
28	4	NRM	30.3	5.7	289	5.4	70.9 N	302.5 E
29	4	NRM	46.8	7.4	242	5.9	80.8 N	274.1 E
Mean field direction			51.9	2.4	24.1	6.6		
Mean VGP					31.9	6.0	84.5 N	274.4 E

N, number of samples; ODF, optimum demagnetizing field; INCL, inclination; DECL, declination; K, precision parameter; A_{95}, radius of 95% confidence; VGPLAT, VGP latitude VGPLONG, VGP longitude. OS07 and OS09 are not included for VGP analyses.

volcanoes exposed in the same island which are 0.4 Ma for Okata volcano and late Pleistocene for Gyojanoiwaya volcano(Kaneoka et al.,1970, Kikawa,1984) and the geological settings suggests that the good selection is to correlate Fudeshima volcano to Brunhes normal polarity chron.

Calculated angular standard deviation of the VGPs between-site is 15.1 with 95% confidence interval between 12.4 and 19.3. This value of ASD agrees well with general tendency of the world-wide paleosecular variation dispersions at the similar latitude during Brunhes epoch(McElhinny and Merrill, 1975;Fig.5). Secular variation seems to be aveaged within the Fudeshima dike swarm. Hence,from these paleomagnetic results,it cannot but be concluded that Fedeshima volcano has undergone no post-cooling tectonic movement.

McElhinny and Merrill (1975) calculated ASD of VGPs for the Japanese region during Brunhes epoch from Japanese paleomagnetic data and reported the value of 13.7 (+1.7, -1.4) which is smaller than their Brunhes-aged ASD of VGPs combined for latitude range between 31 N and 45 N (14.8, +1.0 ,-0.9). Because some of the

Japanese data sets they used are from the regions which underwent some tectonic movement during Brunhes epoch,this value may reflect apparent PSV. ASDs derived in this study (15.1) and other recent studies(for example, 14.6 for Tsunakawa and Hamano(1982), 13.9 for Heki(1983) are slightly larger than this ASD,which indicate that ASD of VGPs caused by PSV for the Japanese region during Brunhes epoch may be between 14 and 15. If so, Japanese ASD during the Brunhes epoch agrees better with that deduced from the world-wide PSV dispersions at the similar latitude of 35 N compiled by McElhinny and Merrill (1975) for the same epoch.

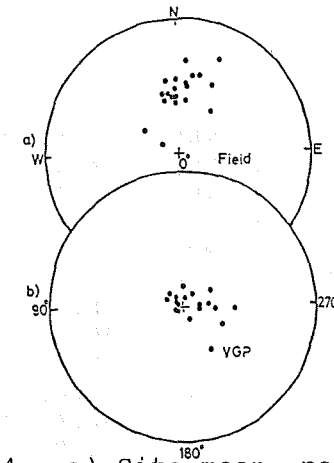

Fig. 4. a) Site mean paleomagnetic vector directions of Fudeshima dike swarm. All means have positive inclinations. b) Virtual geomagnetic poles (VGP).

5. Conclusion

Paleomagnetic results from the Fudeshima dike swarm indicate ASD of VGPs from their mean which coincides with that of global trend. Consequently, Fudeshima dike swarm recorded the paleosecular variation during a time long enough to average it. The paleomagnetic data futher exhibit the mean field direction which is consistent with the geomagnetic field direction of the geocentric axial dipole. These results suggest that the Fudeshima region (Oshima Island) seems to have undergone no post-cooling tectonic movement. Between-site ASD of Brunhes-aged VGPs for the Japanese region may be between 14 and 15.

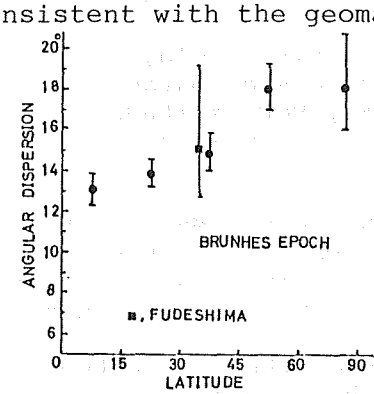

Fig.5. World-wide paleosecular variation VGP dispersions for the Brunhes epoch found by averaging over 15 latitude stripes(McElhinny and Merrill 1975). Star symbol means the value of VGP dispersions for the Fudeshima dike swarm.

References

Harland et al.(1982) A Geologic Time Scale (Cambridge Univ. Press) P.131 Inamoto,A(1974) Graduation Thesis,Fac.Sci.Chiba Univ. Heki,K. and H. Tsunakawa(1981) Rock Mag. Paleogeophys.,8,17 Heki,K(1983) J. Geomag. Geoelectr., 35, 383 Kaneoka et al.(1970) Geochem. J., 4,53 Kikawa,E.(1984)MasterThesis, Fac.Sci.Chiba Univ. McElhinny,M.W. and R.T.Merrilli(1975)Rev.Geophys. Space Phys.,13,687 Nakamura,K. (1977)J.Volcano.Geotherm.Res.,2,1 Nakamura,K(1980)Gekkan Chiky (The Earth Monthly),2,94 Ozima,M. and Y.Aoki(1972)J.Geomag.Geoelectr.,24,471Tsunakawa,H(1982)DoctralThesis,Fac.Sci.Univ.Tokyo Tsunakawa,H. and Y.Hamano(1982)Rock Mag. Paleogeophys.,9,9

PALEOMAGNETISM OF THE IZU COLLISION ZONE

Eiichi KIKAWA* and Hajimu KINOSHITA**

* Earthquake Rsearch Institute, University of Tokyo
Tokyo 113, Japan
** Department of Earth Sciences, Chiba University
Yayoi-cho 1-33, Chiba City 260, Japan

It is widely accepted that the Philippine Sea(PHS) plate is colliding with the Eurasian (EUR) plate and pushing the latter north-northwestward and the Izu Block (Izu Peninsula) is being accreted to south central Honshu. From paleomagnetic results, Tonouchi and Kobayashi (1983), Hirooka et al. (1983) and Koyama (1983) imply that the Izu Block originated in a latitude (23 N) significantly lower than the present position (35 N) and had been drifting northward at a rate of approximately 10 cm/year until it collided with south central Honshu 2 to 3 M.y. ago. This reveals that the Izu Block may have been emplaced to the present location at that time and probably subjected to post-collision deformation processes.

A paleomagnetic investigation was made on six Quaternary volcanoes in the northwestern to southern part of the Izu Peninsula (Ida, Daruma, Tanaba, Chokuro, Jaishi and Minamisaki(Nanzaki) volcanoes) and on Ashitaka volcano situated in the north of the plate boundary between the PHS and EUR plate to test the hypothesis that the Izu Peninsula has undergone possible post-collision deformation(Fig. 1). There have been already several paleomagnetic investigations on Quaternary volcanoes in the eastern part of the Izu Peninsula as will be referred to later.

The mean field directions are summarized in Table1 and Fig.2 The overall average field directions computed from the 19 sites of Ashitaka volcano are I(inclination)=48.7, D(declination)=1.0 with 95% confidence(A_{95}) of 8.6. This mean field direction is consistent with the geomagnetic field direction of the gecentric

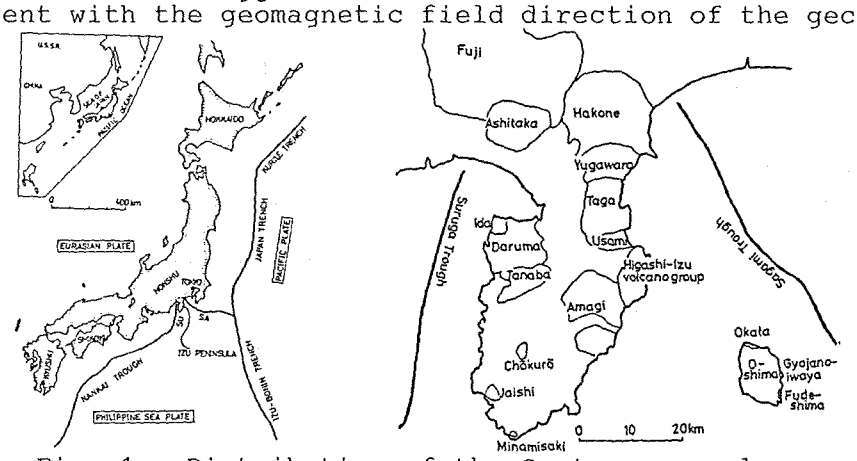

Fig. 1. Distribution of the Quaternary volcanoes in the northern tip of the Philippine Sea plate.

Table 1. Mean Paleomagnetic Vector Directions and Pole Positions

VOLCANO	N	n	DEC	INC	K	A95	VGPLO	VGPLA	K	a95
ASHITAKA (Brunhes)	19	119	1.0	48.7	18.7	8.0	315.8	85.7	15.5	8.8
Northwestern part of the Izu Peninsula										
IDA (0.64Ma)	6	34	4.6	50.6	36.2	11.3	76.5	85.0	36.6	11.2
DARUMA (0.59 to 0.83Ma.)										
*early lava	2	15	174.2	-22.7	470.5	11.5	153.0	-66.2	431.6	12.1
early lava	4	24	33.5	56.7	19.4	21.5	28.3	63.7	14.1	25.4
late lava	22	194	190.7	-49.7	18.7	7.4	240.8	-80.9	17.1	7.7
late lava	29	208	9.2	46.7	18.9	6.3	80.2	80.0	19.1	6.3
TANABA (Matuyama)	8	53	189.9	-47.7	17.5	13.7	70.0	-80.7	14.9	14.8
South-southwestern part of the Izu Peninsula										
CHOKURO (Brunhes)	7	46	352.2	39.5	29.0	11.4	352.1	76.1	29.4	11.3
JAISHI (Matuyama)	9	60	154.9	-58.0	17.1	12.8	72.3	-70.7	13.1	14.8
MINAMISAKI (0.43Ma.)	5	28	348.4	36.9	115.1	7.2	358.4	72.7	101.9	7.6

N, number of flows. n, number of specimens. Dec, declination of mean paleomagnetic vector (MPV). INC, inclination of MPV. K, Fisherian precision parameter of MPV. A_{95}, angle of 95% confidence of MPV. VGPLO, mean VGP(MVGP) longitude. VGPLA, mean VGP latitude. k, Fisherian precision parameter of MVGP. a_{95}, 95% confidence of MVGP. *; not included in the paleomagnetic study.

axialdipole(I=54.7). Ida volcano of normal polarity, Daruma volcano of both normal and reversed polarity and Tanaba volcano of reversed polarity which are all located in the northwestern part of the Izu Peninsula have a trend that the declination of the remanent magnetization is generally deflected clockwise from the present geographic north: Paleomagnetic data of Ida volcano exhibit a direction, I=50.6, D=4.6 with A_{95} of 11.3. Daruma volcanic data for early lava result in a direction, I=56.9, D=33.5 with A_{95} of 21.5 ,and the mean vectors obtained from late lava are I=-49.7, D=190.7 with A_{95} of 7.4 and I=46.7, D=9.2 with $A_{95}$of 6.3. Tanaba volcano indicates a direction I=-47.7, D=189.9 with A_{95} of 13.6 similar to the reversed direction of Daruma volcano. On the other hand, Chokuro volcano of normal polarity,Jaishi volcano of reversed polarity and Minamisaki volcano of normal polarity, located in the south-southwestern part of the Izu Peninsula,show consistently the declination deflected counter

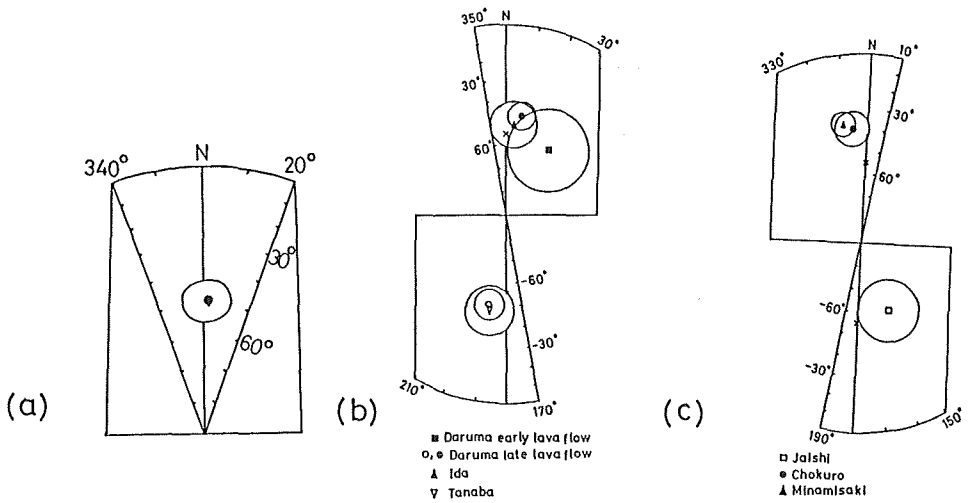

Fig. 2. Paleomagnetic field directions for sites from (a) Ashitaka Volcano, (b) Northwestern part of the Izu Peninsula and (c) South-southwestern part of the Izu peninsula. Symbols are shown in the figure. Solid and open symbols mean positive and negative inclinations, respectively. Note that all means reveal the declinations deflected clocwise in the northwestern part of the Izu Peninsula and counter-clockwise in the south-southwestern part of the Izu Peninsula and the normal and reversed polarity directions are aligned in antipodes.

clockwise: the mean direction of Chokuro volcano is I=39.5, D=352.2 with A_{95} of 11.4 which is close to the average direction of Minamisaki volcano, I=36.9, D=348.4 with A_{95} of 7.2. Here, the inclinations of Chokuro and Minamisaki volcanoes of which values are 39.5+11.4, 36.9+7.2, resepectively are considered to be significantly shallower than the present geomagnetic inclination(I=49). The paleomagnetic data obtained from Jaishi volcano, I=-58.0, D=154.9 A_{95} =12.8 is also deflected counter-clockwise.

Alternating field demagnetization experiment, thermomagnetic measurement and microscopic observation show these magnetization directions to be stable and essentialy free from secondary overprinting because carries of remanent magnetization are fresh, fine-grained titanomgnetites.

As to the paleomagnetic vector directions of the Ashitaka volcano, it is difficult to decipher the effect of paleosecular variations. The average direction which is close to the axial geomagnetic dipole field as mentioned before,nevertheless, suggests that Ashitaka volcano has possibly undergone no post-cooling tectonic movement. This coincides with Tsunakawa and Hamano(1982) in which they reported the paleomagnetic results of twenty-one dikes of Ashitaka volcano whose mean direction recording the paleosecular variation during enough time interval to average it out is also close to the expected geomagnetic field and concluded no tectonic movement of Ashitaka region.

Samples from the Izu Peninsula recorded both normal and re-

Table 2. Paleomagnetic Vector Directions : Eastern Part of the Izu Peninsula

	INC	DEC	A_{95}	Reference
Yugawara Volcano	51.0	351.9	9.9	Akimoto and Terauchi(1981)
Taga Volcano	53.1	340.7	15.7	Nagata et al.(1957)
*Usami Volcano	51.6	337.9	8.1	Kono(1968), Akimoto and Terauchi(1981)
Ajiro Basalts	39.6	335.8	23.6	Akimoto and Terauchi(1981)
Shiofukizaki Basalts	61.6	313.6	9.6	Tonouchi(1981)

INC, inclination; DEC, declination; A_{95}, 95% confidence.
Note: *, This volcano has revealed both normal and reversed polarity.

versed polarities and so were magnetized over tens of thousands of years at least. This result indicates that the duration of volcanism was sufficiently long to average out the secular variation. This is also supported by K-Ar ages. The normal and reversed paleomagnetic directions which are aligned in antipodes indicate the declinations deflected clockwise in the northwestern part of Izu Peninsula and counter-clockwise in the south-southwestern Izu Peninsula. Another paleomagnetic data obtained from Quaternary volcanoes in the eastern Izu Peninsula all reveal the counter-clockwise deflections in declinations similar to those of the south-southwestern part of the Izu Peninsula(Nagata et al.,1957, Kono, 1968, Tonouchi,1981,Akimoto and Terauchi,1981, Fig.3, Table 2). This differential movement may be explained by some tectonic movement within the Izu Block. MacDonald (1980) suggests that in most orogenic zones combined rotations about inclined axes should be a common phenomenon. Nevertheless,if some errors are permitted,it is possible to regard rotation about inclined axes as rotation about vertical axes or rotation about horizontal axes in proportion to the dip of inclined axes. Therefore,considering this dis-

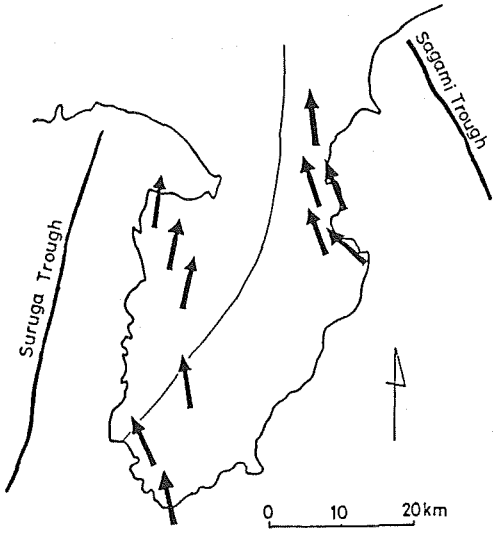

Fig. 3. Arrows indicate paleomagnetic declinations found for the respective volcanoes. An easterly and westerly directed arrows apparently indicate clockwise and counter-clockwise rotation,respectively. The solid line based upon the boundary of the strike of dikes (Nakano et al., 1980) seems also to reveal the boundary of the two groups of declinations.

Table 3. Summary of Results of Paleomagnetic Interpretation Based Upon Rotation about Horizontal Axis

	Strike of Tilting axis	Tilting Angle	Approximate Tilting Direction	Approximate Tilting Rate (degree/m.y.)
Ida Volcano	N43W	6	SW	10
Daruma Volcano	N22W	12	W to WSW	15
Tanaba Volcano	N25W	12	W to WSW	(<12)
Chokuro Volcano	N59E	16	SE	-
Jaishi Volcano	N23W	17	E to ENE	(10)
Minamisaki Volcano	N52E	20	SE	(40?)
Yugawara Volcano	N24E	8	E to ESE	16
Taga Volcano	N 4W	14	E	(28)
Usami Volcano	N 3W	16	E	20
Ajiro Basalts	N22E	26	E to ESE	20
Shiofukizaki Basalts	N34W	28	E to ENE	14

cussion and for the sake of simplicity, the two simple rotations can be applied to analyze and interpret the traces of tectonic movement expected from paleomagnetic directions. It can be assumed that the original magnetic vector is that of the geocentric axial dipole because the geomagnetic field had in average an axial geocentric dipole during the Quaternary (McElhinny, 1973).

The two declination groups in the Izu Peninsula are difficult to explain as due to rotation about vertical axes. If we want to do so,relative two counter-balancing rotations in a small geologic unit are needed. Such rotations are, however, difficult to occur because they would generally be accompanied with both lack and excess of materials. There is no evidence of such geo-

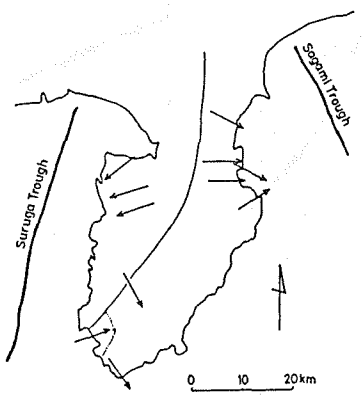

Fig. 4. Arrows indicate tilting directions found for respective volcanoes. Two tilting domains, one of which has been tilted to the W to WSW and the other has been tilted to E to SE, are recognizable.

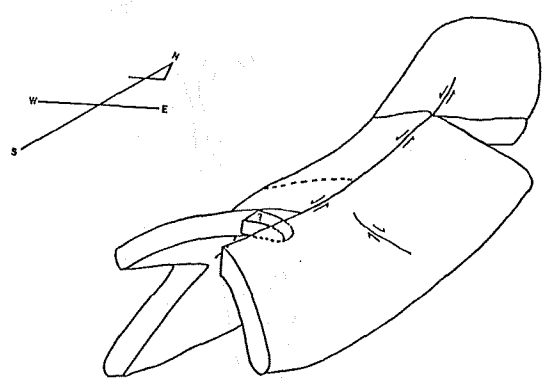

Fig. 5. Block diagram interpretation of the Izu Block collision zone. The view is from SE and shows the deformed Izu Block collision complex. Faults are indicated by arrows showing the sense of lateral motion.

logical events. Rotations about horizontal axes may provide a better explanation. Fig. 4 shows an example of such an interpretation of the paleomagnetic results. In this model, the northwestern Izu Peninsula has been tilted to the west or west-southwest, whereas the northeastern to southern Izu Peninsula has been tilted to the east to southeast. Jaishi volcano seems to be slightly different from the others probably because it may belong to much smaller geological domain and has been affected by small amount of relatively anomalous tectonic movement. The strike of tilting axes and approximate angle and rate of tilting deduced from respective volcanoes are listed in Table 3. Tilting rate is estimated to be 15 dgrees/m.y.

Suzuki et al.(1975) revealed that the Izu Peninsula is deformed as a whole nearly parallel to shore line and tilts toward the sea at a rate of 28 degrees/m.y. on the basis of the data of 1st levelling surveys carried out during 1903 to 1974.Focal depth distribution of earthquakes within the Izu Block(Ishida,1984) exhibits clearly the bending of the Izu Block with deduced anticlinal axis running nearly through the center of the Izu Block. From geological evidence, Kuno(1950, 51) suggested a southeastward tilting of the Taga volcano situated on the eastern row of the Izu Peninsula. These are in consistency with our present interpretation. Bending of geologic domains may be an indication of the post-collision deformation of the Izu Block. A possible interpretation of the shape of the Izu Block is shown in Fig. 5.

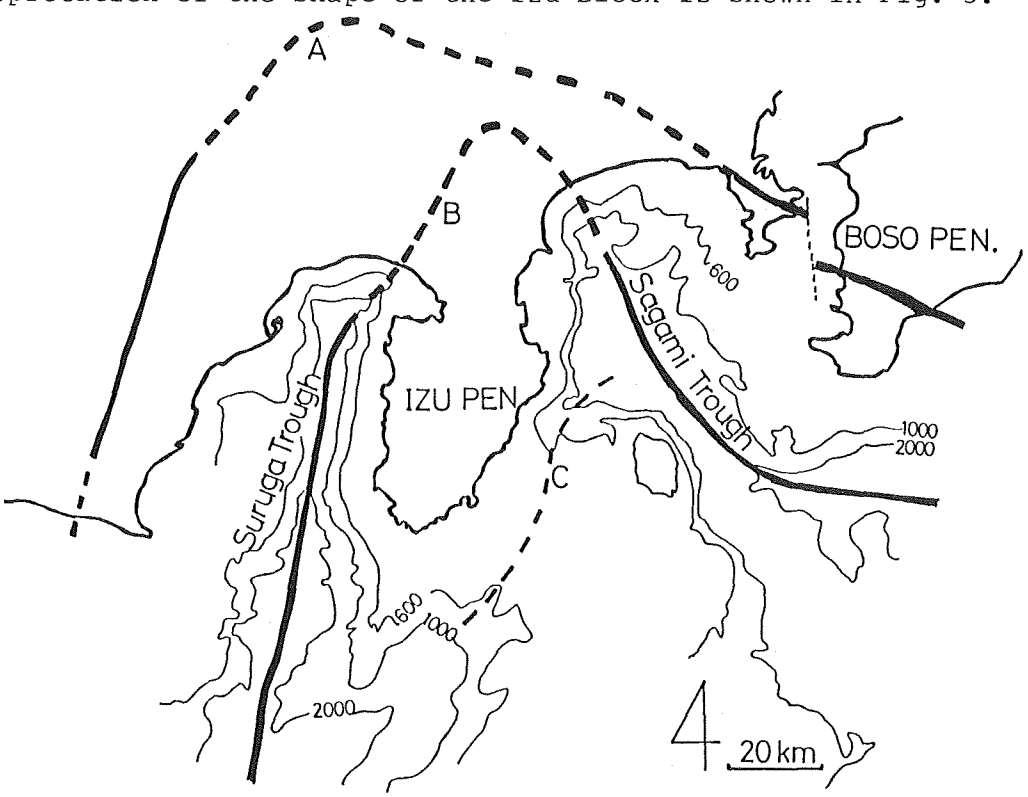

Fig. 6. Schematic illustration of collision in the past(line A), the present(line B) and the future (line C).

Tnouchi and Kobayashi (1983) revealed the existence of the paleosubduction (30Ma-11MaBP) along the Hayama-Mineoka and Setogawa belts from paleomagnetic evidence. As Fig. 6 shows, position of the paleosubduction was quite different from the present trenches, i.e. Sagami and Suruga Trough, indicating that the subduction zone jumped. Ishibashi(1977) suggested a possible embroy of subduction in the south of the Izu Peninsula from seismic study. If so, such a new subduction develops in future and post-collision processes of the Izu Block finish. Consequently, Izu Peninsula will be accreted to the central Honshu.

References

Akimoto, T. and T. Terauchi (1981) Graduation Thesis, Chiba Univ.
Hirooka et al. (1983) Rock Mag. Paleogeophys., 10, 53
Ishibashi, K. (1977) Rep. Coord. Comm. Earthq. Predict., 17, 65
Ishida, M. (1984) J. Phys. Earth, 32, in press
Kaneoka et al. (1982) J. Geolog. Soc. Japan, 88, 919
Kaneoka et al. (1983) Rock Mag. Paleogeophys., 10, 50
Kono, M. (1968) J. Geomag. Geoelectr., 20, 353
Koyama, M. (1983) Rock Mag. Paleogeophys., 10, 61
Kuno, H. (1950) J. Fac. Sci., Univ. Tokyo, sec. II, 7, 257
Kuno, H. (1951) J. Fac. Sci., Univ. Tokyo, sec. II, 7, 351
MacDonald, W.D. (1980) J. Geophys. Res., 85, 3659
McElhinny, M.W. (1973) Palaeomagnetism and plate tectonics, P.357
Nagata et al. (1957) J. Geomag. Geoelectr., 9, 23
Suzuki et al. (1975) Bull. Geol. Surv. Japan, 26, 319
Tonouchi, S. (1981) Doctral Thesis, Fac. Sci. Univ. Tokyo
Tonouchi, S. and K. Kobayashi(1983) Accretion Tectonics in the Circum-Pacific Regions, edited by M. Hashimoto ans S. Uyeda, Terra Scientific Publishing Company, Tokyo, 261-288
Tsunakawa, H. and Y. Hamano (1982) Rock Mag. Paleogeophys., 9, 9

PALEOMAGNETIC MEASUREMENT OF SEVERAL TERTIARY DYKES IN CENTRAL JAPAN

Hideo SAKAI, Kimio HIROOKA and Akira TAKEUCHI

Department of Earth Sciences, Faculty of Science, Toyama University, Toyama 930

Introduction

Tectonic elements such as the distribution and slip-sense of faults and igneous dykes have been used to restore an ancient stress field.

Takeuchi(1980) adopted the so called "dyke method"(Nakamura,1977) and successfully reconstructed the Neogene history of regional stress fields of the southern part of Northeast Honshu Arc. He then concluded the drastic change in axial arrangement of the stress field of the inner zone of south NE Honshu has been occurred at the middle Late Miocene (7~8Ma). The history of the changes in stress field seems to responsible for the evolution of backarc basins on the NE Honshu arc(Takeuchi,1981; Tsunakawa and Takeuchi,1984). We collected the dyke rocks from the region where the paleostress field had been reconstructed and the NRMs were measured. Not all the obtained data are valid, however, they are to be applicable to the study of the history of the stress field especially to calibrate the paleostress orientations. The dyke rock samples are also used for paleointensity studies and for the measurements of magnetic anisotropy.

Sampling sites

Geologic setting of the studied areas were described by Takeuchi(1980). The area covers the southern part of NE Honshu extending from latitude 36.5°N to 38.5°N. Fig.1 shows the sampling localities of dyke rocks. Sampling is carried out at 2 to 5 sites in each locality. Totally 31 sites studied here are distributed in Niigata and Fukushima Prefectures. Tsunakawa and others(1983) studied the K-Ar age of some of these dykes. The determined ages show that the dyke rocks in this area formed in 2.7~23Ma besides basalts of Tenno, about 110 Ma. The rock type of dyke and host rock are shown in Table 1 and the labels correspond to the numerals in Fig.1.

Table 1. Sampling localities.

Label	Locality	Dyke Rock	Host Rock	Site NO.(ND)
1	Tenno	basalt	Pre-Tertiary granite	28,29,30
2	Takanuki	andesite	Pre-Tertiary gneiss	26,27
3	Ryozen	andesite	granite,volcanics	22,23,24,25
4	Southern Aizu	rhyolite	Tertiary volcanics	17,18,19
5	Tadami	basalt	Miocene volcanics	14,15,16
6	Yahiko	ditto	Miocene shale	2,3,9,10
7	Ogi-Sado	ditto	ditto	4,5,6,7,8
8	Kakudasan	andesite	Pliocene volcanics	11,12,13
9	Yoneyama	ditto	ditto	0,1
10	Koriyama	ditto	Miocene sand-stone	20,21

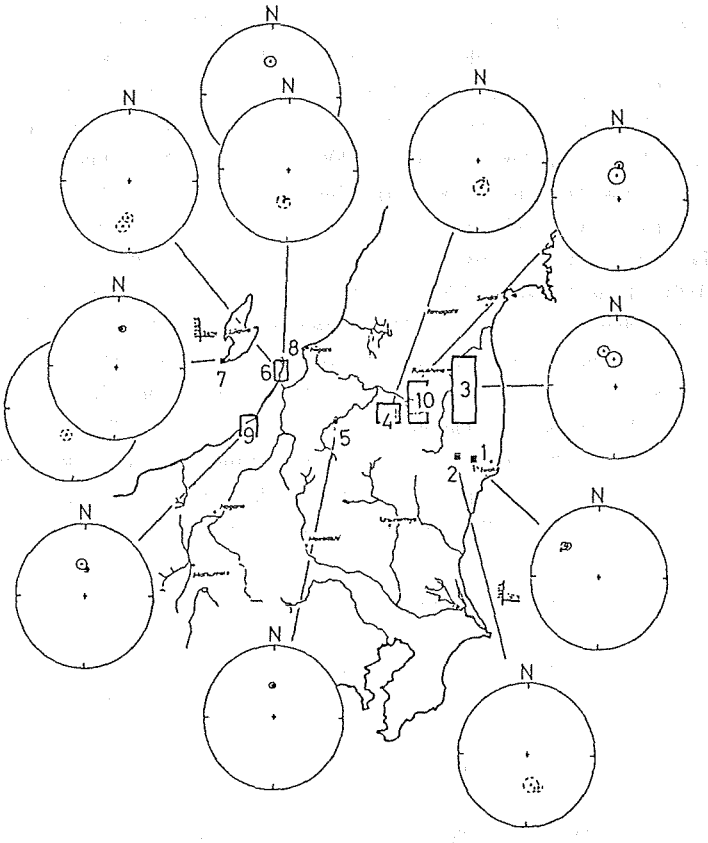

Fig. 1. Map showing the sampling localities: The results of NRM measurements are also shown with the Lambert equal area projection.

Measurement of NRM

Seven to ten hand samples are collected from each site and the plural core type specimens are cut from the sample. As a magnetic cleaning method, Alternating Field (A.F.) demagnetization is mainly adopted. When an area of the alpha 95% reliability ($\alpha 95$) at the most converged A.F. level is more than 10 degree, we do not use the data from such an unstable sample. Stepwise thermal demagnetization is also subjected to several specimens of the each remnant site. No significant difference between the data after A.F. and thermal demgnetizations is detected. Finally, we obtain paleomagnetic data from 20 sites. These data are shown in Table 2 and the mean direction with the circle of $\alpha 95$ for each site are plotted in Fig.1. We represented the paleomagnetic data in Fig.2 where the variation of the declination with age is compared between the data from three regions, e.g., Fukushima Prefecture, Niigata Prefecture and Sado Island. Different marks are used in the figure for the data of each regions. In the case when the NRM shows reversed polarity, declination is replaced by the direction antipodal to NRM.

Dykes in Niigata Prefecture and Sado Island between 2.7 Ma and 13.6 Ma have the somewhat eastern declination. On the other hand, the dykes in Fukushima Prefecture of nearby 22 Ma and 10 Ma in age show the westward direction. Those of about 12 Ma have also a little easterly deflected remanences. Heki and Tsunakawa(1981) reported the fairly westward deflected NRM from the Shimokura dyke swarms of 8Ma in age. Shimokura in Miyagi Pref. is not so far from the Fukushima sampling location. We plot the data of Shimokura in Fig.2 with the mark, large triangle. The declination of dykes in Fukushima Prefecture, a part of southeastern NE Japan, as a whole shows the westward deflection between 23Ma and 8 Ma. As the cause of this feature two cases are considerable. One is the geomagnetic secular variation caused by the change of the nondipole and/or the dipole field and the other is the tectonic movement. In the later case, the westward declination of the basalts in Tenno up to 50° shoud be taken into consideration. Then the declination of southeastern part of NE Japan seems to have changed in the two stages since 110Ma. By the tectonic movement, the first declination change occured between 110Ma and 23 Ma and after 8Ma the declination changed westerly again.

Table 2 Paleomagnetic results of NRMs

	Site no.	D	I	α95	N	A.c. (Oe)	Age (Ma)	Polarity
ND	0	3.6	60.1	3.5	8	150	2.7±0.1	N
	1	-6.3	53.3	6.2	8	100	2.8±0.1	N
	2	188.4	-36.4	6.9	8	200	7.2~14.6	R
	3	182.0	-47.6	6.0	7	200		R
	4	3.9	44.3	3.0	8	200	12.2±0.3	N
	6	195.2	-59.8	6.5	6	100		R
	8	6.7	44.6	4.4	6	150		N
	11	188.1	-53.1	7.6	6	100		R
	12	-2.3	50.3	6.3	7	200	13.6±0.4	N
	13	185.7	-57.3	3.0	6	100	12.2±0.3	R
	16	-2.5	53.4	3.9	8	150	*12	N
	17	171.7	-59.4	8.6	7	250	10.1±0.3	R
	18	164.2	-66.4	4.4	7	200		R
	20	0.3	50.8	5.0	7	200	12.3±0.5	N
	21	-6.3	62.9	10.0	7	150	13.7±0.4	N
	22	-20.3	46.7	6.7	7	200	21.3~22.1	N
	23	-4.4	58.1	9.1	7	250		N
	26	158.6	-50.4	4.6	6	500	22.5±0.6	R
	27	171.6	-55.2	8.5	8	300	23.0±0.6	R
	28	-49.0	33.8	4.5	7	300	111±3	N
	29	-55.2	33.6	2.2	7	200		N
	30	-46.4	37.6	4.4	8	300		N

*;Shimada and Ueda(1979).

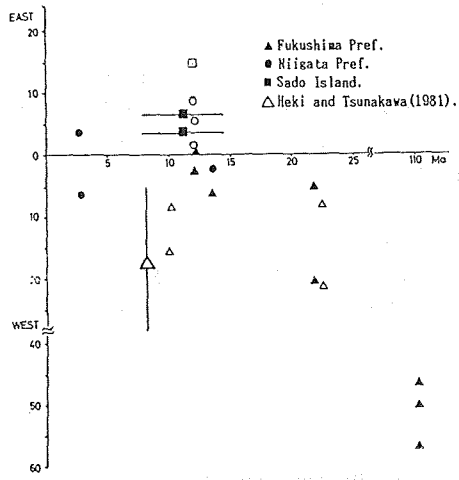

Fig. 2.
Declination data as a function of the K-Ar age. Closed marks show the data with normal polarity and open marks show with reversed polarity. The marks of triangle, circle and quadangle show the data from the dykes in Fukushima Prefecture, those in Niigata Prefecture and those in Sado Island, respectively.

Paleointensity measurements

Thelliers' method was also applied to the dyke samples. One core specimen from each site was submitted. The confidence of data is checked mainly by the linearity between partial n.r.m. and partial t.r.m.. We obtained 8 paleointensity data as shown in Fig.2. In this figure, the relative value of paleointesity compared with the present value is denoted as F/Fo. The site number and the geomagnetic polarity are shown in the left side.

The paleointensities obtained are about six-tenth to eight-tenth of the present one, i.e., the geomagnetic intensity of Neogene age is fairly small. Furhter, there seems no distinct difference between the paleointensity of normal epoch and that of reversed epoch. This feature is concordant with the result of Kono(1968) and Sakai(1980).

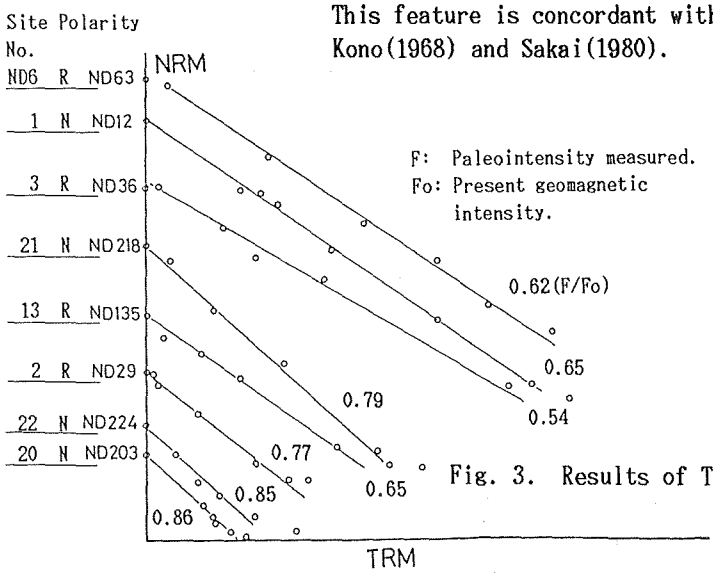

Fig. 3. Results of Thelliers' method.

Anisotropy measurement

Directional arrangement of mineralogical axes causes the lamination structure of sedimentrary rocks and metamorphorsed fabric in rocks. These directional alignments of minerals give the information about the stress condition at the rock formation stage and/or the flow direction of magmas. In this study, dyke rocks were used as the preliminary examples to estimate the directional alignments of minerals from the measurement of magnetic anisotropy. Anisotropy of magnetic susceptibility, AMS(Ellwood, 1978), was measured by the spinner magnetometer.

AMS measurements were carried out for the dyke specimens of 20 sites whose NRMs cluster well within 10° of α95. Samples of dispersed NRMs were also measured to see feature between the AMS and the dispersion of NRMs, however, we have no conclusive idea yet.

To see the mineralogical fabric in the dyke, K-ratio defined as follows were calculated for all specimens.

K=(difference of the AMS magnitudes between the Maximum and Intermediate axes) /(difference of the AMS magnitudes between the Maximum and Minimum axes)

K-ratio shoud be nearly 1 for the needle type mineral alignments assembly and about 0 for the stripe type alignments assembly. K-ratios for the dyke rocks of well clustered NRMs are almost all less than 0.5, that is, the stripe type alighnments are superior.

Significant features of AMS were obtained from 10 sites. Fig.4 shows the typical AMS results obtained from the dykes## of Toyama Prefecture. The large circle in the figure stands for the plane of intrusion of the dyke.

The dykes are Miocene in age and the NRMs deflect quite easterly.

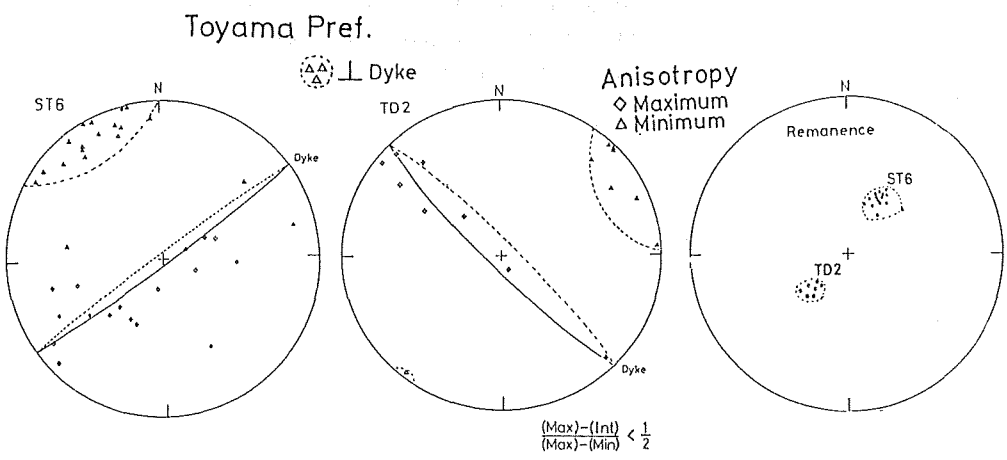

Fig. 4. Results of AMS measurements from the dykes in Toyama Prefecture. NRM directions of the each dykes are shown in the right side by the Lambert equal area projection.

The minimum axes of AMS show a tendency to be normal to the plane of intrusion. It suggests that the alignment of the long-axis of the particle parallel to the dyke wall. The same feature is recognized from the 6 dykes of Fukushima Prefecture and 4 examples are shown as group (A) in Fig.5. On the contrary, the results obtained from 3 sites in Niigata Prefecture show that significant cluster of AMS minimum axes lie in the intrusive plane of dykes. We denote them as group (B) in Fig. 6. We examined the factor that distinguishes the two groups, such as the size(aspect ratio) of dykes, the dynamic relationship at intrusion between the dyke and host rocks, and so on. One explanation adoptable is that the dyke of group (A) is long one, i.e., the horizontal length is more extensive than its thickness. Duff(1975) has suggested that plastic deformation during later stages of magma flow may cause the long-axis alignment normal to streamline in the fluid. According to his suggestion, the long axes of minerals in the thicker dyke tend to be normal to the wall plane of intrusion. The ratio of the length to the thickness in the dyke may cause the difference in the induced stresses and flow direction, and the two types of orientation of minerals, group (A) and (B), appear.

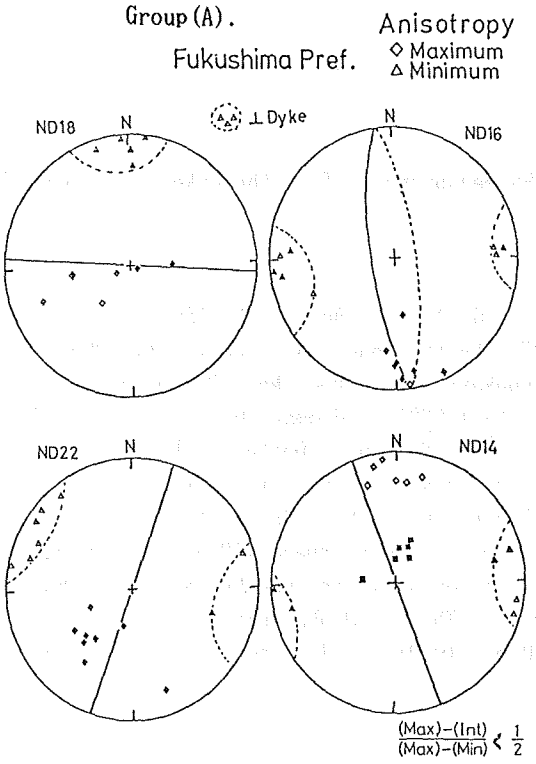

Fig. 5. Results of AMS measurements from the dykes in Fukushima Prefecture.

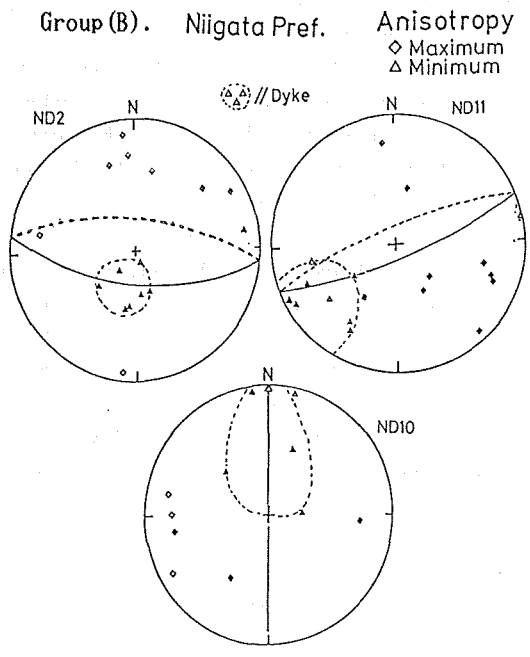

Fig. 6. Results of AMS measurements from the dykes in Niigata Prefecture.

References

Duff, B. A. (1975) J. Geol. Soc. Aust., 22, 159.

Ellwood, B. B. (1978) Earth Planet, Sci. Lett., 41, 254.

Heki, K. and H. Tsunakawa (1981) Rock Mag. Paleogeophys., 8, 17.

Kono, M. and T. Nagata (1968) J. Geomag. Geoelectr., 20, 211.

Nakamura, K. (1977) Jour. Volcanol. Geotherm. Res., 2, 1

Takeuchi, A. (1980) J. Geosci, Osaka City Univ. 23, 1.

Takeuchi, A. (1981) Jour. Geol. Soc. Japan. 87, 737.

Tsunakawa, H., A. Takeuchi and K. Amano (1983) Geochemical Journal, 17, 269.

Tsunakawa, H. and A. Takeuchi (1984) Kagaku (Science), 53, 624.

Sakai, H. (1980) D. Sc. Thesis, Osaka Univ.

Shimada, I and Y. Ueda (1979) J. Jap. Assoc. Miner. Petrol., 74, 387.

PALEOMAGNTIC EVIDENCE FOR THE MIOCENE COUNTER-CLOCKWISE ROTATION OF NORTHEAST JAPAN

Yo-ichiro OTOFUJI* , Takaaki MATSUDA**
AND
Susumu NOHDA***

* Department of Earth Sciences, Faculty of Science, Kobe University, Kobe 657, Japan
** Department of Geology, Himeji Institute of Technology, Himeji 671-22, Japan
*** Kyoto Sangyo University, Kamigamo, Kita-ku, Kyoto 603, Japan

1. Introduction

In recent years Southwest Japan has been the focus of several paleomagnetic investigations (Otofuji and Matsuda, 1983; 1984; Torii, 1983; Hayashida and Ito, 1984): The studies for late Tertiary rocks indicated that the rotation of Southwest Japan relative to the Eurasia started later than 15 Ma. This result gives rise to the hypothesis on the Miocene origin of Japan arc rifting.

The present investigation is focused on the Northeast Japan arc: The study is undertaken to discover the paleomagetic evidence for the Miocene counter-clockwise rotation of the Northeast Japan arc in an attempt to determine the timing of rifting of the Japan arc.

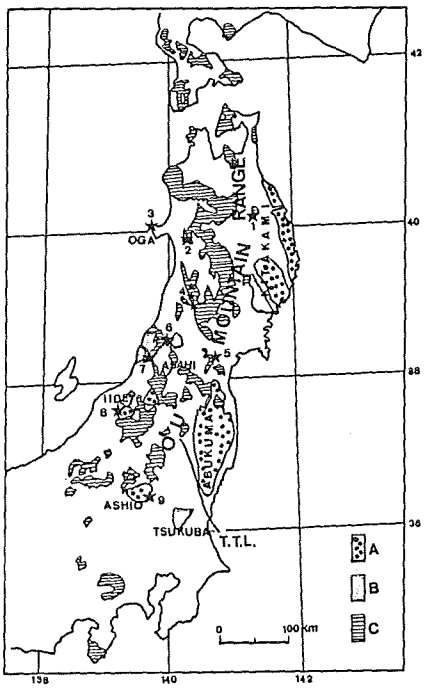

Fig. 1 Locations of paleomagnetic sampling areas (shown by stars) in Northeast Japan together with distribution of Cretaceous granitic rocks (A), Paleogene granitic rocks (B) and Miocene volcanic rocks (C): 1=Ninohe, 2=Taiheizan 3=Oga Peninsula, 4=Yuzawa, 5=Zao, 6=Northern Asahi, 7=Western Asahi, 8=Iide and 9=Ashio. T.T.L.=Tanakura Tectonic Line.

2. Sampling

Our paleomagnetic approach is to analyze the Paleogene to Miocene welded tuffs within igneous materials. Samples were also collected from plutonic rocks of late Cretaceous and early Paleogene when few welded tuffs had been produced. More than 700 samples were collected from nine areas (Fig. 1). Sampling was mainly carried out from the rock unit whose ages had been dated by either K-Ar dating or Fission track dating (Kawano and Ueda, 1966; Nishimura and Ishida, 1972; Suzuki, 1980; Konda and Ueda, 1980; Matsuda et al., 1985).

Samples were taken by hand sampling; a magnetic compass was used for orientation. Each site typically comprised ten independently oriented samples distributed over distance ranging up to 20 m.

3. Paleomagnetism

Individual specimens, 25 mm in diameter and 25 mm long, were prepared from samples in the laboratory. Natural remanent magnetization (NRM) was measured with Schonstedt SSM-1A spinner magnetometer. All samples were magnetically cleaned only by thermal demagnetization, because the thermal demagetization is more suitable technique than that of the alternating field demagetization to erase the secondary magnetic component in welded tuff and granodiorite (Otofuji and Matsuda, 1983; 1984).

3.1 Identification of primary component

Three pilot specimens from each site were progressively demagnetized in steps of 100°C or 150°C to the Curie temperature with increment steps reduced to 30°C or 50°C near the Curie temperature. More than seventy percent of the welded tuffs were found to be magnetically stable: The change in NRM directions of pilot specimens was less than 10 degrees. One specimen from all independently oriented samples for stable site was demagnetized at the optimum demagnetization temperature which produced minimum dispersion for NRM directions from three pilot specimens. All specimens for the unstable sites, granitic rocks and the rest of welded tuffs, were progressively demagnetized. The stable end points during demagnetization runs were identified to be their characteristic directions.

The characteristic direction after thermal demagnetization for each site was accepted as a reliable one provided the following criteria were satisfied: An acceptable site has at least five specimens cut from independently oriented samples and a mean direction from the site has a circle of 95 % confidence less than 15°.

The tilting test was useful to identify the primary component from the reliable characteristic direction. The NRMs of Nyudozaki igneous rocks (51 Ma) and Kuguriiwa rhyolite lava (32, 27 Ma) from Oga Peninsula were judged to be secondary remanence acquired after the peninsula was faulted and folded, because their directions before tilt correction are tightly grouped and are parallel to the present axial dipole field although the NRM of Kuguriiwa lavas showed reversed polarity. No further paleomagnetic investigation was conducted for these sites.

3.2 Paleomagneic directions

Thirty six sites were found to have reliable primary magnetic component through thermal demagnetization and tilting test. Directions of

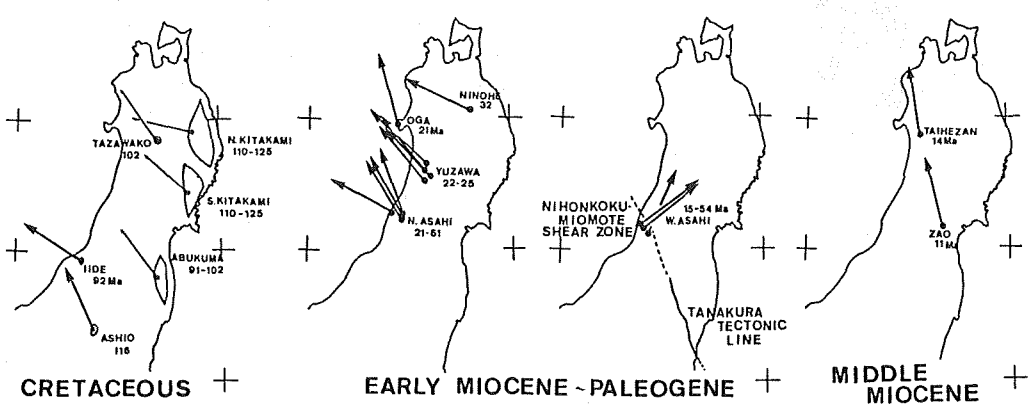

Fig. 2 The declinations of the paleomagnetic directions found for the Cretaceous, the Paleogene to early Miocene and Middle Miocene stages of Northeast Japan. The Paleogene to early Miocene data of Northeast Japan is divided into those of the Western Asahi and other areas. The Cretaceous data from North and South Kitakami,and Tazawako are after Ito and Tokieda (1974), Ito et al. (1980). Data from Abukuma are after Kawai et al. (1971).

TABLE 1 Average paleomagnetic directions of Late Tertiary

Formation Name	N	polarity	$\bar{D}$ (°)	$\bar{I}$ (°)	α_{95}	k	V G P	∂p	∂m	Age (Ma)
[11Ma-14Ma]										
Yamadera	2	R	-14.5	69.7	--	--				11.3(K-A)$^{\delta}$
Okuramata	2	N	-10.1	51.1	--	--				14.1(K-A)$^{\varepsilon}$
Mean (sites)	4		-11.7	60.5	15.3	37.2	70.2N 80.7E	17.7	23.3	
(Formations)	2		-11.7	60.4	--	--	69.5N 80.8E	--	--	
[20Ma-32Ma]										
Higashiohtorigawa	1	R	-27.4	50.5	--	--				21 (F-T)$^{\varepsilon}$
Daijima	2	N	-30.0	47.6	--	--				22$^{\gamma}$,20$^{\beta}$(F-T)
Hatamura	4	R	-43.4	64.5	24.2	15.4				22< <25(K-A)$^{\delta}$
Okatsugawa	6	R	-40.5	54.1	11.6	34.4				25 (K-A)$^{\delta}$
Yunosawagawa	3	N	-43.5	63.1	21.4	34.2				25≦(K-A)$^{\delta}$
Nisatai	1	N	-66.9	39.4	--	--				32 (F-T)$^{\alpha}$
Mean (sites)	17		-41.2	56.5	7.2	25.7	60.8N 57.8E	7.5	10.4	
(Formations)	6		-42.5	54.0	11.0	37.8	57.0N 56.0E	10.8	15.4	

Table 1. Directions are presented as the value at the representative point of Northeast Japan (141°E, 39°N). All data are after tilt correction. N is number of sites, $\bar{D}$,$\bar{I}$ are mean declination and inclination, α_{95} and k are Fisher statistic parameters, and ∂p and ∂m are semiaxes of the oval 95 % confidence around the pole. The mean directions for each stage, 11 Ma-14 Ma and 20 Ma-32 Ma, are calculated by assigning unit weight to formations and sites, respectively. The ages are data from $^{\alpha}$Samata (1976), $^{\beta}$Nishimura and Ishida (1972), $^{\gamma}$Suzuki (1980), $^{\delta}$Konda and Ueda (1980) and $^{\varepsilon}$Matsuda et al. (1985).

the declinations for three periods ,the Cretaceous, the Paleogene to early Miocene, and Middle Miocene, are drawn in Fig. 2. Site mean directions for two stages, 11Ma-14Ma and 21Ma-32Ma, are listed in Table 1.

Cretaceous to Paleogene granitic rocks (110 Ma - 59 Ma)

Declinations of the Cretaceous granite from southernmost part of Northeast Japan (Iide and Ashio areas) show the westward deflection which is consistent with the declination value previously reported from Northeast Japan of the Cretaceous period (Kawai et al., 1971; Ito and Tokieda, 1974; Ito et al., 1980).

The westward deflection is observed for Paleogene granitic rocks from Uetsu area. We measured the same granodiorites (Suganodai) whose NRM had been reported to have easterly declinaton, i.e. D=45° (Kawai et al., 1971). Although the NRM directions of the rocks were dispersed and roughly directed eastward before thermal demagnetization, the NRM after thermal demagnetization above 400°C changed its polarity and grouped at about D=120° , I=-50°. The other rocks from Uetsu area also showed the westerly direction with normal polarity. The westward deflection is probably a more realistic estimate of the declination value for these granitic rocks with age of 60 Ma.

Paleogene to early Miocene welded tuffs (54 Ma - 19 Ma)

Almost all welded tuffs except for those from southern area (Western Asahi) show the westward deflection in declination value. The reliability of the westerly declination is ascertained through the presence of normal and reversed polarities. The declination value of the Paleogene to early Miocene period is also characterized by the westerly declination for a large part of Northeast Japan.

In contrast with the westward deflection, the eastward deflection has been discovered from Paleogene welded tuffs of Western Asahi. The reliability of the easterly direction is ascertained through the presence of normal and reversed polarities. The easterly direction of this area is definitely distinguished from the westerly direction observed in the other areas of Northeast Japan at 95 percent confidence level (D=35.9°,I=59.8°,

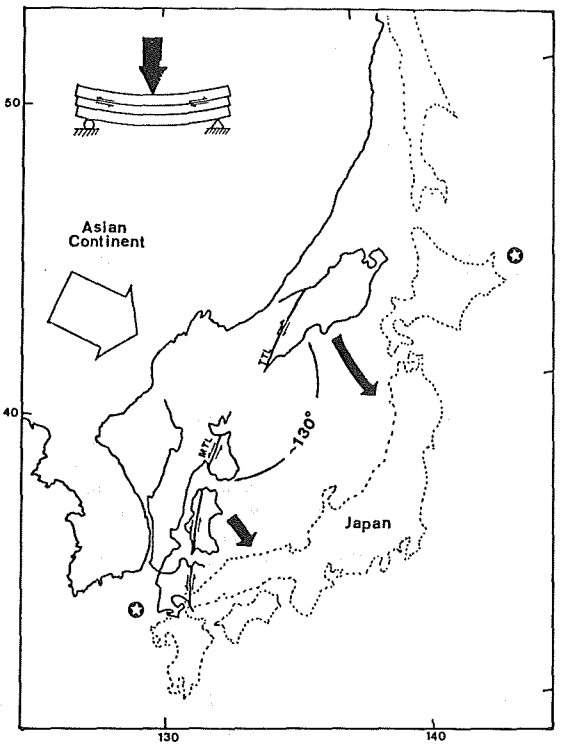

Fig. 3 Rotation model of Northeast and Southwest Japan: Position of the primary blocks of Northeast and Southwest Japan arcs before 21 Ma. The rotation pivots (146°E, 44°N) for Northeast Japan and (129°E, 34°N) for Southwest Japan are shown by stars. The axis of Northeast Japan arc makes an angle of about 130° with that of Southwest Japan arc before both blocks are rifted from Asian continental margin. The inset shows a piled up beam model. A few terraines making up the Japanese island behave as a pile of elastic beams when the primary blocks of Japanese island are subjected to the force which rifts them from the continental margin. A right lateral movement is expected along the Tanakura Tectonic Line (TTL) and a left lateral one along the Median Tectonic Line (MTL).

α_{95}=10.4° vs. D=-41.2°, I=56.5°, α_{95}=7.2°). Since the easterly declination has been found in rocks with age ranging from 54 Ma to about 15 Ma, the easterly declination is not probably attributed to the short time phenomena of geomagnetic field such as the field transition or excursion.

Middle Miocene (11 Ma and 14 Ma)

Miocene welded tuffs were collected from Taiheizan and Zao areas. The mean NRM directions from both areas direct to the present axial dipole field within 95 % confidence limits after tilt correction (see Table 1).

4. Discussion

4.1 Counter-clockwise rotation of Northeast Japan

The Cretaceous paleomagnetic data of this work combined with the previous ones (Kawai et al., 1971; Ito and Tokieda, 1974;Ito et al., 1980) indicate that Northeast Japan of the Cretaceous period is characterized by the westerly deflection in declination (Fig. 2). The westerly directions have been also observed through remeasurements of Paleogene granitic rocks, and discovered from Paleogene to early Miocene welded tuffs. Because well-grouped westerly direction has been obtained after tilt correction for Tertiary welded tuffs, the westerly deflection in declination possibly indicates true tectonic rotation about a vertical axis (MacDonald, 1980). These results imply that the counter-clockwise rotation of Northeast Japan occurred during late Tertiary. Based on the Cretaceous data (Fig. 2), the rotated block is concluded to extend southward to Ashio area.

Easterly declination value in the Paleogene obtained from southern part of Northeast Japan (Western Asahi) is discordant with the data from the rest of Northeast Japan (Fig. 2). The area is expected to have undergone the different block movement from the other areas later than 15 Ma. The easterly declination data could be explained by the clockwise rotation of local block due to dextral strike slip fault (MacDnald, 1980). Sampling sites are situated along the Nihonkoku-Miomote shear zone which is the northwestward extension of the Tanakura tectonic line (Chihara, 1984). Based on the geological observation (Otsuki and Ehiro, 1978; Chihara, 1984), right-lateral displacement is expected to have occurred along the

Nihonkoku-Miomote shear zone and the Tanakura tectonic line during the Miocene. The Paleogene igneous rocks of this area probably record only the local block movement, and tectonic rotation of Northeast Japan may be concealed by this movement.

4.2 Timing and amount of the rotation of Northeast Japan

We can estimate the timing of the counter clockwise rotation from the paleomagnetic data combined with geochronological data of Northeast Japan except for Western Asahi. The K-Ar age determination assigns 14 Ma and 11 Ma for the welded tuffs of Okuramata and Yamadera formations (Konda and Ueda, 1980; Matsuda et al., 1985) whose NRMs direct northward, respectively. Their remanent magnetizations are reasonably accepted to be a primary component, because these data are after tilt correction and thermal demagnetization. The youngest rocks with westerly declination value, Hokakejima dacite and Higashi-Ohtorigawa formation, showed their fission track age of 21 Ma (Nishimura and Ishida, 1972; Suzuki, 1980; Matsuda et al., 1985). Timing of the rotation is presumed to be from 21 Ma to between 14 Ma and 11 Ma.

The rotation angle is evaluated through statistical calculation of the data of rocks between 32 Ma and 21 Ma except for those from Western Asahi (Table 1). The mean direction is D= -41.2°, I= 56.5° and α_{95}= 7.2°. Taking into account of the effect of apparent polar wander since 20 Ma, the rotation angle and its uncertainty is R=46.8° and ΔR=14.1°(the R and ΔR values are after Margill et al. (1981)): we used the paleofield direction and confidence oval at the reference point of Northeast Japan calculated from the 20 Ma paleopole (85°N, 198°E, A95=4°) of Northern Eurasia (Irving, 1977).

Difference between the observed inclination value and the calculated value from the apparent polar wonder path is -4.1°± 9.1°from 30 Ma to 20 Ma, which indicates no significant latitudinal translation for Northeast Japan. Comparing the inclination value at the period 35-20Ma of Northeast Japan with that of Southwest Japan (I=56.5°, α_{95}=7.2° vs. I=48.6°, α_{95}=6.5°)(Otofuji and Matsuda, 1984), the Northeast Japan, as it is at present, appears to have been situated at higher latitude than Southwest Japan. Northeast Japan is concluded to have been subjected to the counter clockwise rotation through 47°± 14°since 21 Ma without suffering significant north-south translation.

The timing of the rotation of Northeast Japan is compared with that of Southwest Japan. The best curve fitting analysis for rotation versus age for all the reliable data from Southwest Japan determines that the climax of the rotation was at 14.9 Ma (Otofuji et al., 1985). Although the paleomagnetic data from Northeast Japan are much smaller in number than those from Southwest Japan to estimate the timing of rotation, the timing of rotation of Northeast Japan (21 Ma to between 15 Ma and 11 Ma) is comparable to that of Southwest Japan. Both Northeast Japan and Southwest Japan probably underwent rotation with respect to Asian continent at almost the same period in middle Miocene.

4.3 Rotation model of both Northeast Japan and Southwest Japan

The following model is proposed to explain the amount of rotation for both Northeast Japan and Southwest Japan (see Fig. 3): (1) The rotation of both arcs were phenomena associated with the rifting process of Japan arc due to back arc opening of the Japan Sea. (2) The differential rotation about different rotation pivots occurred between Northeast Japan and Southwest Japan. (3) Northeast Japan rotated about a northern pivot (146°E, 44°N) through 47°, while Southwest Japan rotated about a southern pivot (129°E, 34°N) through 56°. (4) The timing of rotation of both arcs are between 21 Ma and 12 Ma; The climax of the rotations is at about 15 Ma.

References

Chihara, K. (1984) Personal Communication.
Hayashida, A. and Y. Ito (1984) Earth Planet. Sci. Lett., 68, 335
Irving, E. (1977) Nature, 270, 309
Ito, H. and K. Tokieda (1974) Rock Mag. paleogeophys., 2, 54
Ito, H., K. Tokieda and Y. Notsu (1980) Rock Mag. Paleogeophys., 7, 113
Kawai, N., T. Nakajima and K. Hirooka (1971) J. Geomag. Geoelectr., 23, 267
Kawano, Y. and Y. Ueda (1966) Jour. Japan Assoc. Min. Petr. Econ. Geol., 56, 416
Konda, T. and Y. Ueda (1980) Jour. Japan Assoc. Min. Petr. Econ. Geol. Spec. Issue, 2, 343
MacDonald, W.D. (1980) J. Geophys. Res., 85, 3659
Margill, J., A. Cox and R. Duncan (1981) J. Geophys. Res., 86, 2953
Matsuda, T., S. Nohda and K. Nagao (1985) (in preparation)
Nishimura, S. and S. Ishida (1972) Jour. Japan Assoc. Min. Petr. Econ. Geol., 67, 166
Otofuji, Y. and T. Matsuda (1983) Earth Planet. Sci. Lett., 62, 349
Otofuji, Y. and T. Matsuda (1984) Earth Planet. Sci. Lett., 70, 373
Otofuji, Y., A. Hayashida and M. Torii (1985) Formation of Active Ocean Margins, Nasu et al. eds. (TERAPUB, Tokyo) (in press)
Otsuki, K. and M. Ehiro (1978) J. Phys. Earth., 26 (suppl.), S537.
Suzuki, T. (1980) Jour. Geol. Soc. Japan, 86, 441
Samata, T. (1976) Jour. Geol. Soc. Japan, 82, 783
Torii, M. (1983) Doctoral Thesis, Faculty of Sci. Kyoto Univ.

(Submitted to Earth Planet. Sci. Lett.)

PALEOMAGNETIC STUDY ON TECTONIC SETTING OF HOKURIKU DISTRICT IN MIOCENE: YATSUO AREA

Yasuto ITOH and Masayuki TORII

Departmentof Geology and Mineralogy, Kyoto University
Kyoto 606, Japan

Recent paleomagnetic study revealed that Southwest Japan has undergone as much as 47° clockwise rotation at 15 Ma (Otofuji et al., 1984). Their studied areas are the San'in and Setouchi districts, which are extending in the central part of Southwest Japan. Both eastern and western boundaries of the rotated region have not been definitely determined as yet. In the east of Southwest Japan, general geologic attitude of pre-Neogene rocks is bordered by a major tectonic zone which is called Fossa Magna. It is possible to surmise Fossa Magna as the apparent eastern boundary of the rotated block. However, there are few paleomagnetic works designed to investigate relative movement of Fossa Magna region to Southwest Japan. In this report, we examine paleomagnetic data from Early to Late Miocene volcanic and sedimentary rocks at the Yatsuo area situated on the northwestern flank of the Fossa Magna region (Fig. 1).

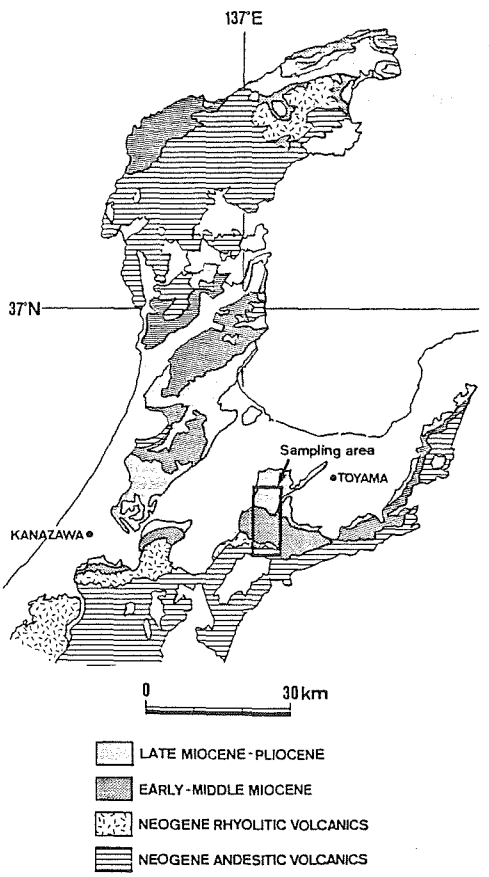

Fig. 1 Simplified geologic map of the Hokuriku district and sampling area.

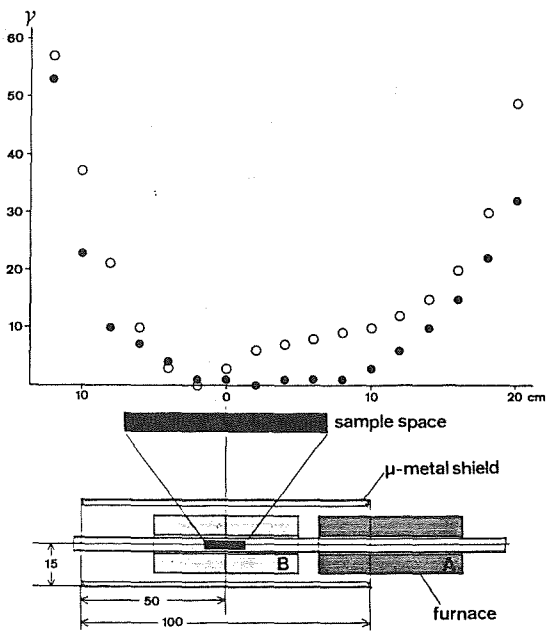

Fig. 2 Sectional plan of the furnace used for thermal demagnetization and residual magnetic field in the furnace. Solid circles: residual field (furnace is located at A for cooling cycle) open circles: residual field (furnace is located at B for heating cycle)

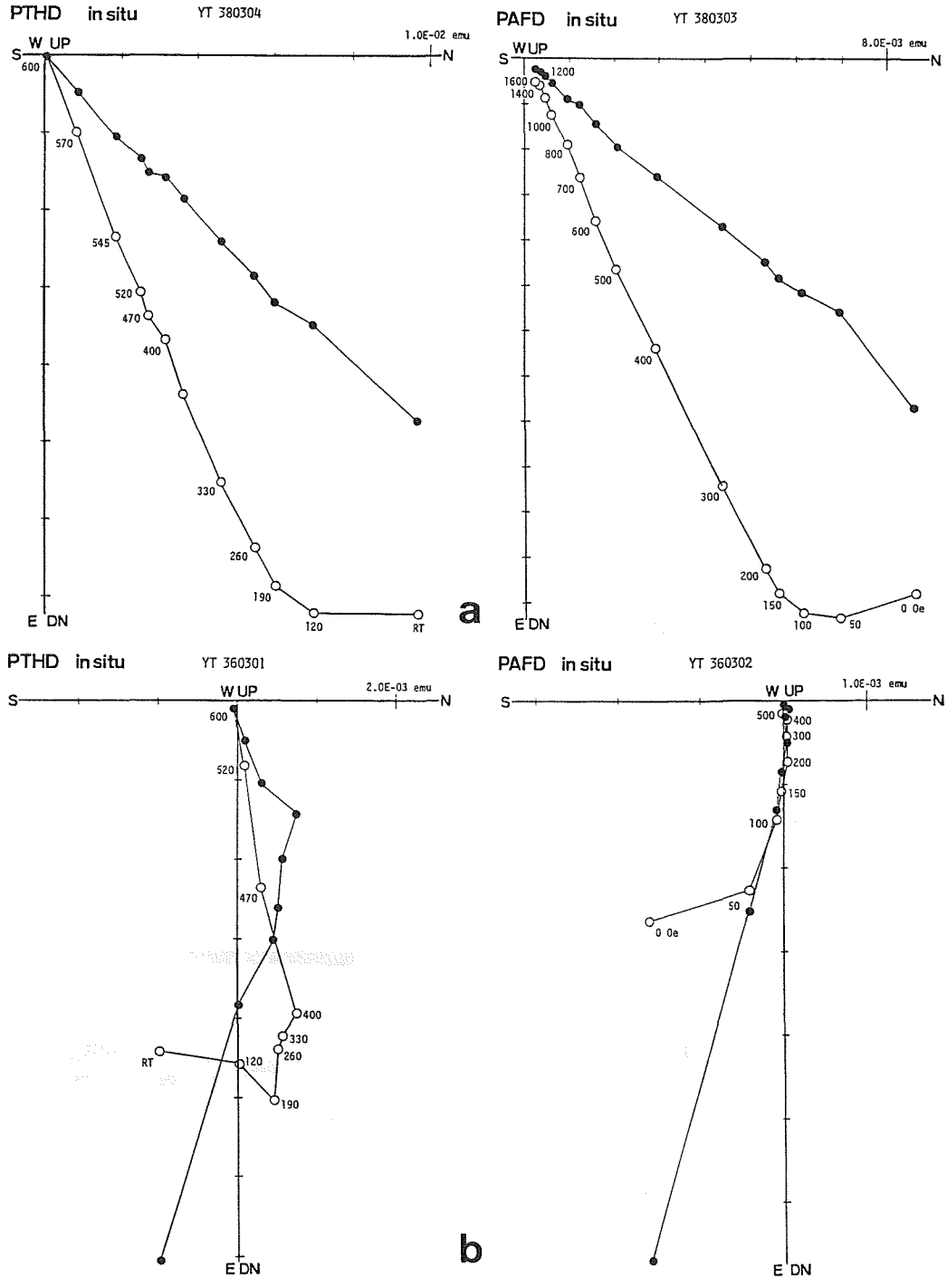

Fig. 3 Typical Zijderveld diagrams of progressive thermal and AF demagnetization of samples from site 38 (a) and site 36 (b). Solid and open circles are projections of vector end points on horizontal and N-S vertical planes, respectively. Numbers adjacent to symbols are peak temperature in °C and field in Oe. In (a), magnetization is regarded as primary component except for the soft secondary component removed upon 190°C or 200 Oe. In (b), secondary component cannot be removed perfectly by AF demagnetization.

In the Yatsuo area, a typical sequence of the Hokuriku Group (Sakamoto, 1966) extends from the east to west about 10 km wide, and is gently folding about north-south axis. Neogene strata of the area comprises thick mafic to felsic volcanic piles (so-called Green Tuff) and fossiliferous marine sedimentary rocks. Total thickness of the strata is almost 3000 m in this area.

Samples of sedimentary and volcanic rocks were collected at 38 sites from 37 horizons covering Lower to Upper Miocene strata. Samples were taken by hand sampling and each site comprises four to ten separately oriented samples. Specimens of 25 mm in diameter and 20 mm in length were prepared from each sample. A Schonstedt SSM-1A spinner magnetometer and a ScT C-112 cryogenic magnetometer were used to measure remanent magnetizations.

Two specimens were selected from each site, and their magnetic stability was tested by means of progressive demagnetizations of thermal and alternating field methods. AF demagnetization was carried out progressively up to 1600 Oe with a magnetically shielded two-axis tumbler. Progressive thermal demagnetization was carried out in more than twelve steps up to 700°C. Specimens were heated in air using a noninductively wounded furnace enclosed in three-layered cylindrical mu-metal shield. Stray field during cooling cycle was reduced less than 10 gamma (Fig. 2).

Zijderveld diagrams were used for the determination of primary components. Stable remanent magnetization after the thermal demagnetization is recognized as a straight trend on the Zijderveld diagram (Fig. 3). We excluded the following sites from the routine demagnetization procedure. Progressive change of the vector end-points did not show straight trend or showed increase of intensity at high temperature range. In such sites, unstable or spurious magnetizations are not negligible. We also excluded the sites of which magnetic directions coincide with the present geomagnetic field direction before tilt correction of the strata. In such sites, stable secondary component acquired parallel to the present field may not be removed effectively. The remaining sites were assumed to have stable primary magnetization. Seven sites among 38 survived these criteria.

Primary components found by thermal demagnetization are also recognized by means of progressive AF demagnetization (Fig. 3-a) in five sites among the seven. For the five sites, partial AF demagnetization was adopted for cleaning of the rest specimens. For other two sites, however, AF demagnetization is not effective to separate the primary component (Fig. 3-b). Partial thermal demagnetization, therefore, was adopted for the

Table 1 Paleomagnetic site mean directions from the Hokuriku Group. Dec,Inc: mean declination and inclination in degrees; N: number of specimens; α_{95}: radius of 95% confidence circle in degrees; k: precision parameter; Lat,Lon: latitude and longitude of virtual geomagnetic pole position (north-seeking pole).

Site	DEMAG LEVEL	Dec	Inc	N	α_{95}	K	Polarity	VGP Lat	VGP Lon
04	400 °C	-164.9	-73.1	10	5.9	68.9	R	65.8	156.3
05	200 Oe	-172.5	-51.7	12	3.2	190.1	R	82.5	-100.5
16	100 Oe	6.9	58.0	10	2.0	572.0	N	84.2	-155.7
18	100 Oe	0.0	52.7	7	5.2	135.3	N	86.7	-42.9
31	200 Oe	-10.4	59.4	11	7.4	39.2	N	81.1	74.2
36	330 °C	18.4	43.1	5	7.2	113.6	N	70.5	-102.0
38	200 Oe	18.3	48.7	8	2.0	790.8	N	73.2	-114.0

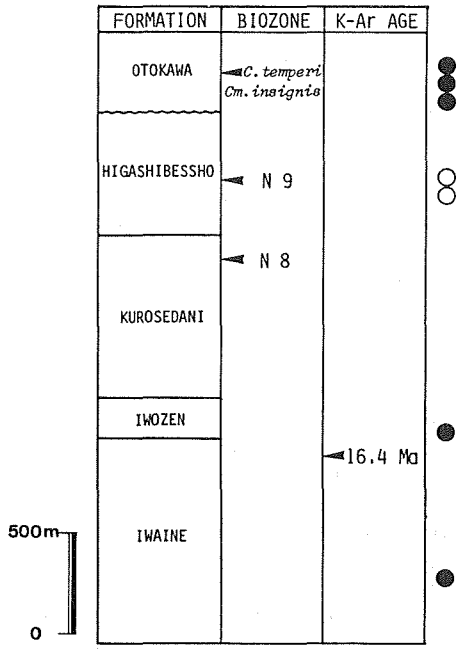

Fig. 4 Summary of lithostratigraphy and biostratigraphy (Hayakawa, 1983; Tanimura, 1979), K-Ar age (Shibata, 1973), and results of paleomagnetic polarity stratigraphy. Solid and open circles represent normal and reversed polarity, respectively.

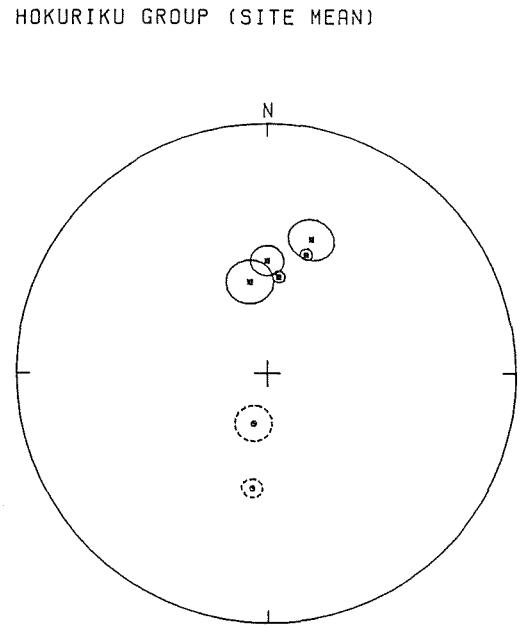

Fig. 5 Site mean directions of remanent magnetization, after tilt correction.

cleaning of the rest specimens. The routine demagnetization was made for five to twelve specimens in a site. Comparing the result of partial demagnetization at three to five steps, an optimum demagnetization level was decided as to give the minimum α_{95} value for each site (Table 1). Mean magnetic direction of each site shows small α_{95} less than 10°.

In Fig. 4, horizons of the paleomagnetic data are plotted on a columnar section of the sampled area, together with radiometric data and biostratigraphical zonations. As shown in the figure, geologic ages of the sites range from 17 to 5 Ma. All sites have declinations less than 20° (Fig. 5). Considering effect of secular variation, we conclude that no significant rotational movement of the area occurred throughout Early to Late Miocene. In San'in and Setouchi district, the change of declination from about 50° east to 0° at about 15 Ma has been observed. This apparent discrepancy may be due to different movement of the sampled area relative to the central part of Southwest Japan in Miocene time.

References:

Hayakawa,H. (1983) NOM (News of Osaka Micropaleontologists), **10**, 1.

Otofuji,Y., A.Hayashida and M.Torii (1984) Formation of Active Ocean Margins (TERRAPUB, Tokyo) in press.

Sakamoto,T. (1966) Rept. Geol. Surv. Japan, **213**, 1.

Shibata,K. (1973) Geol. Soc. Japan, Mem., **8**, 143.

Tanimura,Y. (1979) Fundamental data on Japanese Neogene bio- and chronostratigraphy (IGCP-114 National working group of Japan, Shizuoka) P.83.

ANOMALOUS MAGNETIC DIRECTION OF A MIOCENE ANDESITE DYKE FROM THE WESTERN COASTAL AREA OF THE KII PENINSULA

Masayuki TORII and Naoto ISHIKAWA

Department of Geology and Mineralogy, Kyoto University, Kyoto 606, Japan

Paleomagnetic study of Cenozoic rocks from Southwest Japan introduced that regional clockwise rotation of about 50° has occurred at 15 Ma associated with formation of the Japan Sea (Otofuji et al., 1984). This tectonic interpretation was substantiated by the paleomagnetic studies on well-dated rocks: paleomagnetic directions from the rock units older than 15 Ma showed clockwise rotation from the 'expected' field direction (Otofuji and Matsuda, 1983 and 1984; Hayashida and Ito, 1984). Contrary to this, most of the younger rock units have magnetic directions parallel with the present geomagnetic field (Torii, 1984). The fact that the deflected paleomagnetic directions are common for rocks prior to 15 Ma enable us to make a paleomagnetic test to assume age of rocks having no age-diagnostic data based upon their paleomagnetic directions in Southwest Japan. In this short report, we will discuss age of a single andesite dyke rock which intruded into the lower Miocene sediments.

The andesite dyke is located at Haneta, Tanabe Town in the western coastal area of the Kii Peninsula (Fig. 1). The dyke rock crops out on a cut wall of a small hill of which half was removed last year. It intruded into a conglomerate bed, the A1 member of the Asso Formation which is the lower most member of the Tanabe Group (Miyake et al., 1984). The country rock shows no significant tilt judging from gentle dipping of thin seems of mud stone. The dyke strikes in the direction N75°E, dipping vertical. The dyke rock can be classified into a high-magnesian andesite based on its low FeO^*/MgO ratio (less than 1.0; Miyake et al., 1984) after the definition by Tatsumi and Ishizaka (1982). Age of the Tanabe Group was estimated to be Lower Miocene from evidence of age-diagnostic planktonic foraminiferal fossils, which were correlated to N8 zone of Blow (Tanabe Research Group, 1981).

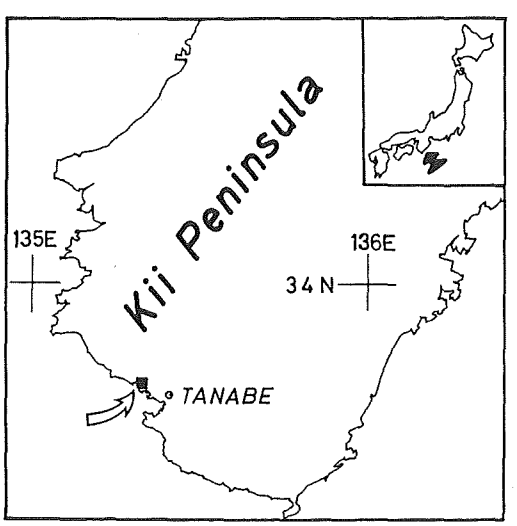

Fig. 1 Location of sampling site at Haneta, Tanabe Town.

For paleomagnetic work, 17 hand samples were collected. Two sub-samples of cylindrical shape were made from each sample for two parallel experiments: thermal (TH) and alternating field (AF) demagnetizations. Several thin-sliced samples (about 2 mm thick) were also prepared for TH demagnetization. Each sub-sample was stepwisely demagnetized, and analyzed

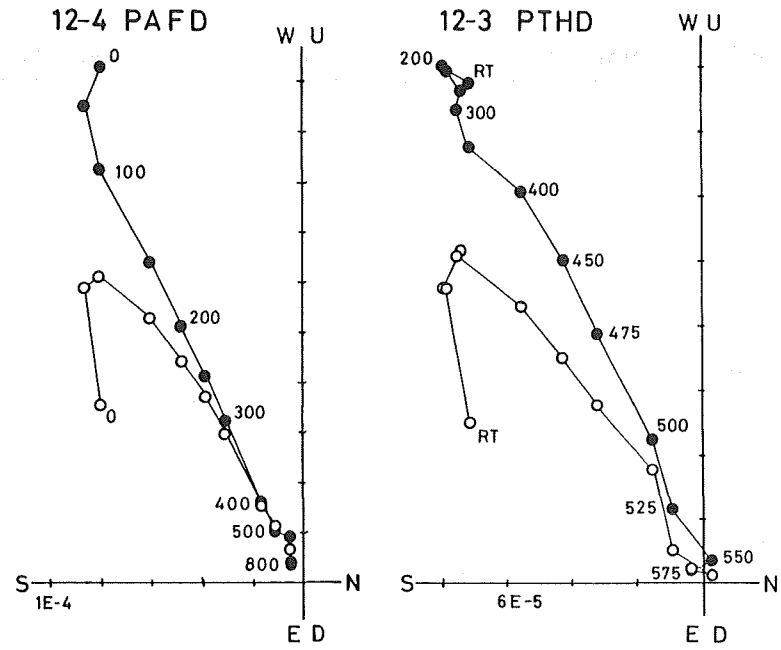

Fig. 2 Typical examples of progressive AF and TH demagnetizations are shown by vector orthogonal projection. Solid (open) circles are projection on horizontal (N-S vertical) plane. Numerals denote demagnetization level in Oe or °C. Unit of coordinate is bulk intensity in cgs unit.

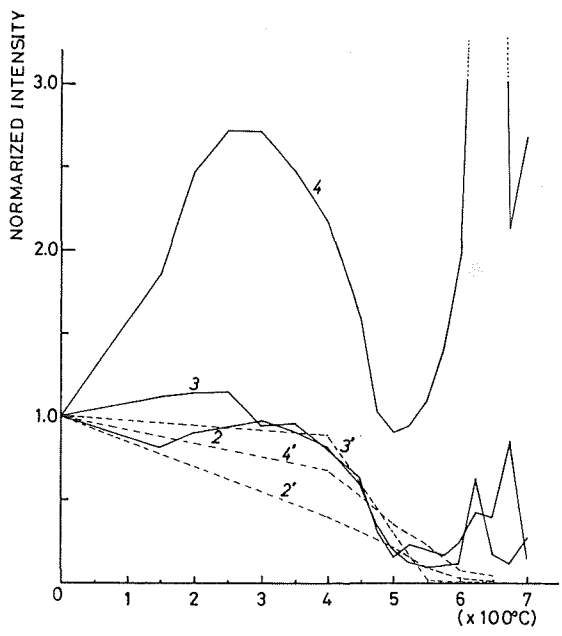

Fig. 3 Intensity of magnetization after TH demagnetization. Solid lines indicate progressive change of standard cylindrical samples (No. 2, 3, 4). Dashed lines are those of thin-sliced samples (No. 2', 3', 4'). For example, samples of No. 2 and No. 2' were prepared from same block sample. Irregular increase of intensity at high temperature range is not observed for thin-sliced samples.

by means of vector orthogonal projection. Typical examples of the progressive demagnetization experiments are shown in Fig. 2. An unstable component was successfully erased by AF demagnetization up to 300 Oe. While TH demagnetization also removed the soft component by heating up to 400°C, it sometimes resulted irregular increase of magnetization at a higher temperature range. Such a increase of magnetic intensity at higher temperature range was not observed for thin-sliced samples which could be easily oxidized during thermal treatment (Fig. 3). The increase of intensity can be therefore attributed to formation of a new magnetic mineral within the sample itself, where chemical condition may be less oxidizing.

Mean magnetic direction of the 17 samples obtained after AF demagnetization in the peak field of 300 Oe is D=238.2°and I=-44.4° (Fig. 4). Precision parameter and radius of the 95% confidence circle are 35 and 6.1°, respectively. Absolute value of the mean inclination is comparable with that of the present geomagnetic field at the sampling site. On the other hand, the mean declination is fairly anomalous, showing almost 60° clockwise deflection from the south.

Possible interpretations for the anomalous magnetic direction of the dyke rock are as follows; (1) an instantaneous record of geomagnetic field swing such as a pat of secular variation or polarity reversal: (2) tectonic rotation of the surrounding land block after intrusion of the dyke rock. The first cause, however, does not seem to be persuasive. More than 60° deflection is too much to attribute to the geomagnetic secular variation (Doell and Cox, 1972). Although there may be a little chance to record a transient field direction during polarity transition, it does not sound reasonable to attribute the anomalous record to a mere chance.

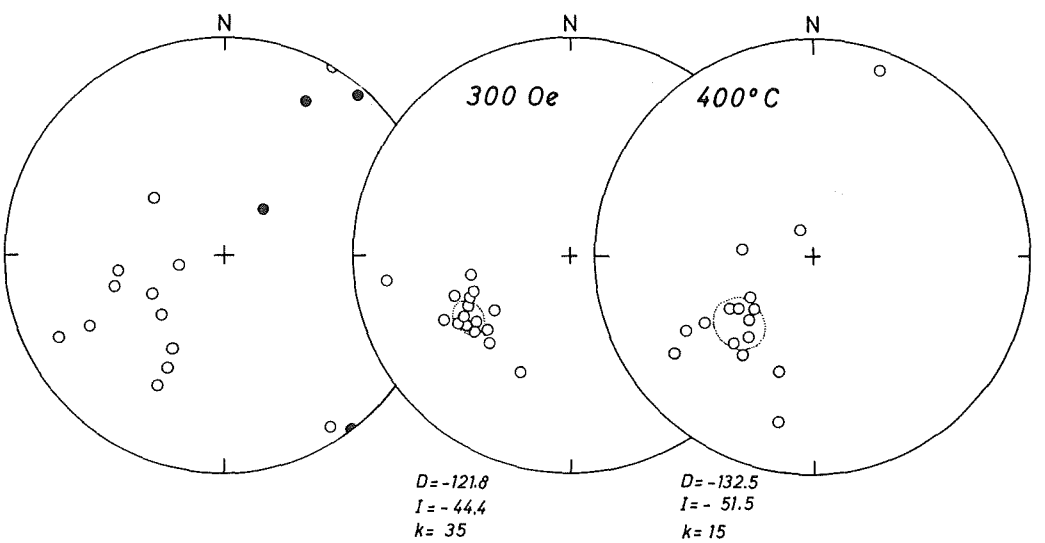

Fig. 4 Remanent directions before demagnetization, after partial AF demagnetization of 300 Oe (peak field) and partial TH demagnetization of 400°C. Dotted ovals indicate 95% confidence circles. Cleaned directions after AF and TH demagnetizations show no significant difference, but well clustered by AF method.

On the other hand, tectonic rotation is a likely interpretation. As mentioned before, the most extent of Southwest Japan has undergone clockwise rotation as much as 50° at 15 Ma (Otofuji et al., 1984). For instance, paleomagnetic directions from the nearby Kumano acidic rocks, a huge volcano-plutonic complex dated at about 15 Ma, are pointing almost 60° east of the present declination (Tagami, 1981). The Kumano acidic rocks were intruded into the Kumano Group along the eastern coast of the Kii Peninsula. The Kumano Group is marine sedimentary sequences correlated to the Tanabe Group based on biostratigraphic evidences (Tsuchi et al., 1979). After the intrusion of the Kumano acidic rocks, the Kii Peninsula has undergone clockwise rotation as a part of Southwest Japan. The clockwise shift of declination of the dyke from the western coast of the Kii Peninsula is possibly attributed to the regional rotation of Southwest Japan. This interpretation leads us to estimate the upper limit of intrusion age of the dyke as to be 15 Ma. We can conclude that the dyke intrusion occurred after the deposition of the country rock (N8: about 17 Ma) and preceded the time of tectonic rotation of Southwest Japan (about 15 Ma).

References:

Doell, R.R. and A.Cox (1972) in 'The Nature of the Solid Earth' (McGraw-Hill, New York) p.245.

Hayashida, A. and Y.Ito (1984) Earth Planet. Sci. Lett., 68, 335.

Miyake,Y., N.Ishikawa, S.Ishida and M.Torii (1984) submitted to J. Geol. Soc. Japan.

Otofuji, Y. and T.Matsuda (1983) Earth Planet. Sic. Lett., 62, 349.

Otofuji, Y. and T.Matsuda (1984) Earth Planet. Sic. Lett., 70, 373.

Otofuji, Y., A.Hayashida and M.Torii (1984) in 'Formation of Active Ocean Margins' (TERRAPUB, Tokyo) in press

Tagami, T. (1982) NOM, 9, 23.

Tanabe Research Group (1981) 'Chikyu Kagaku' (Earth Sci.), 38, 249.

Tatsumi,Y. and K.Ishizaka (1982) Earth Planet. Sci. Lett., 60, 293.

Torii, M. (1984) in preparation

Tsuchi,R., et al. (eds) (1981) Neogene of Japan -- Its biostratigraphy and chronology -- (Kurofune Printing, Shizuoka) p.91.

WHEN WAS THE JAPAN SEA OPENED? : PALEOMAGNETIC EVIDENCE FROM SOUTHWEST JAPAN
(Abstract)

Yo-ichiro OTOFUJI[1], Akira HAYASHIDA[2] and Masayuki TORII[3]

[1]Department of Earth Sciences, Kobe University, Kobe 657
[2]Department of Earth Sciences, Doshisha University, Kyoto 602
[3]Department of Geology and Mineralogy, Kyoto University, Kyoto 606

Formation of the Japan Sea is viewed from paleomagnetic direction data reported from the southwestern part of Japan. Reliable paleomagnetic data-set is compiled to investigate exact timing of clockwise rotation of Southwest Japan. The following guidelines are adopted for selection of the data: (1) Samples were from the area about 800 km long between Amakusa and Toyama, where the clockwise declination shift in the Cretaceous and Paleogene rocks was already known. (2) Stability of remanent magnetization was examined by alternating field and thermal demagnetization treatments. (3) Paleomagnetic direction was obtained after tilting correction of strata. (4) Age of the rocks was determined through radiometric dating, correlation with a paleomagnetic polarity time scale, or biostratigraphic data of marine microfossils. Plot of the declinations, corrected for the apparent polar wonder effect, in respect to the age shows that southwest Japan was abruptly rotated through about 50° at about 15 Ma (Fig. 1). The best fit curve is obtained to describe the rotational motion; climax of the rotation is at 14.9 Ma and its duration is 0.6 m.y. Since the rotational motion of Southwest Japan is attributed to the back-arc spreading between Japanese Islands and the Asian Continent, it is concluded that the Japan Sea was opened at about 15 Ma.

In press in "Formation of Active Ocean Margins"
Eds. N. Nasu et al., TERRAPUB, Tokyo, Japan

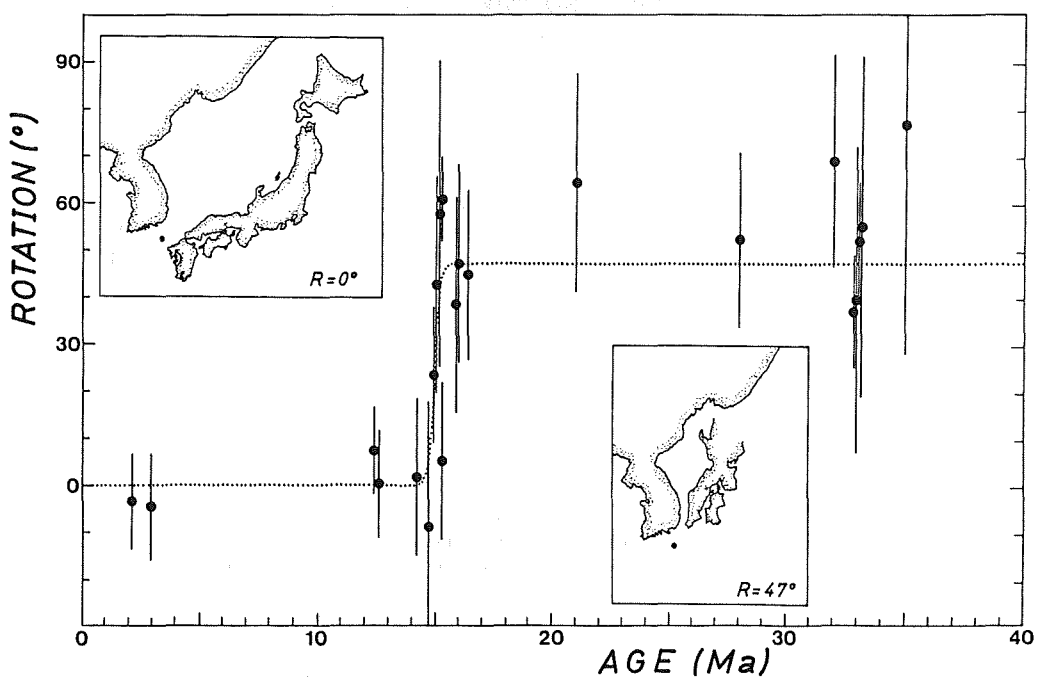

Fig. 1 Plot of rotation angles (R) as a function of age (t). Error bars shows uncertainty in rotation at 95% confidence level. The dotted line shows the best fit curve:

$$R(t) = Ro \left(1 - \frac{1}{\exp((t - to)/T) + 1} \right)$$

Rotation angle, R(t), reaches Ro/2 at time to, when the angular velocity of rotation is maximized. Four fold of T represents duration of rotational motion. These parameters are estimated as follows: Ro = 47.1 (°), to = 14.9 (Ma) and 4T = 0.6 (m.y.).

PALEOPOSITION OF SOUTHWEST JAPAN AND PLATE CONVERGENCE BETWEEN EURASIA AND PACIFIC PLATES IN PRE-NEOGENE TIME
(Abstract)

Akira HAYASHIDA[1], Yo-ichiro OTOFUJI[2] and Masayuki TORII[3]

[1]Department of Earth Sciences, Doshisha University, Kyoto 602
[2]Department of Earth Sciences, Kobe University, Kobe 657
[3]Department of Geology and Mineralogy, Kyoto University, Kyoto 606

Recent paleomagnetic studies on Neogene rocks established that Southwest Japan was subjected to a rapid clockwise rotation through 47° at 14.9 Ma. Pre-Neogene rocks in the Mino-Tamba and Shimanto belt are memorizing deflected paleomagnetic directions acquired prior to the rotation; Cretaceous igneous rocks of the Inner Zone have clockwise deflected magnetic directions, and the similar directions are also observed in the secondary magnetic component of allochthonous rocks found in the Mino-Tamba subduction complex. These data suggest that Southwest Japan had been situated on the eastern flank of the Asian Continent since the Cretaceous until the clockwise rotation occurred at about 15 Ma. The paleoreconstruction of Southwest Japan shows that convergence plate boundary between Eurasia and an oceanic plate was extending along the azimth N30°E in the coordinate fixed to Eurasia. This result, combined with the recent estimation on past relative motions between the Pacific and Eurasia plates, lead the following conclusion on the condition of plate convergence which formed the Shimanto belt (Fig. 1): (1) Oblique subduction with significant left-lateral components was dominant between 66 Ma to 48 Ma. (2) Lateral component of convergence changed its direction from sinistral one to dextral at about 43 Ma.

Submitted to Geological Society of London Special Publication
"The Cretaceous-Recent Evolution of the SW Japan Active Margin"
(Editers; J. K. Leggett and A. Taira)

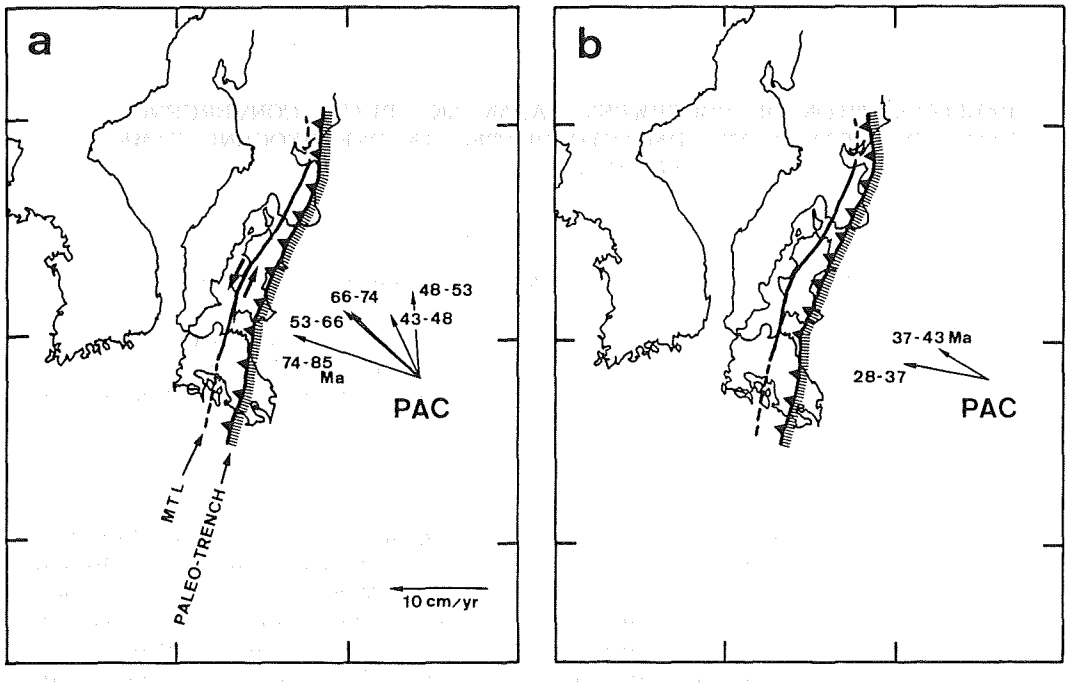

Fig. 1 Plate convergence around Southwest Japan in pre-Neogene time: (a) until 42 Ma, (b) 42 Ma to 30 Ma. Arrows indicate convergence vectors of the Pacific (PAC) or Philippine Sea (PHI) plate relative to the Eurasia. MTL: Median Tectonic Line. Paleoposition of Southwest Japan was estimated using paleomagnetic data and assumption that the rotation was caused by opening of the Japan Sea. Reconstruction after 30 Ma was abandoned, because configulation of the plate boundary in this period is uncertain.

PALEOMAGNETIC STUDY OF CRETACEOUS GRANITIC ROCKS FROM THE INNER ZONE OF EHIME PREFECTURE, SHIKOKU

Yoshihisa NISHIYAMA*, Akira TOKUYAMA**
and
Haruaki ITO***

* Saijo Senior High School, Saijo-shi, Ehime 793
** Hyogo University of Teacher Education, Yashiro-cho, Kato-gun, Hyogo 673-14
*** Shimane University, Nishikawatsu-cho, Matsue 690

1. Introduction

The Median Tectonic Line (MTL) is the great fault that divides Southwest Japan into the Inner and Outer Zones. It is generally defined as the fault being located between the Ryoke and Sanbagawa belts.

In central Shikoku, it is difficult to observe the MTL directly because the border between the Ryoke and Sanbagawa belts is mostly covered by thick marine sediments of the Izumi group. However, the geological structure of the Ryoke and Sanbagawa belts is thought to be fairly affected by tectonic movements of the MTL. Some traces caused by tectonic movements of the MTL may be somewhat recorded in various rocks of the Ryoke or Sanbagawa belt. To understand paleotectonics of the Ryoke belt is not so easy, because the belt consists mostly of granitic rocks

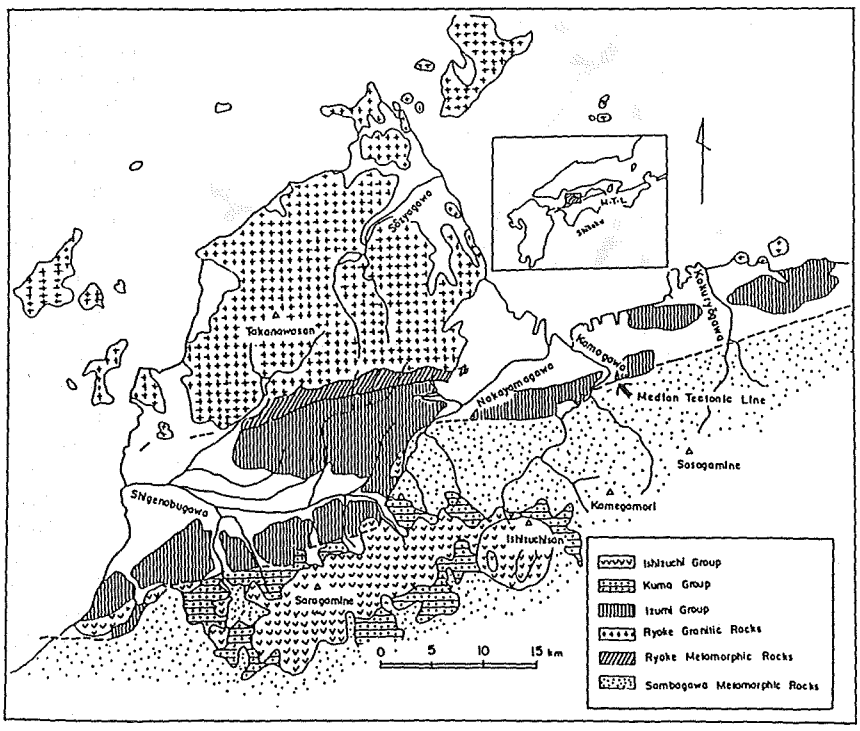

Fig. 1 Geological sketch map of northeastern part of Ehime Prefecture (after Nagai et al., 1980).

having poor structural elements. We carried out paleomagnetic study on the Ryoke granitic rocks and dike rocks which intrude into the Ryoke belt in order to find out significant records of tectonic movements of the MTL.

2. Geological setting

The area studied is mostly the Takanawa peninsula and its vicinity, Ehime Prefecture. The Ryoke granitic rocks in this area are widely exposed to the north of the Izumi group as shown in Fig. 1. The MTL in this area is the fault lying between the Izumi group and Sanbagawa belt. The Ryoke granitic rocks are composed of diorite, granodiorite and granite and they are classified into nine rock types (Miyahara and Hiraoka, 1970). Many dikes of hypabyssal and basic rocks intrude into the Ryoke granitic rocks. K-Ar age of 87 Ma for a quartz diorite sample and Rb-Sr age of 93 Ma for a granite sample in this area are given by Kawano and Ueda (1966) and Hayase and Ishizaka (1967) respectively. It suggests that the Ryoke granitic rocks emplaced at the time of normal polarity representing the Cretaceous magnetic smooth zone (Larson and Pitman, 1972).

3. Sampling and measurements

A total of 440 hand samples were collected from 55 sites in granitic rocks of the Ryoke belt and 10 sites in dike rocks. One or two core samples were drilled from each hand sample in the laboratory. The NRM of all core samples was measured with a Schonstedt spinner magnetometer at Shimane University. Most of core samples at each site were progressively demagnetized in alternating field up to 600 oe and the remaining cores thermally demagnetized.

As a result, samples taken at 16 sites of the Ryoke granitic rocks and 6 sites of dike rocks were found to have stable components of magnetization. The sites having the stable NRM are shown in Fig. 2 and results of measurements are given in Table 1.

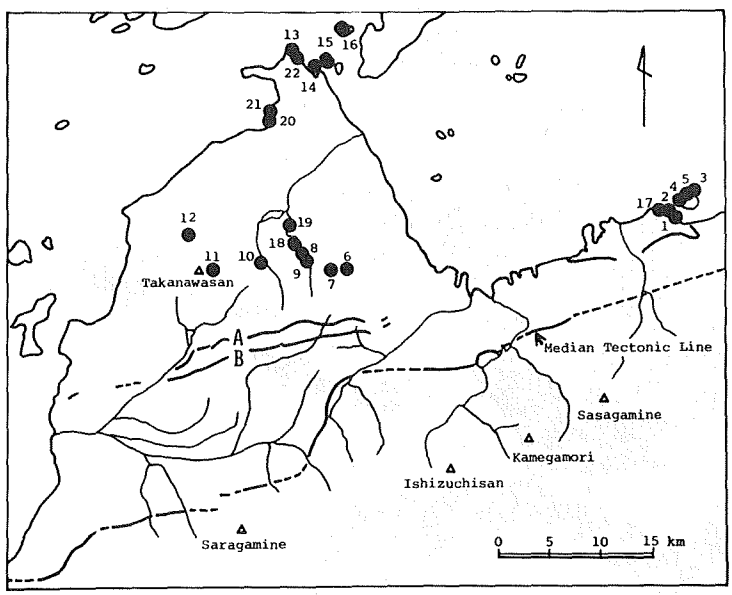

Fig. 2 Sampling sites of the Ryoke granitic rocks and dike rocks with stable NRM. Line A denotes the boundary between the Ryoke granitic and metamorphic rocks. Line B denotes the northern boundary of the Izumi group.

4. Discussion

All the samples from the

Table 1. Paleomagnetic data for the Ryoke granitic rocks and dike rocks

	Site	Rock Kind	N	D(°E)	I(°)	K	α_{95}	I_r (emu/gr)	VGP Lat.	VGP Long.	dp	dm
A	1	Diorite	8	359	19	64.9	6.9	1.66×10^{-6}	66N	44W	3.8	7.2
	2	"	7	356	24	57.8	8.0	2.51×10^{-6}	68N	36W	4.6	8.6
	3	"	9	3	11	11.9	15.6	3.67×10^{-7}	61N	54W	8.0	15.8
	4	"	6	24	15	57.1	8.9	8.04×10^{-7}	56N	93W	4.7	9.2
	5	"	6	10	20	11.7	20.4	3.23×10^{-7}	64N	71W	11.1	21.3
	6	"	8	10	40	70.0	6.7	3.97×10^{-6}	76N	88W	4.8	8.0
	7	"	10	6	37	81.3	5.4	1.33×10^{-6}	76N	72W	3.7	6.3
	8	"	11	349	23	12.6	13.4	4.99×10^{-7}	66N	20W	7.6	14.2
	9	"	10	1	22	7.4	19.0	4.03×10^{-7}	68N	51W	11.6	20.1
	10	Granodiorite	7	14	10	9.7	20.4	2.15×10^{-7}	58N	74W	10.4	20.6
	11	Diorite	7	29	26	59.2	7.9	2.59×10^{-6}	57N	107W	4.6	8.6
	12	"	8	27	19	6.8	22.9	3.75×10^{-6}	55N	99W	12.5	23.9
	13	"	11	27	53	43.0	7.0	5.50×10^{-5}	67N	143W	6,7	9.7
	14	"	10	358	70	84.6	5.3	3.30×10^{-5}	70N	130E	7.9	9.1
	15	"	7	352	65	52.2	8.4	8.24×10^{-5}	76N	110E	11.0	13.6
	16	"	3	22	50	3892.5	2.0	5.49×10^{-5}	72N	133W	1.8	2.6
B	17	Porphyrite	5	15	37	300.0	4.4	4.34×10^{-7}	71N	97W	3.1	5.2
	18	"	7	356	28	86.1	6.5	1.53×10^{-6}	71N	34W	3.9	7.2
	19	"	4	357	45	78.7	10.4	1.15×10^{-6}	82N	26W	8.3	13.1
	20	Basic dike rocks	6	238	-53	18.3	16.1	6.53×10^{-7}	42S	26E	15.4	22.2
	21	"	5	245	-51	48.8	11.1	2.66×10^{-6}	36S	26E	10.1	15.0
	22	"	5	18	52	88.3	8.2	2.78×10^{-6}	75N	136W	7.6	11.2

A : Granitic rocks
B : Hypabyssal and basic dike rocks
N : Number of samples measured
I_r : Intensity of NRM after A.F. demagnetization
K : Fisher's precission parameter
α_{95} : Semi-angle of cone of 95 percent confidence
dp,dm : Semi-axes of ovals of 95 percent confidence

Ryoke granitic rocks are normally magnetized as predicted by radiometric dating. Site-mean directions of the NRM of the granitic rocks are shown in Fig. 3. The directions of NRM obtained were obviously different with those from Cretaceous rocks in Southwest Japan. In paticular, it is noteworthy that NRM directions at sites near the MTL have low inclinations. The inclinations become gradually steep with distance from the northern boundary of the Izumi group as seen in Fig. 4. The difference in inclination between the southern and northern parts in the Takanawa peninsula is about 40°. The difference can be explained by bending movements of the Ryoke belt as

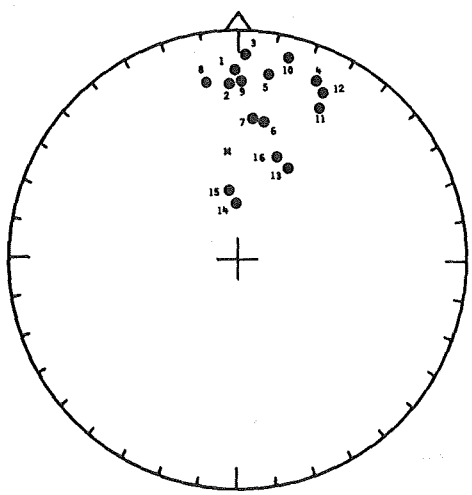

Fig. 3 Site-mean directions of NRM obtained from the granitic rocks.

shown in Fig. 5. The bending movements are considered to be due to downward thrusting of the MTL after the implacement of granitic rocks. However, it is still impossible to determine whether the bending is due to relative underthrusting of the Sanbagawa belt against the Ryoke belt or relative overthrusting of the Ryoke belt against the Sanbagawa belt from only the present paleomagnetic data. It is necessary for us that the more detailed work has progressed further.

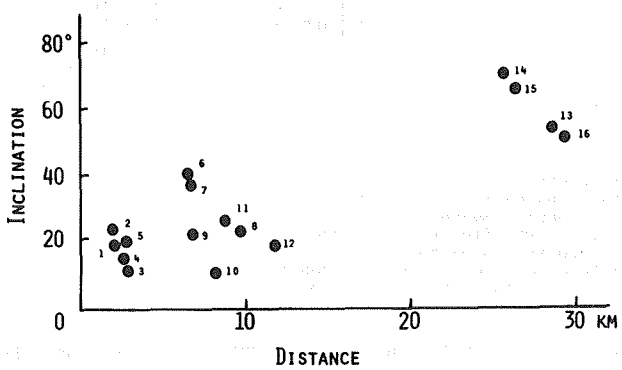

Fig. 4 Change in inclination of NRM of the granitic rocks with distance from the northern boundary of the Izumi group.

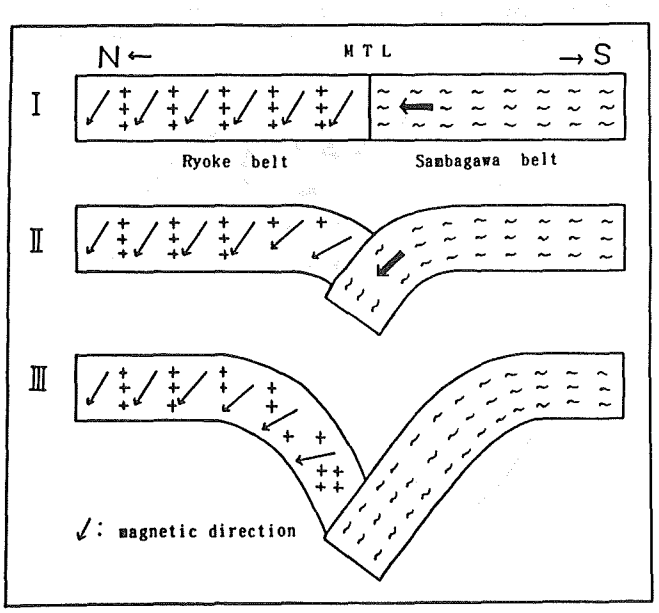

Fig. 5 Bending process of the Ryoke belt.

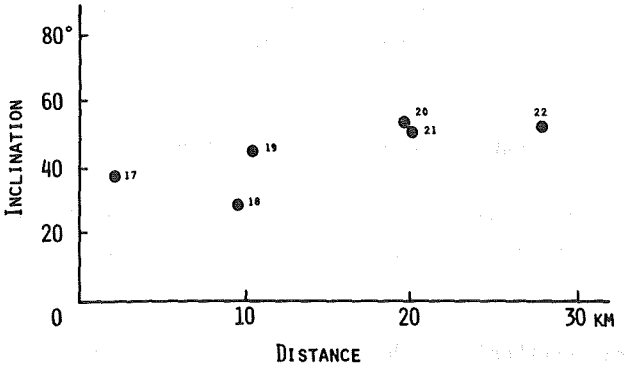

Fig. 6 Change in inclination of NRM of the dike rocks with distance from the northern boundary of the Izumi group.

Hypabyssal and basic dike rocks are considered to have intruded into the Ryoke granitic rocks before the deposition of the Izumi group (Ochi, 1982). Changes in inclination obtained from these dike rocks are shown in Fig. 6. The inclinations are almost no change with distance from the northern boundary of the Izumi group. This fact implies that the bending of the Ryoke granitic bodies had ceased before the deposition of the Izumi group. It is likely that a tectonic basin had been formed between the Ryoke and Sanbagawa belts throughout the bending movements of the Ryoke belt. The depth of the basin is estimated more than 6 km at least. Many structural features of the Izumi group are well explained by assuming that the Izumi group was formed in such a basin.

References

Hayase, K. and K. Ishizaka (1967) J. Japan. Assoc. Min. Petr. Econ. Geol., 58, 201-202.

Kawano, Y. and Y. Ueda (1966) J. Japan. Assoc. Min. Petr. Econ. Geol., 56, 191-211.

Larson, R. L. and W. P. Pitman (1972) Geol. Soc. Am. Bull., 83, 3645-3662.

Miyahisa, M. and T. Hiraoka (1970) Mem. Ehime Univ., Sci. Ser. D, Vol. IV, No 3, 21-33.

Nagai, K., K. Horikoshi, S. Sato, M. Miyahisa, N. Kashima, J. Takahashi, S. Doi and T. Hiraoka (1982) Geological Map of Ehime Prefecture, Ehime Eath-Science Association.

Ochi, S. (1982) J. Geol. Soc. Japan, 88, 511-522.

PALEOMAGNETIC STUDY OF SAWADANI GREENSTONES IN JURASSIC SUBDUCTION COMPLEX, SW JAPAN

Hideo SAKAI* and Shigenori MARUYAMA**

* Department of Earth Sciences, Faculty of Science, Toyama University, Toyama
** Department of Earth Science, Faculty of Education, Toyama University, Toyama

Introduction

Plate tectonic synthesis of the Japanese Islands has been tried by many authors since Matsuda & Uyeda(1971). After the classical work by Matuda & Uyeda, the small ocean basin model for the Mesozoic Japan such as back-arc basin by Horikoshi(1972), Ichikawa et al.(1972) and Sugisaki et al.(1972), though the details are different among the authors, and the strike-slip mobile belt model by Taira et al.(1983) were proposed. These three different models are come partly from the insufficient data on the paleomagnetism. Along this philosophy, Hirooka and his coworkers have given paleomagnetic constrains for the tectonic evolution of the Japanese Islands (Hattori & Hirooka, 1979; Hirooka et al., 1983). This paper is also to offer the new data on the accreted fragments, the Sawadani Permo-Carboniferous seamount.

Geological outline and Age

In Sawadani region of Tokushima Prefecture, east Shikoku in Japan, the greenstones are widely distributed. The Sawadani greenstone complex, 4 x 30km^2 in size, occurs showing the beautiful profile of the Permo-Carboniferous seamount surrounded by the Jurassic clastic sedimentary rocks in eastern Shikoku(Maruyama & Furutani, 1982). It is composed mainly of earlier mildly alkaline basalt and fractionated rocks, and later oceanic tholeiites(Maruyama, 1979). Maruyama(1979) revealed from field survey that the Sawadani seamount was formed by the two episodic volcanic events with a dormancy. In Fig.1, region(I) is the zone formed by first volcanic activity and region(II) is by the second volcanism. The northern part of the Sawadani seamount is affected by the Sanbagawa zeolite or prehnite-pumpellyite facies metamorphism, while the southern part by the lower grade of the pumpellyite-actinolite facies metamorphism.

The age of the seamount was estimated to be latest Carboniferous to early Permian by fusulinids in small limestone lenses intercalated with pillow lava flows and the capped limestone mass(Kanmera, 1969). However, the emplacement of the seamount is much later presumably middle to late Jurassic, because the surrounding clastic rocks contain early Jurassic radioralia(Isozaki et al., 1981), and are covered unconformablly by the early Cretaceous molasse type fore-arc basin deposits.

The greenstones of the Sawadani seamount were collected at 20 sites.

Measurements and the cleaning procedure of remanence

Measurements were made with a spinner magnetometer. For specimens of

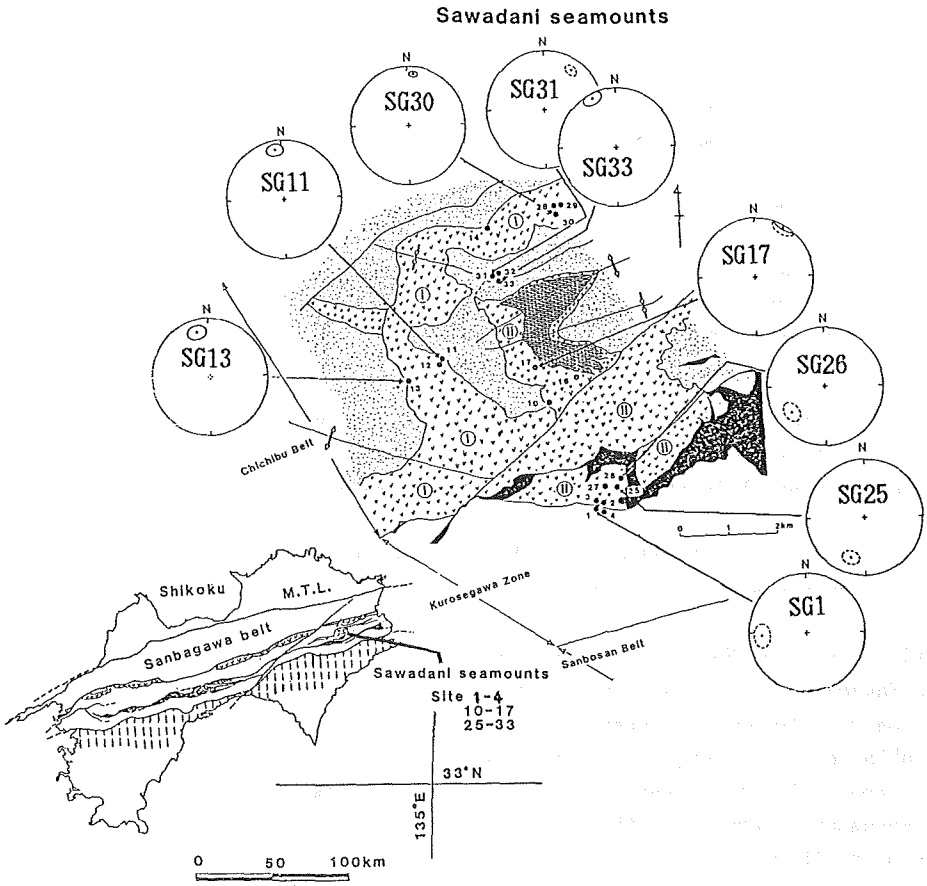

Fig. 1. Sampling localities of Sawadani greenstones and the paleomagnetic results represented by Lambert equal area projection.: The number I and II denote the eruption stage of Sawadani seamount.

respective site, stability of remanent magnetizations and the degree of dispersion were examined by progressive alternating field(A.F.) and thermal demagnetization. Through the magnetic cleaning treatment, we adopt the paleomagnetic data from 9 sites in this study.

The data are obtained as follows. The directions of the natural remanent magnetization(n.r.m) for all specimens, were measured. We adopted the cleaning method to the several pilot specimens of every site to define the optimum demagnetizing field(ODF) or optimum demagnetizing temperature (ODT). The remaining specimens were demagnetized in the ODF or ODT and the site-mean of the direction of remanence and Fisher's parameters were calculated. When two sets of core specimens were obtained from hand samples we adopted both cleaning methods on the specimens of the site. In the other cases, A.F. cleaning methods are used to obtain the site-mean data and thermal cleaning was applied to several specimens to check the data. When the result gave $\alpha 95$ larger than 20° and K smaller than about 10 we rejected the data. The

Table 1.Paleomagnetic results of Sawadani greenstone mass

Site No.	D	I	ODF(ODT)	Dc	Ic	P.L.	α95	K	N
SG 1	233.8	-8.0	4500e	-93.3	-24.0	12.5	13.9	24.3	6
11	-23.5	38.6	2000e	-8.0	17.3	8.9	10.1	26.8	9
13	-28.6	21.9	380°C	-14.6	22.8	11.9	11.5	24.3	8
17	27.2	28.0	2000e	31.8	-4.1	-2.0	12.4	21.0	8
25	193.4	-6.5	3000e	199.5	-27.4	14.6	10.8	20.8	10
26	-82.6	-63.4	3000e	233.5	-29.4	15.7	12.0	22.1	8
30	4.4	24.3	380°C	7.4	14.3	7.3	4.9	111.0	9
31	31.9	47.8	300°C	35.9	-21.0	-10.9	7.7	45.7	9
33	-33.3	24.2	2500e	-26.0	9.4	4.7	10.7	32.8	7

Table 1. Dc,Ic are declination and inclination after bedding correction, P.L. is the paleolatitude, α95 and K are Fisher's statistic parameter, and N is the number of specimens measured.

paleomagnetic results are tabulated in Table 1, where the data after bedding correction are also summarized.

Paleomagnetic results of Sawadani greenstones

In the Sawadani region, the grade of metamorphism increases gradually southward from zeolite/prehnite-pumpellyite facies in the northern half to the lower subfacies of the pumpellyite-actinolite facies in the southern half. We briefly compare the rock-magnetic behavior of the specimen in two region with their metamorphic grade and their age.

(1) Results of northern region(I)

Fig.2 shows the cleaning experiments of the northern site, SG30. The Schmidt equal-area projection of the n.r.m. and the direction after thermal treatment at 300°C are also compared in this figure. Remanent directions cluster well at the stage of n.r.m. and no significant change of direction was observed from the treatment of both A.F. and thermal cleaning. Reffering the results of progressive thermal demagnetization of pilot specimens, we adopt the mean direction at 380°C as the site-mean value. Similary, the site-mean directions are adopted from the 5 sites in the northern region(I). All these remanences after bedding correction dip northwards in the equal-area projection and have shallow inclinations.

(2) Results of southern region(II)

In the region (II), we obtained the paleomagnetic data from 4 sites, SG25, SG26, SG1 and SG17. Site SG17 consists of uppermost pillow lava layer just beneath the capped reefy limestone. As shown in Fig.1, SG 25, SG26 and SG1 are the neighboring sites and are apart from SG17 about 3 km southward. The remanences of the former 3 sites have the different behavior from that of the site SG17, that is, remanent directions of SG17 are thickly clustered in the stage of n.r.m., however, those of the other 3 sites scattered to some extent.

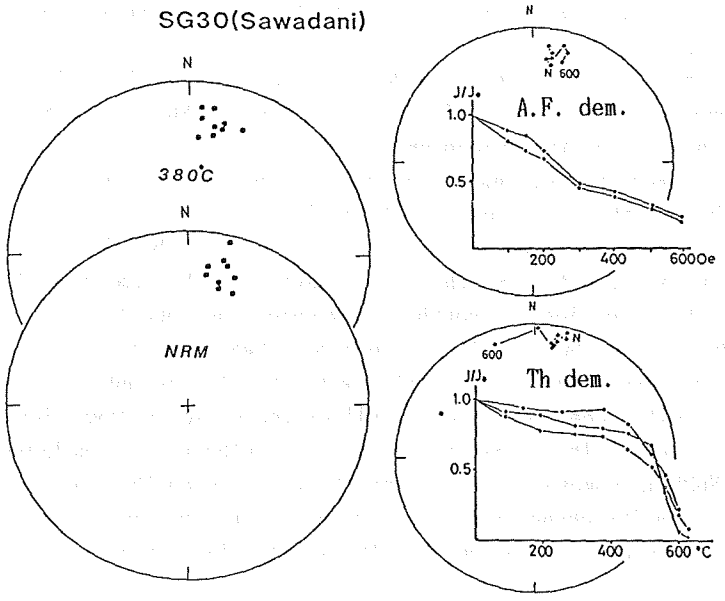

Fig.2.
Paleomagnetic results of site SG30.

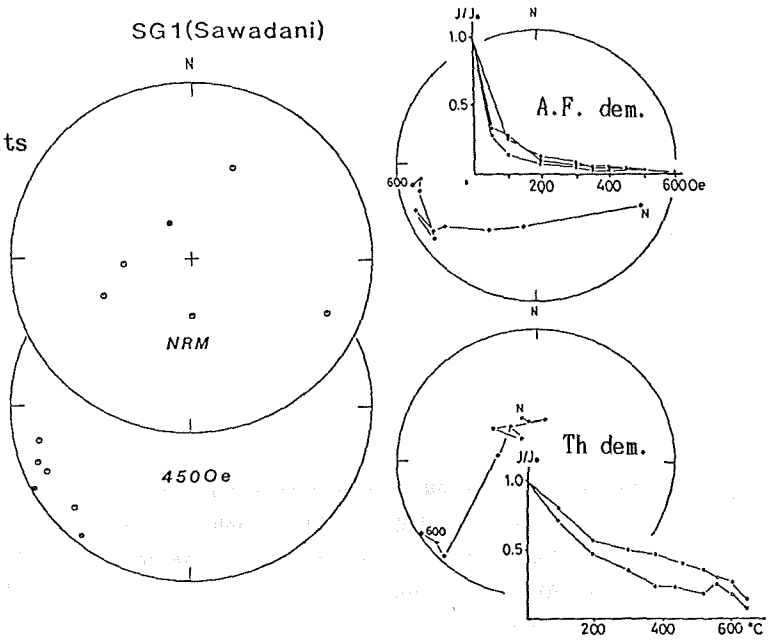

Fig.3.
Paleomagnetic results of site SG1.

Fig.3 shows the cleaning result of SG1. By cleaning the unstable component, the remanent direction migrated southwestward to form a well-clustered orientation. Similarly, the unstable component can be removed and the well clustered directions are obtained from SG25 and SG26. Such the intense secondary magnetizations recognized above may be caused from the metamorphic process affected in the southern part of the region(II). We calculated the directions of cleaned component from the specimens of sites SG25 and SG26, whose bedding planes are quite different. The cleaned components are calculated from the vector difference between the n.r.m. and the remanence after A.F.

demagnetization at 3000e. They are shown in Fig.4. The cleaned component and the direction after A.F. cleaning are denoted by the marks, romboric and asterisk, respectively.
Regardless where they are in situ or after bedding corrected, the directions of the cleaned components in SG25 are different from those in SG26. Further, these directions are apart from the paleomagnetically normal or reversed direction. The soft component is, thus, considered to be acquired in the metamorphic process before the greenstones emplaced in the place.

As shown in Fig.2 ,the site-mean inclination of SG17 after bedding correction displayed positive with a northern declination. The remaining 3 sites, however, have the directions of southern hemisphere and are fairly antipodal with the data of the SG17. The difference between the directions after structural corrections seems to be related with the stratigraphic difference. The four sites compared here are all of the pillowed lava flows at the second stage, however, the formative age of the southern part including sites SG1, SG25 and SG26 is somewhat earlier than that of the northern part, SG17. Geomagnetic polarity change might be occured during the 2nd stage volcanism. All the data of this region show the shallow inclinations.

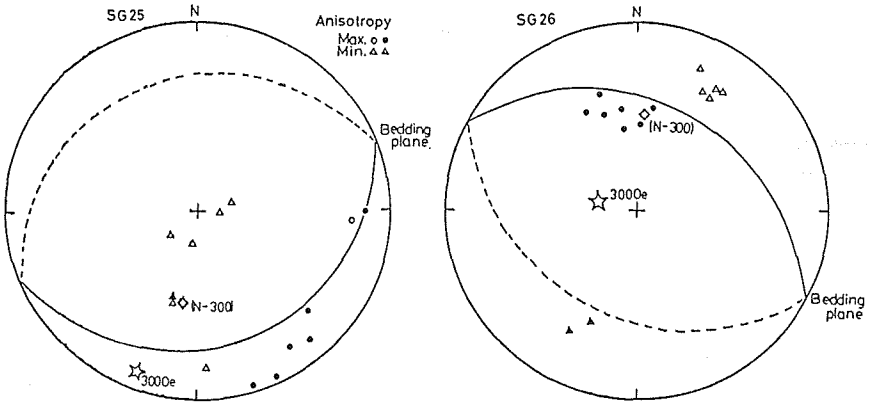

Fig. 4. The results of AMS measurements and the A.F. cleaning experiments of site SG25 and SG26.: The rhomboric and asterisk marks denote the direction of the cleaned magnetic component and the remnant component after 3000e A.F. demagnetization. Large circle show the bedding plane of the each site.

(3) Measurement of magnetic anisotropy

In Fig.4, the Maximum and Minimum axes of the anisotropy of magnetic susceptibity(AMS) are also shown. Maximum axes of AMS denoted as the circles tend to be parallel to the bedding plane, however, no corelation with the remanent direction is observed. Several investigators(e.g.,Ellwood and Whitney, 1980) mentioned that the AMS may be the indicator of flow direction of the lava. Employing their ideas, the anisotropy data of these sites may show

the direction of the pillow lava flow which is roughly in accordance with the measured direction of pillow tubes.

(4) A sort of conglomerate test

To examine whether the measured remanences maintain the primary one or not, sites SG31 and SG33, several meters apart from each other were chosen. Both greenstones are the olistlithes set in the same matrix of mudstone. The site-mean directions of the each site are clealy different regardless where in situ or after bedding correction. This may offer a sort of conglomerate test and the obtained results enhance the notation that these two sites acquired the remanences before they became oliststrome. The remanence of these sites shows also the inclination of lower angle.

Summary and Discussion

In Fig. 5., the paleomagnetic data before and after bedding correction are compared. The site-mean directions after bedding correction clustered better than those in situ, suggesting the structural disturbance such as folding or faulting after primaly magnetization. The direction obtained from the southern region are in the southern hemisphere of equal area projection and are rather antipodal to the direction of northern region. The geomagnetic polarity change may contribute to these antipodal directions. The obtained site-mean directions after bedding correction in all show the shallow inclinations.

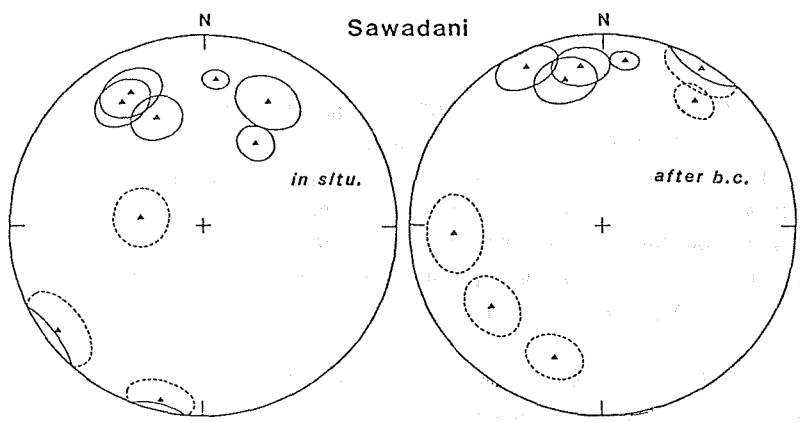

Fig. 5. Summary of site mean directions of Sawadani seamounts with a95 confidence circles. The site means in situ are in the left side, and those after bedding correction are in the right side. Projections are equal area. Solid symbols are on the lower hemisphere and open symbols are on the upper hemisphere.

We tried to measure the palaeo-latitudes of the surrounding slate-shale matrix (Jurassic) of the seamount, but the magnetic directions at each site are rather scattered, and could not get reliable paleolatitudes.

Summarizing the results from Sawadani region, the followings are led:

1. The specimens of northern sites have the stable remanences. Specimens of the northern sites have some unstable components, however, that can be subtructed by A.F. and thermal cleaning method. These magnetic features seem to be coincidence to the regional difference of metamorphic grade.

2. The remanent directions after bedding correction of southern sites (the earlier period of the 2nd stage volcanism) are antipodal to those of northern sites (1st stage volcanism) and of the site in the later period of the 2nd volcanism. Systematic polarity changes from normal, reverse and normal found through n.r.m. are with ascending order of stratigraphy, i.e., the polarity change in the primary magnetization reflects the eruption history of the seamount. Sawadani seamount had grown during these stages of geomagnetic polarities at latest Carboniferous to early Permian.

3. All the paleomagnetic data obtained from the Sawadani region show the much shallower inclinations than the present-day Japanese Islands.

The paleolatitude of the late Carboniferous-early Permian are calculated from the inclination of Sawadani region. In the calculation, the directions in the southern hemisphere are regarded to be reversal ones.

The obtained paleolatitudes of the seamount vary to some degrees, however, the averaged value of 7.0°N is still clearly shallower than the present-day Japanese Islands.

References

Ellwood, B. B. and J. A. Whitney (1978) J. Geophys. Res., 85, 1481.

Hattori, I. and K. Hirooka (1979) Tectonophys.,57,211.

Hirooka, K., T. Nakajima, H. Sakai, T. Date, K. Nittamachi and I. Hattori (1983) Accretion Tectonics in the Circum-Pacific Regions, ed. Hashimoto and Uyeda (TERRAPUB, Tokyo) p.179.

Ichikawa, K., T. Matsumoto, M. Iwasaki (1972) Kagaku, 42, 181.

Isozaki, Y., W. Maejima and S. Maruyama (1981) J. Geol. Soc. Japan, 87, 555.

Kanmera, K. (1969) Sci. Rep. Fac. Sci., Kyushu Univ. Geol., 9, 237.

Maruyama, S. (1979) Chikyu-Kagaku, 33, 255.

Maruyama, S. and H. Furutani (1983) Mem. Fac. Education, Toyama Univ., B, 31, 51.

Matsuda, T. and S. Uyeda (1971) Tectonophys., 11, 5.

Sugisaki, R., S. Mizutani, H. Hattori, M. Adachi and T. Tanaka (1972) Tectonophy, 14, 35.

Taira, A., Y. Saito and M. Hashimoto (1983) Geodynamic Series, Vol. 11, AGU, 303.

NATURAL REMANENT MAGNETIZATION OF DIRT ICE LAYERS COLLECTED FROM ALLAN HILLS, ANTARCTICA

Minoru FUNAKI

National Institute of Polar Research
9-10, Kaga 1-chome, Itabashi-ku
Tokyo 173

1: Introduction

Although the wide surface of Antarctica is covered with snow and firn snow, the bare ice areas exist around the mountains and the coast line in Antarctica. The dirt layers of right gray or yellow, which are usually a few centimer to less than 1 meter in width, are recognized in the bare ice surface. In the 2164m ice core samples obtained from Byrd Station, approximately 2000 individual dirt layers, resulting volcanic ash, were presented from the lower half of the cores (Gow and Williamson, 1971). Nishio et al. (1984) reported the existence of these dirt layers from Yamato Mountaines, Queen Maud Land, and Allan Hills, Southern Victoria Land: they found the volcanic ashes fragments in the samples collected from these dirt ice layers.

In 1979 austral summer season, the author collected 5 blocks of dirt ice samples from one layer and 1 block of the clean ice one with orientations at Allan Hills Meteorites Ice Field (site A) due to the preparation of the existence of NRM for those kind of dirt ice layers, but the orientations disappered during the transportation from the field to the laboratory. On the other hand Nishio collected the dirt ice samples with orientation for glaciological investigations from a dirt ice layer at Allan Hills (sit B) in 1980. A part of this sample was proffered for this magnetic investigations.

There is no report for rock magnetic and paleomagnetic studies about these kind of dirt ice layers up to the present. Although N. Kawai had a trial of NRM measurement of the clean ice samples collected from Antarctica by an astatic magnetometer before, any significant magnetization could not be detected from the samples.

2. samples

The dirt ice layer of site A tilts to 14° in the southwestward direction. The southeast edge disappears due to the snow accumulations and the northwest one has a boundary with clear ice. The average width is about 12cm, although it expands about 1m at the northwest one: The length on the traceable layer is about 70m. The pale yellow in color is visible for this layer in the field, but it can not be detected in the hand ice samples by naked eyes. The clear ice, called ordinary ice, was collected 1km southwest from site A. The layer of site B tilts to 16° in the southwestward direction and

the thickness is 8cm. The lightness of this layer is darker than that of site A.

These block ice samples were cut out based on the most flat plain for site A samples and a horizontal plain for a site B sample by a band saw in the -20°C laboratory. Obtained cubic specimens from these block samples are 18-35 g in weight and then their surfaces were melted by water due to taking off the contaminations. These specimens were stored at -20°C in the refrigerator.

3. Measurements of the magnetizations

The NRM of every specimens was measured by the superconducting rock magnetometer and then the representative specimens were demagnetized by AF field up to 500 Oe in room temperature. The NRM intensities of the site A layer are very uniform; it ranges from 1.4 E-7 to 9.6 E-8 emu/g among 5 different block samples. The stabilities of NRM against AF demagnetization are fairly good as for intensities and directions; the value of MDF exceeds 450 Oe. Total of 13 specimens, having same coordinate collected from one block sample, show that their NRM directions are almost parallel one another after AF demagnetization to 100 Oe as shown in Table 1. However there are no significant NRMs in the ordinary ice specimens. It suggests that the intensity of NRM of ordinary ice specimens is less than 2 E-8 emu/g.

The specimens of site B layer have also very stable NRMs against AF demagnetization. Their original intensities, ranged from 2.5 to 3.4 E-6 emu/g, are demagnetized gradually up to 500 Oe, and the MDF values exceed 500 Oe; the directions have almost no shift up to that demagnetization. Total of 14 specimens, including the dirt layer at least in a part of one, have almost same directional NRMs one another as shown in Table 1. The mean direction of NRMs after 100 Oe demagnetization and after the bedding correction is -72° and 120° respectively, as illustrated in Fig. 1. Since the geomagnetic field direction at sampling site (illustrated in Fig. 1) is about -77.2° in inclination and 159.3° in declination, the mean direction of NRM after bedding correction is almost parallel each other. The calculated VGP position from this mean NRM is 49.1°S in latitude and 113.4°E in longitude as shown in Fig.1(3).

The sliced specimens of 18 numbers about 5mm in thickness from bottom (No. 1) to top (No. 18) of site B block sample are measured the NRM intensity variations among each slice. The results are shown in Fig. 2. In this block sample, the dirt layer is only recognized within the No. 5 to 12 specimens by naked eyes. However no colored specimens near the colored one have some significant magnetizations. Their intensities increase gradually from No. 3 to 8 and steeply from No. 8 to 9; the maximum value, 4.6 E-6 emu/g, is observed at No. 10 specimen; it decreases steeply from No. 11 to 14. The directions are almost parallel one another from No. 5 to 13. However that of No. 1 to 4 and No. 14 to 18 have fairly week intensities as less than 1.7 E-7 emu/g and have no significant directional NRMs.

Table 1. Paleomagnetic results of dirt ice layers collected from Allan Hills Meteorites Ice field.

sampling site	bedding correct.	demag.	N	In E-7 emu/g	Inc	Dec	K	a95	pLat °S	pLon °E
site A	—	0	13	1.38			60	5.4°		
		100		1.33			184	3.1		
site B	before	0	14	22.1	-69°	-164°	241	2.6		
	after	0			-72	119				
		100		21.8	-72	120	347	2.1	49	113

Fig. 1 NRM directions of the dirt ice specimens collected from site B.

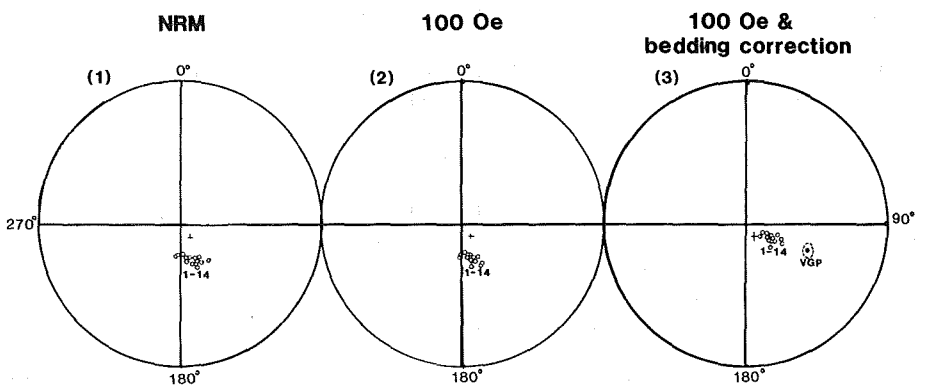

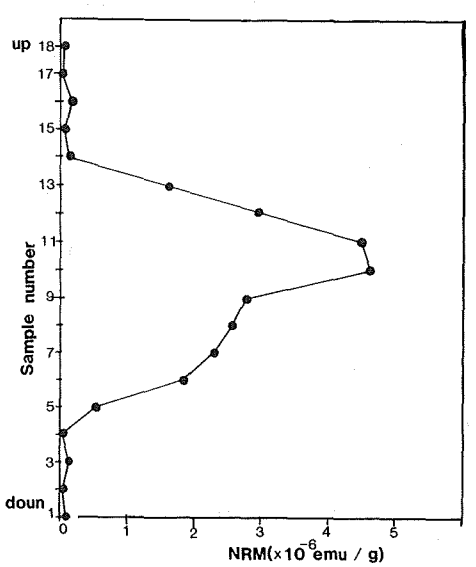

Fig. 2 The NRM intensity variations of the dirt ice specimens collected from site B.

The volcanic ashes were collected from the specimens B by means of the evaporation of melted water at 90°C for measurement of the hysteresis properties at room temperature by vibration sample magnetometer. The obtained values are as follows: the saturation magnetization (Is)=1.13 emu/g, the saturation remanent magnetization (Ir)=0.28 emu/g, the coercive force (Hc)=152 Oe and the remanent coercive force (Hrc)=402 Oe. The thermomagnetic curves were measured for that volcanic ashes under 1.1 E-2 pa in atmospheric pressure. Obtained the reversible curves show the Curie point 570°C of magnetite.

4. Discussion

The NRM carrier of dirt ice specimens of site B is doubtless almost pure magnetite grains by the results of thermomagnetic curves. Day et al. (1977) examined the relationships between the domain structures and the hysteresis properties. Since the ratios of Ir/Is=0.25 and Hrc/Hc=2.65, the magnetic grains is to be psudosingle domain structure. Therefore the reliability of NRM is supported not only by these analyses but also AF demagnetization analyses.

The possibilities of NRM acquisitions of the dirt layers may be estimated and have some problems for respective estimations as follows.

(1): The possibility of acquisition of DRM is seemed to be very difficult on the surface of Antarctica due to the constantly strong wind called Katabatic Wind compared with that of the ordinally sedimentation. Therefore if the snow acquires the DRM by sedimentations of volcanic ashes in Antarctica, the intensity should be extremely week compared with the tuffaceous sediments deposited in the deep seas and lands. Since the specimen of site A includes the volcanic ashes in amount of 2.1 E-3 wt% and has the NRM intensity of 9.6 E-8 emu/g, the NRM intensity of volcalic ashes is estimated to be 4.57 E-3 emu/g. The same order of NRM intensity is obtained from the volcanic ashes in the specimens of site B. It is very strong one compared with the sediments or sedimentary rocks. The alignment of NRM directions among the each block is fairly good as a95=3.1° and 2.1° for the specimens of site A and B respectively. From the view points of this intensities and this alignment of directions for NRM, the characteristics of dirt ice layer is similar to the TRM rater than the DRM. Therefore it seems that the NRMs of diry ice layer may be acquired after sedimentation of volcanic ashes on the surface of snow accumulations.

(2): The snow contacted with volcanic ash grains are molten partially by the sun radiations, consequently the magnetic grains aligned to the geomagnetic field direction at that time. However, it may be difficult to assume the mechanism at the inside of the Antarctica due to the meteorological circumstances.

(3): During the formations of the ice from the snow under the condition of some pressures by the snow accumulations, the magnetic grains are aligned to the geomagnetic field without melting ice. However, there is no report about this

magnetization up to the present.

(4): The ice contacted with volcanic ash grains are molten partially at the surface of Meteorites Ice Field by the same reason of (2), but it has to be same problems of (2). Furthermore this may be rejected by the result of NRM directions after bedding correction.

From those obtained data and estimations, we can not decide when and where the NRM was acquired for the dirt ice layers in Antarctica. However it is important to clarify of the reliability of the estimation (3). Because, every sedimentary rock has a possibility of NRM acquistions during the diagenesis; there is a possibility of realignment the NRM to the geomagnetic field directions when the sediments change to the sedimentary rocks, due to the growing of the some silicate and calcite cristals arond the magnetic grains in the sediments.

The VGP displacement angles and the variations of non-dipole component of geomagnetic field are systematically great in the high latitude region of southern hemisphere as mentioned Cox (1964): it exceeds 18°at the 70°s in latitude. Therefore, it is difficult to limit the sedimantation place and the age from the VGP. However the NRM directions are useful for the identification of individual dirt layers among different regions and for the informations about the flow lines of the ice sheet.

The NRM variations of the site B dirt ice layer are estimated the reflection of the aboundance of the magnetic grains, if there is no differentations for the magnetic propertises among each slice specimen. It may be therefore that the sedimentations of volcanic ashes on the snow acumulations gradually increased in the first step, steep by increased in the second step and steep by decreased in the third steps.

References

Cox, A. and Doell, R. (1964): Bull. Seismol. Soc. Am., 54, 6, 2243-2270.

Day, R., Fuller, M. and Schmidt, V. A. (1977): Phys. Earth Planet. Inter., 13, 260-267.

Gow, A. J and Williamson, T. (1971): Earth Planet. Sci. Lett., 13, 210-218.

Nishio, F., Katsushima, T., Ohmae, H., Ishikawa, M. and Takahashi, S. (1984): Mem. Natl Inst. Polar Res., Spec. Issue, 34, in press.

SUSPENSION METHOD: CHARACTERIZATION OF FINE MAGNETIC GRAINS IN SEDIMENT

Ikuo KATSURA and Shoji YOSHIDA*

Department of Geology and Mineralogy, Faculty of Science,
Kyoto University, Kyoto, 606, Japan

A new method to determine the amount and moment distribution of fine magnetic grains in sediment is proposed. The method is applied to the dilute suspension made of the sediment, and named "suspension method".

The amount of magnetic grains in sediment is defined by "complete alignment magnetization (CAM)" as a sum of magnetic moment of sedimentary grains in natural condition. The classical paramagnetic gas theory could be applied to a non-interacting assemblage of magnetic grains in suspension (Collinson, 1965). The assemblage attains an equilibrium state as "equilibrium magnetization M(B)" under the effects of thermal agitation as the Brownian motion and magnetic field (flux density B). Since the grain moment ranges in an extent, the M(B) becomes

$$M(B) = N \cdot \int_0^\infty f(m) \cdot m \cdot L\left(\frac{mB}{kT}\right) dm, \qquad (1)$$

where N and m are number and moment of magnetic grains, $L(\frac{mB}{kT})$ is the Langevin function, k is Boltzmann's constant, T is absolute temperature, and f(m) is the probability density function of the moment distribution. When we measure the equilibrium magnetization as a function of field intensity and temperature, the CAM and the moment distribution could be determined by the least-squares fitting of the theoretical M(B) curve to the observed values.

To apply this method, the magnetic grains must be in non-interacting state. This condition was examined to the suspension specimens with various concentrations (Table 1). The source sediments were reddish brown clay (GH76-2 D148; Honza, 1977) and calcareous ooze (KH73-4-8; Kobayashi et al., 1980). Since only the reddish brown clay has contained coarse grains, it was sieved down and centrifugalized to remove coarser fractions. The sediments were loosened in water by agitating in an ultrasonic bath, and dispersed with aid of peptizer, sodium hexametaphosphate. The suspension

Table 1. Concentration of specimens.

sediment type	specimen No.	concentration* (g/ml)	relative concentration	water content**
reddish brown clay	B1	1.6×10^{-1}	1	5.76
	B2	1.1×10^{-1}	1/1.5	8.98
	B3	6.3×10^{-2}	1/2.5	15.2
	B4	3.2×10^{-2}	1/5.0	31.0
	B5	1.6×10^{-2}	1/10	62.7
	B6	7.9×10^{-3}	1/20	126
	B7	4.0×10^{-3}	1/40	254
	B8	2.0×10^{-3}	1/80	518
	B9	9.9×10^{-4}	1/160	1020
calcareous ooze	C1	2.0×10^{-1}	1	4.62
	C2	9.8×10^{-2}	1/2.0	9.79
	C3	3.9×10^{-2}	1/5.0	24.9
	C4	2.0×10^{-2}	1/10	51.4
	C5	9.8×10^{-3}	1/20	103
	C6	4.9×10^{-3}	1/40	200

* concentration = (weight of solid)/(volume of suspension).
** water content = (weight of water)/(weight of solid).

*Present address: OYO Corporation, Daitakubo 2-2-19, Urawa, 336, Japan

was prepared by the more addition of an appropriate amount of water, and filled in a glass tube (24 mm both in diameter and height) with a silicone rubber plug (7 mm thick). The magnetization of the tube with plug was less than 5×10^{-11} Am^2. Prior to each run of the experiment, the specimen was agitated in an ultrasonic bath for 30 sec and then shaken by hand. Every run was conducted under the same temperature as 23 °C.

The magnetic relaxation was observed at first. The magnetization of specimens was measured on a cryogenic magnetometer (ScT C-112). The specimen was inserted into the sample test region (residual field 4×10^{-8} T downward) of the magnetometer and vibrated by hand to randomize the alignment of magnetic grains. After the magnetization was reduced to possible minimum (less than 5×10^{-11} Am^2), the specimen was pulled up to the position 45 cm above the center of sample test region. The field at this position was 3.8×10^{-6} T in downward. The specimen was kept there for 15 sec to be magnetized, and quickly inserted into the center of sample test region. The change of the magnetization (vertical component) was observed. The relaxation patterns (Fig. 1) are classified into the following three classes. The concentration is in descending order:

class 1. Magnetization shows little decrease (B1, B2, C1).

class 2. Magnetization decreases quickly and changes its polarity, then approaches to zero (B3, B4, B5, B6, C2, C3, C4).

class 3. Magnetization decreases monotonically to zero as a same exponential form independent of concentration (B7, B8, B9, C5, C6).

The behaviors of classes 1 and 2 indicate that the interaction between grains influences the grain motion and the viscous drag is important to the chained grains. The relaxation pattern in class 3 is corresponding to the expected one from the Brownian motion in a field free space. This result shows the grains in class 3 suspension is in non-interacting state.

Next, the magnetic acquisition was observed. A flux-compensated coil was set in the sample test region. The coil is designed to equalize the flux produced by the inner coil with the flux (opposite polarity) produced by the outer one. The noise of the net field produced inside the inner coil was less than 1×10^{-10} Am^2 (as equivalent magnetization). Every specimen was examined in eight levels of the field up to 1.1×10^{-5} T. The specimen was inserted into the center of sample test region, where the field was previously generated, and vibrated by hand. After the magnetization reached the possible minimum, the specimen was kept there quietly. Then, the change of the magnetization (vertical component) was observed for 20 to 30 sec. The acquisition patterns (Fig. 2) are classified into three classes as same as the relaxation patterns. The behaviors of the magnetic grains could be understood in the same manner as

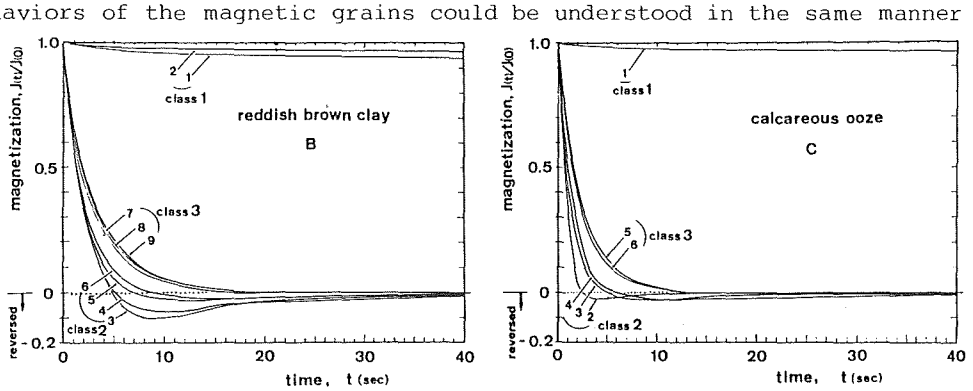

Fig. 1. Typical examples of relaxation patterns of magnetization in a magnetic field free space as a function of time. The magnetization is normalized by the maximum value at the time the specimen was inserted.

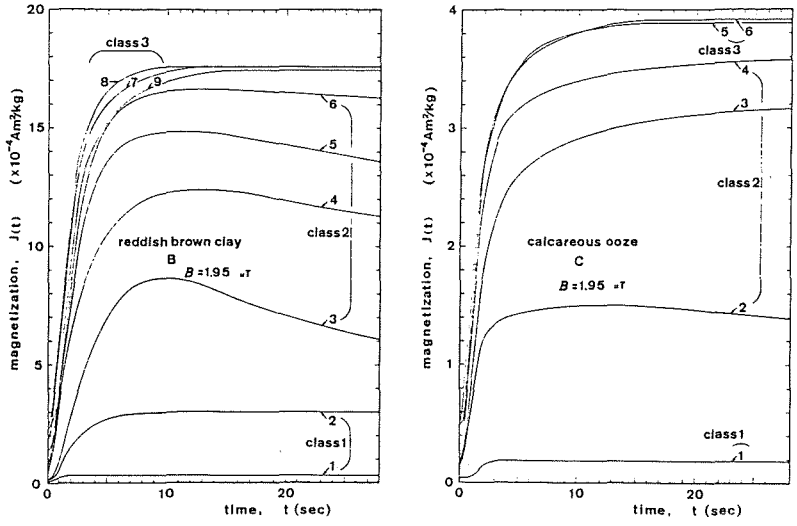

Fig. 2. Typical examples of acquisition patterns of magnetization in a steady magnetic field (1.95×10^{-6} T) as a function of time. The magnetization is normalized by weight of solid.

the behaviors in a field free space. For the class 3, the saturation level represents the equilibrium magnetization.

The magnetizations acquired in a steady field are represented by the saturation-like value (class 1), the peak or final value (class 2), and the equilibrium magnetization (class 3) with respect to the concentration (Fig. 3). The pattern is divided into two parts. The magnetization per unit weight of solid is constant until the concentration increases to a critical value. Above the critical value, the magnetization decreases monotonically. The critical concentration is 4.0×10^{-3} g/ml for the reddish brown clay and 1.0×10^{-2} g/ml for the calcareous ooze. These values are corresponding to the boundary concentration between class 2 and class 3 for both the relaxation and acquisition. In the class 3 suspension, the individual grains are free to rotate without interaction. We can now distinguish a suspension in non-interacting state from that in interacting state by the observation of relaxation pattern only.

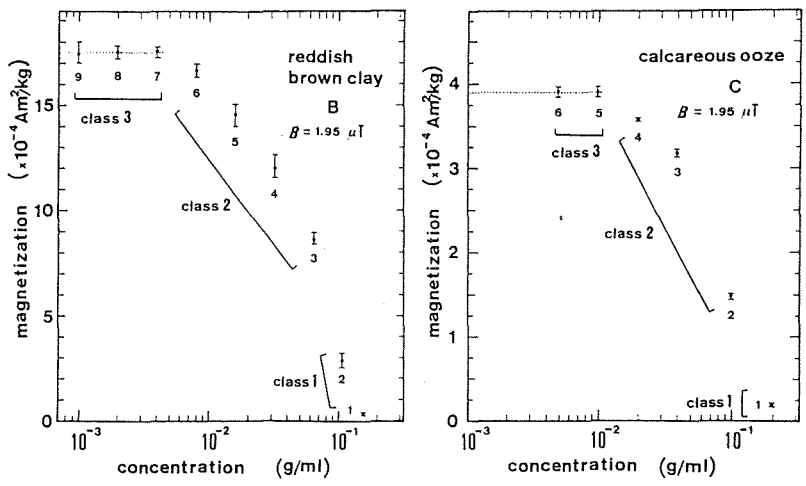

Fig. 3. Variation of magnetization (per unit weight of solid) acquired in a steady field (1.95×10^{-6} T) with respect to the concentration of suspension. The bar attached to the mean data point (solid circle) shows the range between minimum and maximum in five runs for one specimen. Dotted line on class 3 points shows the level of equilibrium magnetization.

The equilibrium magnetization of class 3 suspensions was measured by the same manner mentioned above. The increase of the equilibrium magnetization is apparently accompanied by the increase of field intensity without saturation (Fig. 4). This fact confirms that the magnetic grains are subjected to the thermal agitation and that the equilibrium magnetization could be explained by the paramagnetic gas theory.

When we adopt the log-normal distribution of grain moment, the equilibrium magnetization, M(B), is given by the eq.(1) with log-normal probability density function, f(m). In this case, the M(B) becomes (hereafter the base of logarithms is e)

$$M(B) = \frac{M_0}{\sqrt{2\pi}\cdot \log a \cdot m_A} \cdot \int_{-\infty}^{\infty} \exp\left(x - \frac{(x - \log m_G)^2}{2\cdot(\log a)^2}\right) \cdot L\left(\frac{e^x B}{kT}\right) dx, \qquad (2)$$

where $x = \log m$; logarithmic moment,

$m_A = \exp(\log m_G + (\log a)^2/2)$; arithmetic mean moment,

$M_0 = Nm_A$; CAM,

$\log m_G$; mean of logarithmic moment (m_G is geometric mean moment),

$\log a$; standard deviation of logarithmic moment.

The least-squares method applies to eq.(2) with three fitting parameters, M_0, $\log m_G$ and $\log a$. Optimum fitting parameters were evaluated by the use of the nonlinear least-squares fitting program "SALS" (Nakagawa and Oyanagi, 1980). The integral in eq.(2) was executed for the range $\pm 5\cdot\log a$ around $\log m_G$ by the numerical definite integration (SSL-II, FACOM).

The CAM, m_G and a are 4.5×10^{-3} Am^2/kg, 3.7×10^{-16} Am^2 and 3.8 for the reddish brown clay and 1.3×10^{-3} Am^2/kg, 1.6×10^{-16} Am^2 and 4.3 for the calcareous ooze, respectively (Table 2). The goodness of the fit is evaluated by the deviation d;

$$d = \frac{1}{n} \cdot \sum_{i=1}^{n} \left| \frac{M_{obs}(B_i) - M_{calc}(B_i)}{M_{obs}(B_i)} \right|, \qquad (3)$$

where n is number of measurements and the suffixes of $M(B_i)$ denote "observed" and "calculated", respectively. The estimated curves of M(B) (Fig. 4) apparently demonstrate good coincidence with the observed data.

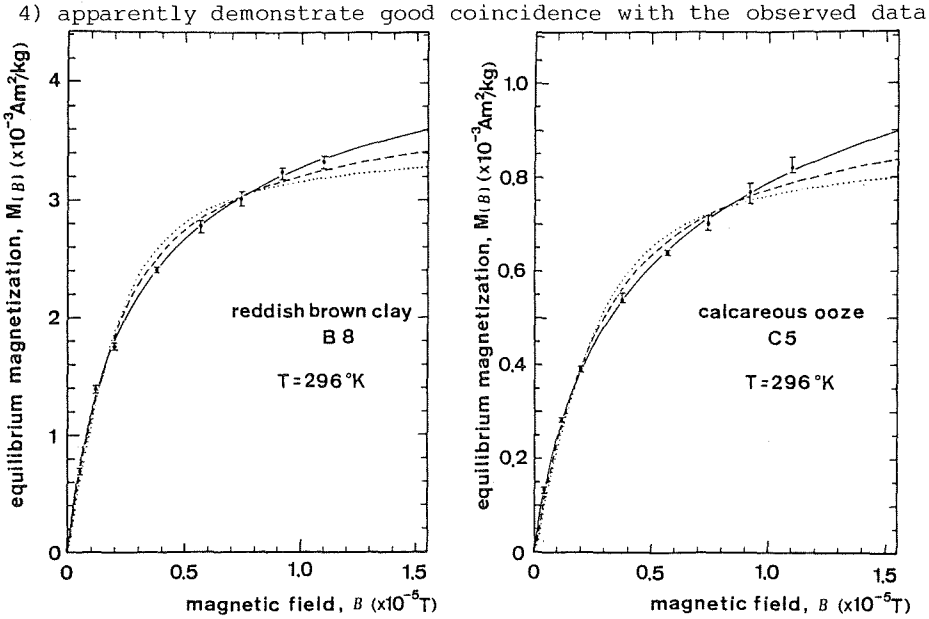

Fig. 4. Examples of equilibrium magnetization (per unit weight of solid) as a function of field intensity. The bar attached to the mean data point (solid circle) shows the range between minimum and maximum in five runs. The curves are results of least-squares fittings. Solid curve is log-normal grain moment distribution. Broken and dotted curves are log-uniform and unit distributions, respectively.

Table 2. Results of least-squares fitting by log-normal distribution.

(T=296°K)		reddish brown clay			calcareous ooze	
		B7	B8	B9	C5	C6
<fitting parameters>						
CAM	$M_0(\times10^{-3}Am^2/kg)^*$	4.28	4.53	4.65	1.28	1.21
geometric mean (median)	$m_G(\times10^{-16}Am^2)$	6.0	3.7	2.1	1.6	1.7
	a	3.3	3.8	4.5	4.3	4.4
<deviation>	d(%)	1.6	1.3	2.5	1.9	1.8
<related parameters>						
arithmetic mean	$m_A(\times10^{-16}Am^2)$	12.	9.0	6.6	4.6	4.9
mode**	$m_o(\times10^{-17}Am^2)$	14.	6.0	2.3	2.0	1.9
standard deviation***	$sd(\times10^{-15}Am^2)$	2.2	2.0	1.9	1.2	1.4
number of magnetic grains	$N(\times10^{+9}/g)^*$	3.5	5.0	7.0	2.8	2.5

* CAM (M_0) and number (N) are normalized by weight of solid.

** $m_o = \exp[\log m_G - (\log a)^2]$

*** $sd = \exp(\log m_G)(\exp[2(\log a)^2] - \exp[(\log a)^2])^{1/2}$

The other two distributions, log-uniform distribution with moment between 0 and m_{max} (Stacey, 1972; Barton et al., 1980) and fictitious unit distribution with identical moment m_c, were assumed and the least-squares fittings were carried out. The estimated M(B) curves (Fig. 4) tend to saturate early in lower field intensity levels. The behavior of the magnetic grains, therefore, is well described by the log-normal type.

The domain state could be estimated from the ratio of CAM to SIRM (saturation isothermal remanent magnetization). The SIRM intensity was 1.37×10^{-2} Am^2/kg for the reddish brown clay and 3.14×10^{-3} Am^2/kg for the calcareous ooze. Then, the ratios are 0.33 and 0.41, respectively. These ratios suggest that the magnetic grains of both sediments are almost composed of single-domain (SD) and pseudo-single-domain (PSD) grains. This result does not contradict the estimated grain size distribution from the moment distribution: As the dominant magnetic mineral is magnetitic for both sediments (Curie temperature was both 570 °C), the m_G values of B8 and C5 are corresponding to the equivalent diameter of magnetite 0.11 μm and 0.09 μm, respectively. The magnetic grains are smaller than the uppermost size of 5 μm to act the Brownian motion (Jirgensons and Straumanis, 1962).

The suspension method has been successful with the use of dilute suspension made of sediment to avoid the interaction of the surrounding grains. This method solves the problem of overestimate of MD grains by the use of weak magnetic field (less than geomagnetic field). The suspension method contributes new abilities to the study of magnetization of sediment in viewpoints of magnetic concentration (CAM), moment distribution (m_G, a, etc.), mineral composition, and microstructure (e.g. domain state, size).

References

Barton, C.E., N.W. McElhinny and D.J. Edwards (1980) Geophys. J. R. astr. Soc., **61**, 355-377.

Collinson, D.W., (1965) J. Geophy. Res., **70**, 4663-4668.

Honza, E., (1977) Rep. Geol. Surv. Japan Cruise, **7**, 1-9.

Jirgensons, B., and M.E. Straumanis (1962) A short text book of colloid chemistry, 2nd ed., Macmillan Co., New York, 425pp.

Kobayashi, K., S. Tonouchi, T. Furuta and M. Watanabe (1980) Bull. Ocean Res. Inst. Univ. Tokyo, **13**, 148pp.

Nakagawa, T., and Y. Oyanagi (1980) in Matusita, K., ed., Recent developments in statistical inference and data analysis, North Holland Publ. Co., Amsterdam, 221-225.

Stacey, F.D., (1972) Pure Appl. Geophys., **98**, 139-145.

(Submitted to Geophys. J. R. astr. Soc. in detailed form by Yoshida and Katsura)

THICKNESS OF THE LOCK-IN ZONE OF POST-DEPOSITIONAL REMANENT MAGNETIZATION IN DEEP-SEA SILICEOUS CLAY

Toshitsugu YAMAZAKI

Marine Geology Dept., Geological Survey of Japan
Yatabe, Tsukuba, Ibaraki, 305, Japan

1. Introduction

Many laboratory experiments (for example, Kent, 1973; Løvlie, 1974, 1976) revealed that a post-depositional process plays a substantial role in detrital remanent magnetization (DRM) of deep-sea sediments and that an apparent time delay (depth-lag) in the fixation of the remanence exists. In the zone-magnetization model (Niitsuma, 1977) remanent magnetization becomes permanent gradually within a finite thickness of sediments (lock-in zone) below the sediment/water interface. Experiments by Hamano (1980) and Otofuji and Sasajima (1981) showed that the post-depositional remanent magnetization (pDRM) is acquired with the density change of sediments. If their experimental results can be adopted to the actual deep-sea sedimentary environment, the lock-in zone corresponds to the depth range in which the density change of the sediments by burial compaction mainly occur.

In contrast to many works about the pDRM based on laboratory experiments, studies on naturally deposited deep-sea surface sediments, especially within several tens of centimeters of the sediment/water interface, are scarce. The purpose of this paper is to show subsurface changes of density and magnetization in siliceous clay which is one of the typical lithologies of deep-sea sediments, and to estimate the thickness of the lock-in zone and the magnitude of the time delay caused by the depth-lag. It is important to make clear them because a time gap between magnetostratigraphic time scale and biostratigraphy caused by the depth-lag is likely not to be small enough to be ignored in the pelagic environment where a sedimentation rate is very slow.

2. Box core sample

A piston corer which is widely used to obtain deep-sea sediments was not suitable for studying the very surface sediments because it often misses or considerably disturbs surface sediments of several tens of centimeters. A GSJ type double-spade box corer (Kinoshita, et al., 1981) which was developed for the purpose to study in situ relation between manganese nodules and surface sediments was used to take undisturbed soft sediments of about 50cm x 50cm x 40cm.

Table.1 Location of sampling sites.

Sample No.	Latitude	Longitude	Water depth	Sampler
B 80	0° 53.25'S	166° 12.59'W	5510 m	Box-corer
P 171	1° 30.45'S	165° 52.52'W	5537 m	Piston-corer
P 355	0° 50.34'S	166° 09.43'W	5164 m	Piston-corer

Box core B80 was obtained in the Central Equatorial Pacific (Table.1). The surface sediments of 38cm long show no disturbance, and there was no sign that several manganese nodules on the top of the sediments were rolled by sampling procedure. The site is in equatorial high productivity province of biogenic opal, and its water depth, 5,510m, is deeper than CCD (Calcium Carbonate Compensation Depth) of this area which is thought to be about 5,000m at present. Therefore, siliceous fossil rich clay has been deposited at this site. The sediments are quite homogeneous and show no lithologic changes, which is suitable to detect the changes of density and magnetization accompanied with burial compaction. Grain size distribution analyzed at 5cm intervals shows no significant difference. Clay, silt and sand content are about 60%, 30% and 10%, respectively. The sedimentation rate at this site estimated from paleomagnetic stratigraphy of several piston cores taken around this site is about 2 to 4 m/Ma (Yamazaki, in prep.). Thus, the age of the bottom of Core B80 (depth of 38cm) is estimated to be 100,000 to 200,000 years.

3. Density change

Water content of Core B80 was determined at 2cm intervals from the weight of the sample before and after drying. The results after the correction of salinity are shown in Fig.1(a) (dry base). Density and porosity (Fig.1(b)(c)) are calculated from the water content and the density of the solids, 2.58 g/cm^3, measured by the pycnometer method. The most important result shown in figures is that a steep increase of density (or decrease of water content) of the surface sediments is restricted within only about 10cm. Under 10cm the water content (density) of siliceous clay settles at the value of about 360% (1.18 g/cm^3). It is known that the water content of siliceous sediments is higher than that of other common lithologies in pelagic environment (i.e. calcareous or zeolitic sediments) (Tsurusaki and Saito, 1982).

4. Remanent magnetization and intensity of ARM

Samples for magnetic measurements were taken from the core in succession by small cubic case of $10cm^3$ immediately after the box-core recovery. Samples were sealed up as firm as possible to prevent dehydration before measurements. A cryogenic rock magnetometer (SCT Model 113) was used for measurements of the remanence. Direction of NRM are plotted in Fig.1(c)(d). Declination values are relative because a box core was not azimuthally oriented. Direction of NRM is nearly uniform except for an uppermost sample. This supports the visual inspection that the core suffered little disturbance. It is difficult to clarify the polarity of the remanence from inclination which is nearly equal to zero. It can be, however, definitely assigned to Brunhes normal epoch based on siliceous microfossils of this core and magnetostratigraphy of several piston cores around this site (Yamazaki, in prep.).

Next, ARM (anhysteretic remanent magnetization) was given to the samples by using peak alternating field of 30 mT and a DC field of 0.025 mT. Fig.1(e) shows the intensity of ARM together with that of NRM. To compensate apparent changes of the intensity accompanied by

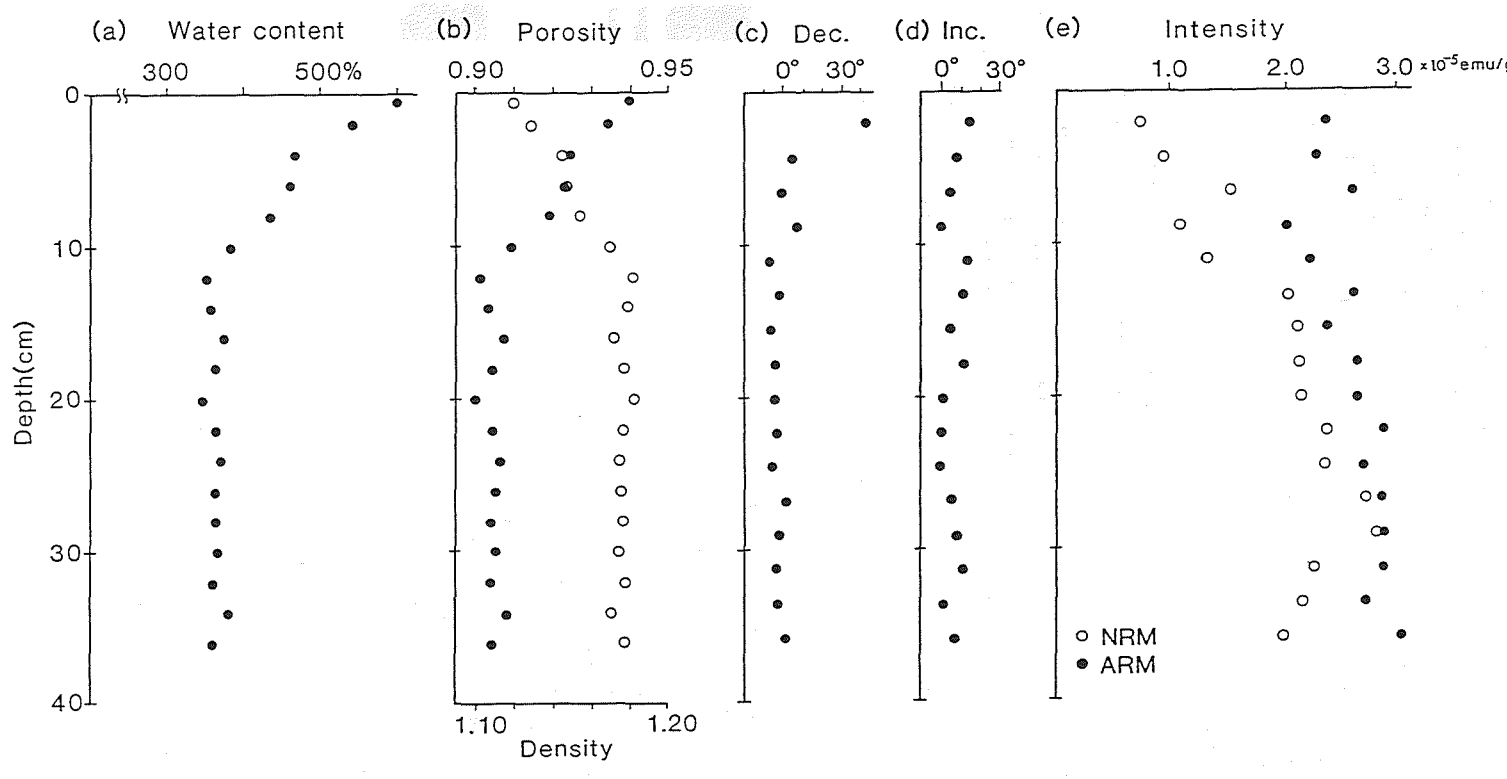

Fig.1 Vertical changes in some properties of surface sediments of Box-core B80. (a) Water content (dry base). (b) Calculated porosity (solid) and density (open) using the density of solids, 2.58 g/cm^3. (c) Relative declination of NRM. (d) Inclination of NRM. (e) Intensity of NRM (open) and ARM (solid). Difference of the amount of the solids is compensated (see text).

changes of the amount of the solids, the weights of solids in each samples shallower than 10cm are normalized to that of below 10cm. The intensity of NRM increases steeply downward to about 10cm deep and settled below it although the intensity of ARM shows only slight downward increase. The approximate uniformness of the intensity of ARM in this core supports the idea of constant sedimentary environment inferred from its lithology. The change of the intensity of NRM can be explained by the idea that the remanent magnetization of uppermost 10cm had not been fixed yet and the remanence carried by the components whose relaxation time are less than two months (the time from the sampling to the measurements) were lost.

5. Discussion.

As shown in Fig.1, the depth range of 0 to 10cm in which the change of the intensity of NRM is observed agrees with that of the density change, and the fixation of the remanence would take place within this width. No remarkable decrease in water content below 40 cm is confirmed at least within 8m (Fig.2) using a piston-core sample (Core P171) of homogeneous siliceous clay (Tsurusaki and Saito, 1981) which was taken near the site of Core B80 (Table.1). The conclusion from laboratory experiments that the thickness of the lock-in zone corresponds to the depth range in which the density change occurs may hold true in the actual deep-sea environment. There is, however, a noticeable discrepancy between the experiments and this study. Hamano (1980)'s experiments using deep-sea red clay show that the sediments acquire the remanence with the range of void ratio from 6 to 3. In siliceous clay of this study, however, the remanence has already been fixed at porosity of 0.9 (void ratio of 9). A part of this disagreement may be explained by the difference of the composition of the sediments, but it seems that a fundamental reason will be the extreme difference in the sedimentation rate between laboratory experiments and the natural pelagic environment.

In deep-sea sediment cores a decrease of the intensity of NRM around the polarity reversal horizon has been recognized formerly (for example, Ninkovich et al., 1966). Using the zone magnetization model (Niitsuma, 1977), the intensity drop can be explained as the cancellation of the components magnetized in the opposite direction. The width of the remanent intensity drop is equivalent to the thickness of lock-in zone if a duration of the intensity drop of the geomagnetic

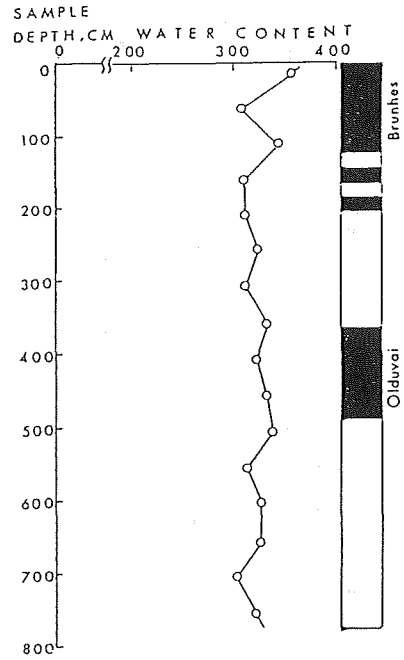

Fig.2 Water content (dry base) of Core P171 (after Tsurusaki and Saito, 1982). Paleomagnetic result is from Joshima (1982).

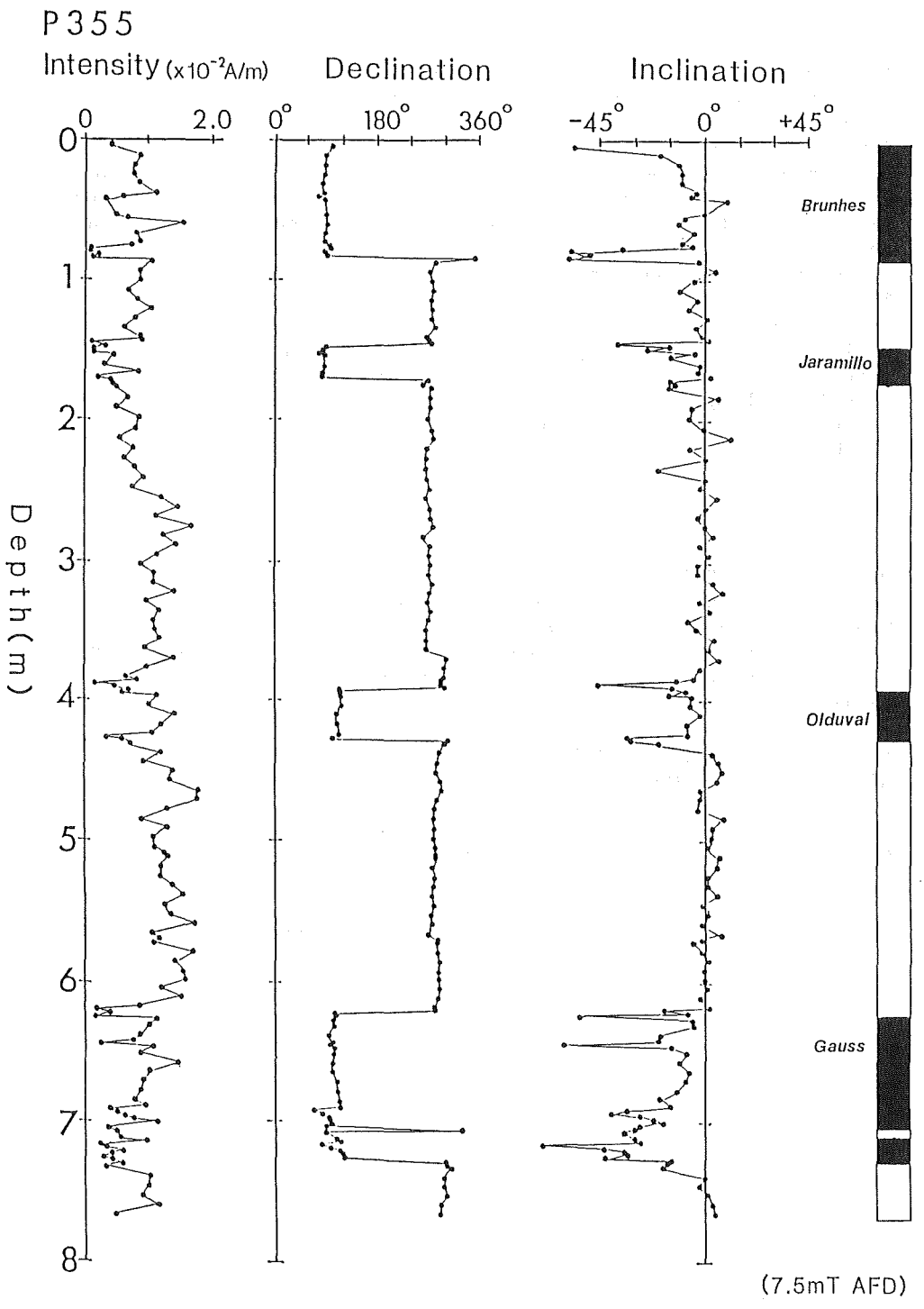

Fig.3 Remanent magnetization of Core P355 after cleaning by peak alternating field of 7.5 mT. Declination is relative.

field at a polarity change is short enough compared with the time interval which corresponds to the thickness of the lock-in zone. This model is applied to Core P355 obtained from the site close to that of Core B80 (Table.1). Most part of this core is also composed of homogeneous siliceous fossil rich clay. Remanent magnetization after cleaning by alternating field of 7.5 mT in peak field is shown in Fig.3. Magnetic reversal sequence from the Brunhes epoch to the Gauss epoch is identified by siliceous microfossils. As shown in figure, the width of the remanent intensity drop is 10 to 15 cm in this core. The effect of the field intensity decrease at a polarity transition can be ignored because only about 1cm thick sediments would deposit during it at a sedimentation rate of 2 to 3 m/Ma (the mean of this core) if a period of 5,000 years of the weak field intensity at a polarity change is assumed. This result well agrees with the thickness of the lock-in zone estimated from the surface sediments of the box core.

References

Hamano, Y. (1980) Earth Planet. Sci. Lett., 51, 221.

Joshima, M. (1982) Geol. Surv. Japan Cruise Rept., No.18, 276.

Kent, D.V. (1973) Nature, 246, 32.

Kinoshita, Y., K.Handa, K.Tsurusaki, S.Nakao and T.Moritani (1981) Geol. Surv. Japan Cruise Rept., No.17, 251.

Løvlie, R. (1974) Earth Planet. Sci. Lett., 21, 315.

——— (1976) Earth Planet. Sci. Lett., 30, 209.

Niitsuma, N. (1977) Rock Magn. Paleogeophys., 4, 65.

Ninkovich, D., N.Opdyke, B.C.Heezen and J.H.Foster (1966) Earth Planet. Sci. Lett., 1, 476.

Otofuji, Y. and S.Sasajima (1981) Geophys. J. R. astr. Soc., 66, 241.

Tsurusaki, K. and T.Saito (1982) Geol. Surv. Japan Cruise Rept., No.18, 124.

(to be submitted to Mar. Geol.)

ELECTRON MICROPROBE AND THERMOMAGNETIC ANALYSIS
OF BASALT SAMPLES FROM HOLE 597C

Tadashi NISHITANI

Institute of Mining Geology, Mining College,
Akita University, Akita 010, Japan

1. Introduction

Electron microprobe and thermomagnetic analysis of selected basalt samples from Hole 597C were performed. The main purpose of this report is to investigate and estimate the degree of oxidation using the ratio of Fe to Ti and Curie temperature, which is obtained from thermomagnetic curves.

2. Results of electron microprobe analyses

Twenty-five samples were selected and 204 points were analysed using an electron microprobe analyzer (JXA-5). Analyzed components are FeO, TiO_2, Al_2O_3, MgO, MnO, CaO, SiO_2 and K_2O. Qualitative analysis showed no trace of Na (sodium) and V (vanadium). Some samples were analysed quantitatively for the components of As (arsenic) and S (sulfer); however, their quantities were not detected except as pyrrhotite. Correction factors were calculated according to Bence and Albee (1968).

Figure 1 (a),(b) shows the variation of each component as a function of depth. Bars in these figures indicate standard deviations. The weight percentages of MnO, CaO, SiO_2 and K_2O are almost constant. Generally, the values of Al_2O_3 and MgO decrease with depth of the hole.

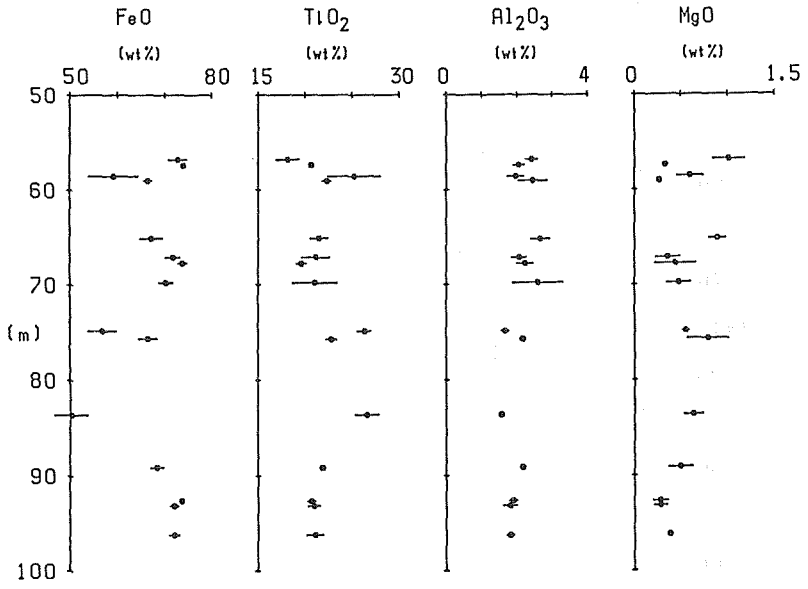

Fig. 1 (a) Variation of components, FeO, TiO_2, Al_2O_3 and MgO as a function of depth.

The ratio of Fe and Ti is calculated and is shown in Table 1 as Fe/(Fe+Ti). The x values can be obtained in the $FeO-Fe_2O_3-TiO_2$ system ignoring other components. Fe/(Fe+Ti) and x are represented as a function of depth (Fig. 2). This figure shows that the titanomagnetite composition (x) of Hole 597C is generally 0.6 - 0.7; the mean value of x is 0.68 ± 0.12. This value is similar to that reported in the previous DSDP samples.

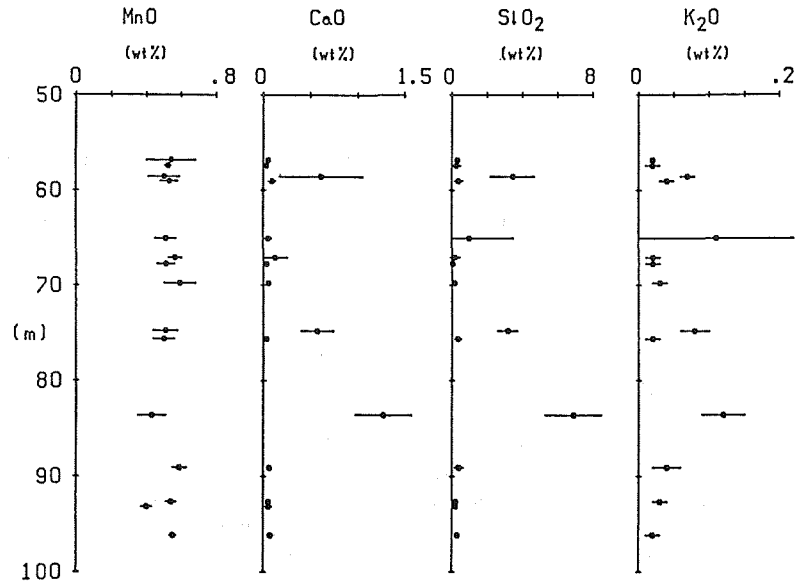

Fig. 1 (b) Variation of components, MnO, CaO, SiO_2 and K_2O as a function of depth.

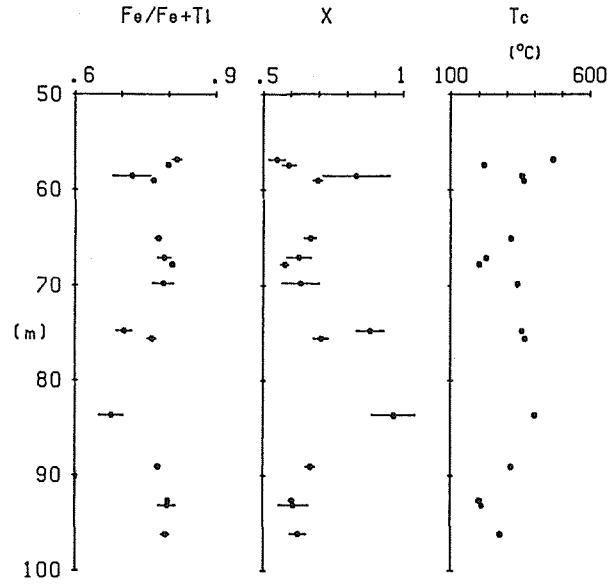

Fig. 2 The ratio of Fe and Ti, x values and Curie temperature (T_c).

3. Thermomagnetic analysis

Thermomagnetic curves were obtained for 24 samples in a magnetic field of 4 kOe. A weight of 200 - 400 mg of sample was heated in the balance, which was constantly evacuated (below 1 x 10^{-5} Torr), at temperatures up to 650 °C. Some thermomagnetic curves are shown in Figs. 3, 4 and 5.

As indicated by the existence of lamella, it is inferred that samples from deeper than 100 m had been affected by high-temperature oxidation. For example, the thermomagnetic curves of 597C 9-3 88-91 (113.39 m) and 597C 9-4 103-106 (115.05 m) show high Curie temperature in a heating process and the heating and cooling curves are almost the same, which indicate the effect of high-temperature oxidation (Fig. 3). All samples below 100 m show a similar tendency to high-temperature oxidation.

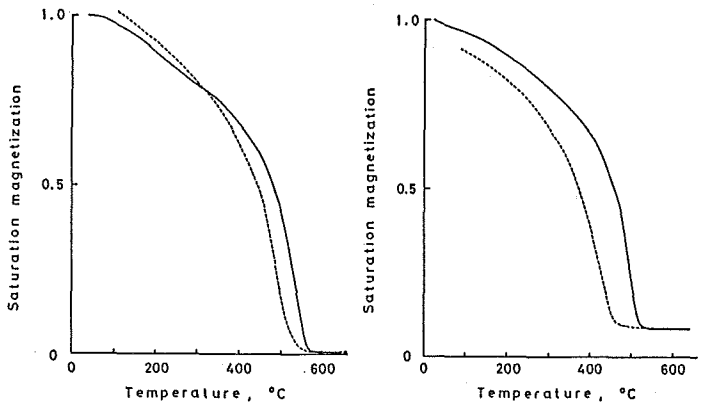

Fig. 3 Thermomagnetic curves, 597C 9-3 88-91 (left) and 9-4 103-106 (right). The solid line indicates heating process and the dotted line indicates cooling process.

Heating curves of 597C 3-1 131-134 (56.83 m) and 597C 4-1 60-63 (65.12 m) are cone-shaped at temperatures above 400 °C and cooling curves, whose Curie temperatures are above 500 °C, rise sharply (Fig. 4). These curves are typical examples which were affected by low-temperature oxidation.

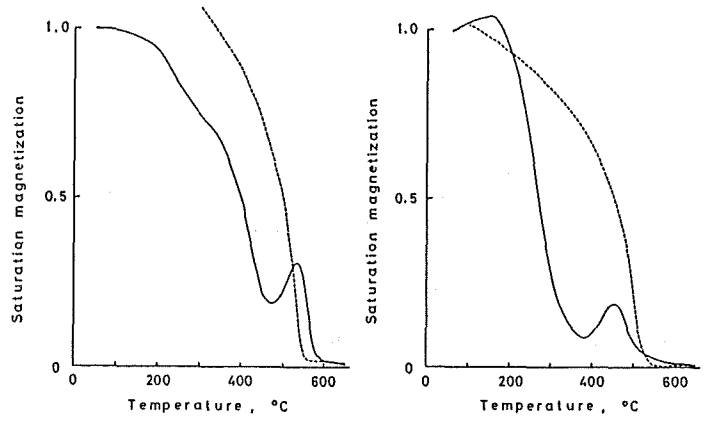

Fig. 4 Thermomagnetic curves, 597C 3-1 131-134 (left) and 4-1 60-63 (right).

On the other hand, samples 597C 4-3 27-30 (67.79 m) and 597C 7-1 115-118 (92.67 m) showed little effect from low-temperature oxidation, as thermomagnetic curves are almost interchangeable and indicating low Curie temperatures of 160 - 210°C (Fig. 5).

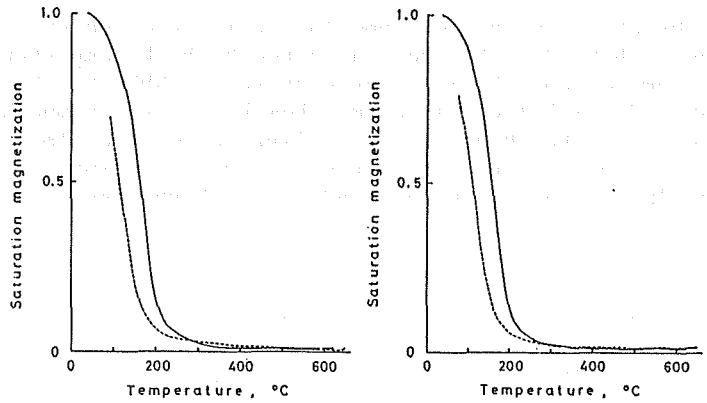

Fig. 5 Thermomagnetic curves, 597C 4-3 27-30 (left) and 7-1 115-118 (right).

Table 1. The ratio of Fe and Ti, x, Curie temperature and oxidation parameter.

sample	Fe/(Fe+Ti)	x	T_1	T_2	T_3	z_1	z_2	depth (m)
3-1 131-134	0.817 (0.010)	0.550 (0.030)	468	578	545	0.90	0.33 (0.42)	56.83
3-2 40-43	0.799 (0.002)	0.594 (0.025)	219		162	0.18	-0.04 (0.17)	57.42
3-3 5-8	0.722 (0.040)	0.834 (0.119)	356	677	541	-	1.31 (0.36)	58.57
3-3 52-55	0.768 (0.006)	0.697 (0.017)	364	589	538	0.77	1.03 (0.18)	59.04
4-1 60-63	0.777 (0.007)	0.669 (0.021)	315	506	518	0.60	0.74 (0.23)	65.12
4-2 111-114	0.790 (0.014)	0.629 (0.043)	226		350	0.30	0.25 (0.19)	67.13
4-3 27-30	0.807 (0.005)	0.579 (0.016)	201		160	0.10	0.10 (0.21)	67.79
4-4 76-79	0.788 (0.022)	0.635 (0.067)	340	518	492	0.62	0.45 (0.12)	69.78
5-1 129-132	0.706 (0.016)	0.883 (0.049)	355	577	545	-	1.71 (0.41)	74.81
5-2 63-66	0.764 (0.009)	0.708 (0.027)	366	592	546	0.78	0.93 (0.32)	75.64
6-1 109-112	0.678 (0.026)	0.966 (0.077)	401	586	550	-	2.23 (0.31)	83.61
6-5 58-61	0.777 (0.006)	0.670 (0.017)	316	563	532	0.61	0.70 (0.23)	89.10
7-1 115-118	0.798 (0.004)	0.605 (0.012)	200		166	0.13	0.002 (0.03)	92.67
7-2 16-18	0.797 (0.018)	0.610 (0.053)	210		163	0.18	0.31 (0.10)	93.17
7-4 18-21	0.792 (0.009)	0.625 (0.028)	275	508	483	0.40	0.23 (0.10)	96.20
8-3 130-133	-	-	500		408	-	-	104.82
8-4 102-105	-	-	484		382	-	-	106.04
8-7 9-12	-	-	449		422	-	-	109.61
9-3 88-91	-	-	556		519	-	-	113.39
9-4 103-106	-	-	506		456	-	-	115.05
10-1 112-115	-	-	504		335	-	-	119.64
10-5 84-87	-	-	492		502	-	-	125.36
10-7 42-45	-	-	497		449	-	-	127.93
11-4 62-64	-	-	508		308	-	-	132.63

Note : T_1, the first Curie temperatures observed during heating.
T_2, the highest Curie temperatures observed during heating.
T_3, Curie temperatures observed during cooling.
z_1, oxidation parameters determined using the T_c-z diagram of Nishitani and Kono (1983).
z_2, oxidation parameters determined by electron microprobe analysis assuming that the difference 100 minus the total percentage by weight is excess oxygen.
Parenthesis means standard deviation.

4. Estimation of the oxidation parameter

The oxidation parameter z can be estimated from the T_c-z diagram of Nishitani and Kono (1983), using the x values obtained by microprobe analyses and the Curie temperatures obtained from thermomagnetic curves. However, Nishitani (1981) showed that the Curie temperature decreases as the amount of Al and/or Mg increases. Electron microprobe analyses show that the amount of Al_2O_3 in Hole 597C basalts is much greater than the amount of MgO, so the effect of MgO is ignored here. The amount of Al_2O_3 is about 2% by weight, which may decrease the Curie temperature by a maximum of 50°C. Thus the Curie temperatures determined from thermomagnetic curves may be offset due to the presence of Al_2O_3, and estimates of the quantity of the titanomagnetite oxidation parameter z may consequently be in error.

There is another way to calculate the oxidation parameter. This is to assume that the difference of 100 minus the total percentage by weight is excess oxygen. Values obtained by this method are shown in Table 1 as z_2. However, this method leads to excessive error: Sample 3-2 40-43 indicates negative oxidation state, and samples 3-3 5-8, 3-3 52-55, 5-1 129-132, and 6-1 109-112 indicate values greater than one. It is therefore assumed here that better estimates of the oxidation parameter can be obtained using Curie temperature and the ratios of Fe and Ti, although the effect of impurities is ignored. The amounts of the oxidation product so obtained are listed in Table 1 as z_1 and plotted on Fig. 6. The z values vary widely, but they have a tendency to decrease as depth increases.

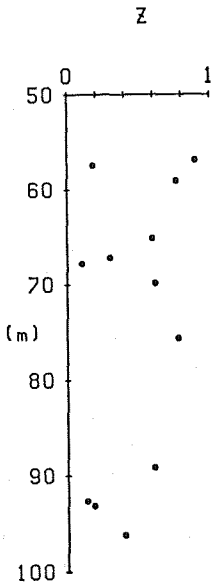

Fig. 6 Oxidation parameter (z) as a function of depth.

As already described, samples from deeper than 100 m had been affected by high-temperature oxidation considering a microscopic observation of lamellae and of the characteristics of the thermomagnetic analysis. We can conclude that the magnetic properties of Hole 597C change at the sub-bottom depth of 100 m and that low-temperature and high-temperature oxidation processes prevail at above 100 m and at below 100 m, respectively.

References

Bence, A.E. and L.L. Albee (1968) J. Geology, 76, 382.
Nishitani, T. (1981) J. Geomag. Geoelectr., 33, 171.
Nishitani, T. and M. Kono (1983) Geophys. J. R. astr. Soc., 74, 585.

ON THE IRREVERSIBLE CHANGE TO A SLIGHTLY LESS MAGNETIC PHASE IN THE THERMOMAGNETIC CURVE

Eiichi KIKAWA

Earthquake Research Institute, University of Tokyo
Tokyo 113, Japan

1. Introduction

At temperatures of several hundred degrees centigrade titanomaghemites which are metastable phases unmix(invert) to a mixture of two(or more) stable phases on a laboratory time scale. On the basis of above fact , an interpretation of the characteristic irreversible change in the thermomagnetic curve in submarine basalts (Type I Js-T curve, hereafter, see Fig. 1) has been proposed by Ozima and Larson (1970), Ozima and Ozima (1971) and Readman and O'Relly(1972). Moderately oxidized titanomaghemites commonly unmix to titanomaghemite plus ilmeno-hematite in case of Type I Js-T curve,causing an increase in both saturation magnetization and Curie temperature. Unmixing of cation deficient spinels is usually manifested by an irreversible change in Js-Tcurve during heating. Type II Js-T curve (Fig. 1) is one of the other typical irreversible type. In type I Js-T curves, the change is to a more magnetic phase; in type II Js-T curves to a slightly less magnetic phase. So far, many curves of type II have not be interpreted clearly. An attept is made to interpret them in this paper.

Irreversible character of Type II Js-T curve may be due to phase change of included titanomaghemites during the heating process. Therefore samples showing typical Type II Js-T curves were prepared as polished thin sections and coated with a thin carbon layer for carrying out chemical analyses of contained titanomaghemites before and after the thermal treatment.The instru-

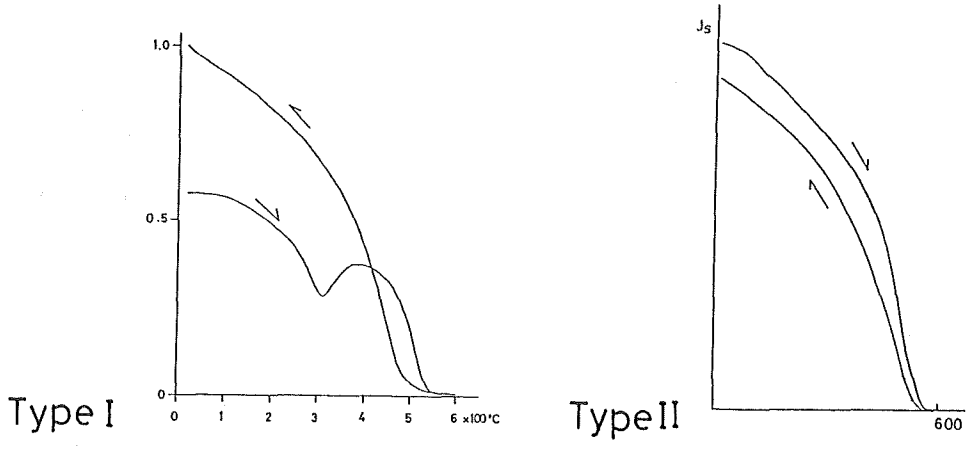

Fig. 1. Typical examples of irreversible thermomagnetic curves.

ment used was a JEOL JCXA-733 electron microprobe analyser located at the Ocean Research Institute, University of Tokyo. Sixty one measurements were made and all grains were analyzed for Fe,Ti,Al,Mg,Mn,Cr,V, Ni, Na and Si. Finally the chemical compositions measured were projected on the FeO-Fe_2O_3-TiO_2 ternary diagram for futher consideration.

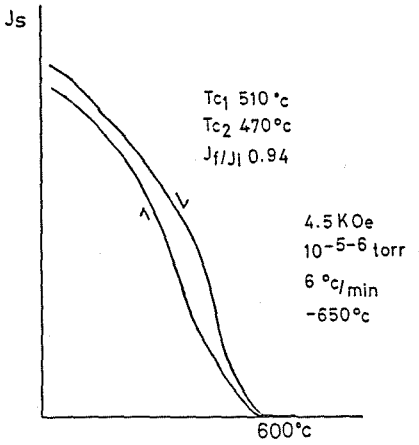

Fig. 2. Thermomanetic curve of the sample,DR3302B. It reveals a typical Type II.

2. Results of Experiments

1) Before the thermal treatment

Measured sample is a basaltic andesite, DR3302B from Daruma Volcano(late lava flow) situated in the northwestern part of the Izu Peninsula. Chemical compositions of(hemo)ilmenite (α phase), titanomagnetite (β phase) and titanomaghemite (γ phase), which were all appreciated by the microscopic observation, were measured(Fig. 2a,b). Fig. 3 summarizes the results. As seen in Fig. 3,β phase and γ phase clearly distribute apart from each other in the diagram. Curie temperature of 510°C obtained from the heating process is consistent with that of the most oxidized γ phase compositions determined from the contours of equal Curie temperature offered by Nishitani and Kono(1983).

2) After the thermal treatment

The grains which were considered to have originally been titanomaghemites were analyzed. Fig. 4 summarizes the results and indicates Curie temperature of cooling process of 470°C is in consistency with the value expected from the compositions of most oxidized γ phase.

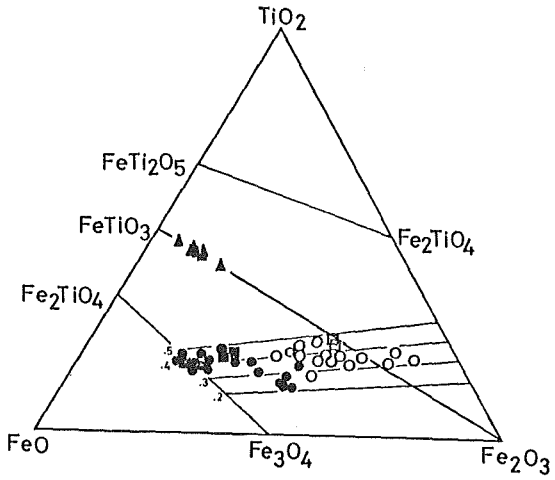

Fig. 3. Chemical compositions before the thermal treatment projected on the ternary diagram. Solid circle: titanomagnetite, Open circle: titanomaghemite, Solid triangle:(hemo)ilmenite.

3. Interpretation

Decrease in both Curie temperature and saturation magnetization due to the thermal treatment must be explained for the Type II Js-T curves. From Figs. 3 and 4, the decrease in Curie temperature can be interpreted by comparing the chemical compositions obtained with the contours of equal Curie temperature. It appears impossible, however, to interpret the decrease in saturation magnetization from these results. Increase in saturation magnetization would rather be expected from the experimental results. In the polished thin section made from the thermal-treated sample,sub-micro grains with length of less than 1μm within one host grain can be recognizable. Provided that the sub-micro grains were products of the phase change of the titanomaghemites, chemical compositions analyzed were average of each sub-micro grain. Chemical compositions of each sub-micro grains were impossible to be measured because the size of the grains is too small for the microprobe analysis.

Inoue (1982) observed that the unmixed intergrowth of exsolution lamellae of ilmeno-hematite and ilmenite in the titanomaghemite grain caused by heating is homogenized to Ti-richer titanomagnetite at temperature between 500 °C and 800 °C and called this phenomenon "mixing". A qualitative interpretation of decrease in both Curie temperature and saturation magnetization in this case seems to be made by mixing. Because Ti-richer titanomagnetite produces both lower Curie temperature and smaller saturation magnetization than the original phase. For further quantitative investigation, various parameters (for example effects of the grain size, etc.) must be essential and now experiments are being carried out.

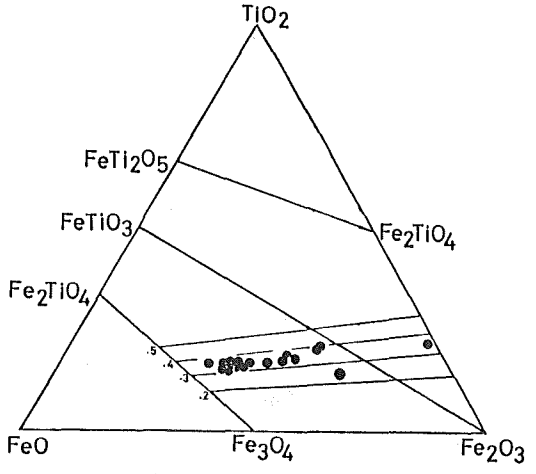

Fig. 4. Chemical compositions of the grains considered to have been titanomaghemites after thermal treatment are projected on the ternary diagram.

References

Inoue, Y. (1982) J. Geomag. Geoelectr., 34, 431

Nishitani, T and M. Kono(1983) Geophys. J. R. astr. Soc., 74, 585

Ozima, M. and E.E.Larson(1970) J. Geophys. Res., 75, 1003

Ozima, M. and M. Ozima (1971) J. Geophys. Res., 76, 2051

Readman, P.W. and W. O'Reilly (1972) J.Geomag.Geoelectr., 24, 69

PROGRESS NOTE ON THERMOMAGNETIC ANALYSIS OF SOME IRON-SANDS OF WEST JAPAN

Haruo DOMEN

Institute of Physical Sciences, Faculty of Education,
Yamaguchi University, Yamaguchi 753, Japan

Therty years ago, the present author studied on the effect of grinding to the thermomagnetic charachteristics of rock-forming ferromageetic grain such as the single crystal of magnetite and iron-sand (Domen, 1954, 1955). And also twenty years latter, thermomagnetic and X-ray analyses of iron-sands sampled nationwidely, from Hokkaido to Kyushu Island, Japan were carried out and only a part of these results obtained was published (Domen, 1977a).

In this brief note, the present author shows likewise result newly obtained of some iron-sands from the west Japan.

Specimen and method

Test specimens submitted to the present study are from 6 sites in west Japan: two from Yamaguchi Prefecture; (1) Kiwado, northern coast, (2) Higashi-Kiwa, southern coast and 4 from Kyushu Island, (3) Top of Mt. Aso, (4) Kusa-Senri, within the outer crater of Mt. Aso closed to site (3), (5) Nada Coast, southeastern coast of Kunisaki-Peninsula, (6) Hime-Shima Islet, eastern nighbour of Kunisaki-Peninsula.

The previous study (Domen, 1977a) covered all of those sampling sites, where the specimens submitted to the present study were re-sampled afterwards.

Thermomagnetic sanalysis was carried out by means of a home-made micro balance (Domen, 1968, 1977b) and less than 100 mg of specimens were analyzed at once in each treatment. X-ray analysis was also performed of each specimen.

Firstly, the specimen from each site was measured as a bulk, say in natural grain of specimen, sometime classified acording to grain sizes. Then, samples were ground into fine powder in the open air and sifted, and analyzed thermomagnetically.

Result

Obtained results of thermomagnetic analysis are shown in figures 1-6, and numerals of these data are shown in Table 1, in which mean lattice constants of each specimen were also sited. The chemicall composition of each sample were estimated by Curie point and lattice parameter obtained mentioned above are plotted in the ternary diagram as in Fig. 7.

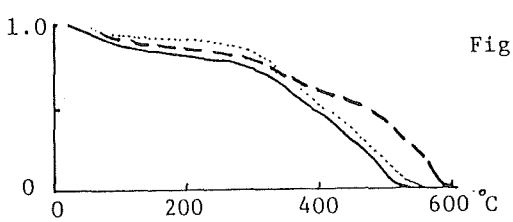

Fig. 1. Js - T curves for (1) Kiwado (natural)

— 100 meshes
--- 200 "
..... less than 250 meshes

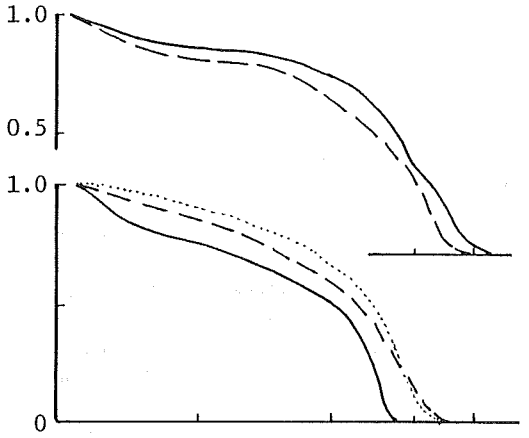

Fig.2. Higashi-Kiwa

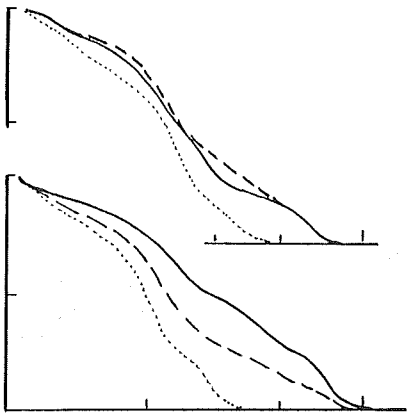

Fig.3. Top of Mt. Aso

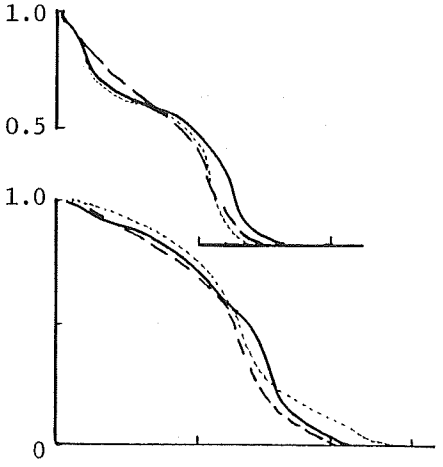

Fig.4. Kusa-Senri, Mt. Aso

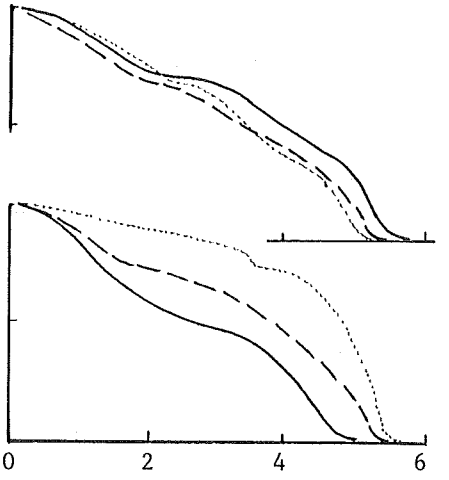

Fig.5. Nada, Kunisaki Pen.

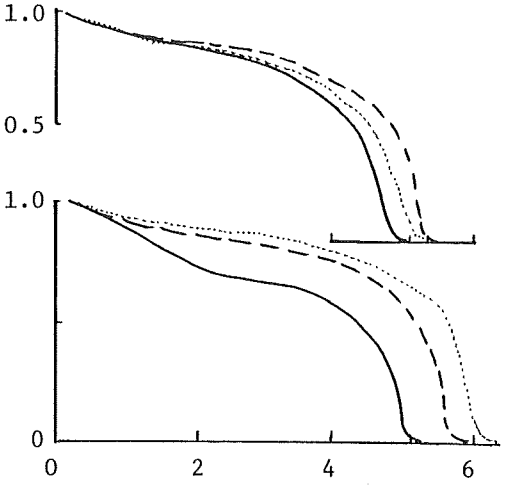

Fig. 6. Hime-Shima

Figs.2~6. Typical examples of Js-T curve (initial heating cureves only).
Top of each figure stands for the natural grain.
Bottom for pulverized one.
Abscissa; Temper. in °C,
Ordinate; Js/Jo.
Hex = 3,000 Oe,
in open air.

— 100 meshes
- - - 200 "
····· 250 m. & less

Table 1. Main Curie Point and Lattice Constant of Yamaguchi and Kyushu Island, west Japan.

Sampling Site	Main Curie Point (Mean value for natural grains)	Lattice Constant
Yamaguchi Iron-sand		
(1) Kiwado Northern coast	580 °C	8.40 Å
(2) Higashi-Kiwa southern coast	550	8.39
Kyushu Iron-sand		
(3) Mt. Aso Top of,	370	8.41
(4) Mt. Aso Kusa-Senri	270	8.41
(5) Nada Kunisaki Pen.	520	8.39
(6) Hime-Shima	533	8.39

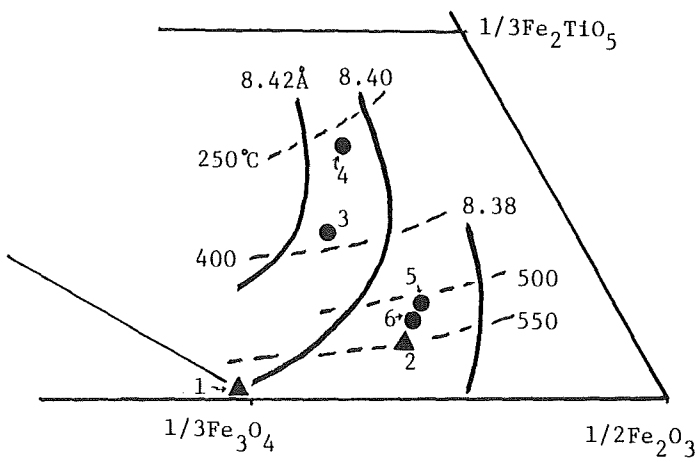

Fig.7. Chemical composition estimated by Js-T and X-ray analyses (ternary diagram after O'Reilly & Readman, 1971).

References

Domen, H., 1954. Bull. Fac. Educ., Yamaguchi Univ., 4(1), 7-13 (in Japanese).
" 1955. Kagaku (Iwanami Book Co.,Ltd.), 25(2), 88-89 (in Japanese).
" 1968. Bull. Fac. Educ., Yamaguchi Univ., 17(2), 19-21.
" 1977a. Rock Mag. Paleogeophys., 4, 5-7.
" 1977b. Bull. Fac. Educ., Yamaguchi Univ., 27(2), 17-23.
O'Reilly, W. and Readman, P.W., 1971. Z. Geophys., 37:321.

THERMAL HISTORY OF THE RYOKE BELT BY FISSION TRACK DATING

Takahiro TAGAMI and Susumu NISHIMURA

Department of Geology and Mineralogy, Kyoto University
Kyoto 606, Japan

Fission track dating has been carried out on zircon and apatite separated from the granitic rocks in the Ryoke belt. Samples were taken from following two routes which are nearly perpendicular to the Median Tectonic Line (MTL). One route is located from Ichishi to Iinan in Mie prefecture, Kinki district, and the other route is from Sakuma in Shizuoka prefecture to Ena in Gifu prefecture, Chubu district (Fig.1).

Dating procedure was mainly according to Naeser (1978) and Nishimura (1981). External detector method was applied to natural surface of zircon and to polished internal surface of apatite (Fig.2). Zircon crystals were etched by an equivolume 48%HF:98%H_2SO_4 etchant for 7 to 19 hours at 180°C under the vapor pressure in a teflon-stainless steel double walled bomb. Apatite crystals were etched with 1%HNO_3 for 2 to 6 minutes at 25°C. Muscovite detectors were etched with 48%HF for 20 to 40 minutes at 18 - 25°C. Geometry factor of 1.0 was used for zircon ($\rho 2\pi/\rho$e.d.) and 0.5 for apatite ($\rho 4\pi/\rho$e.d.).

The dating results are presented in Table 1 and the relation between the fission track age and the distance from the MTL is shown in Fig.3. Fission track zircon ages are approximately consistent with each other, and the mean value of them is 62 ± 5 Ma. Fission track apatite ages from the area more than 8 km apart from the MTL roughly coincide around 30 Ma. In the area within 8 km of the MTL, the apatites indicate much younger ages of 2 - 20 Ma.

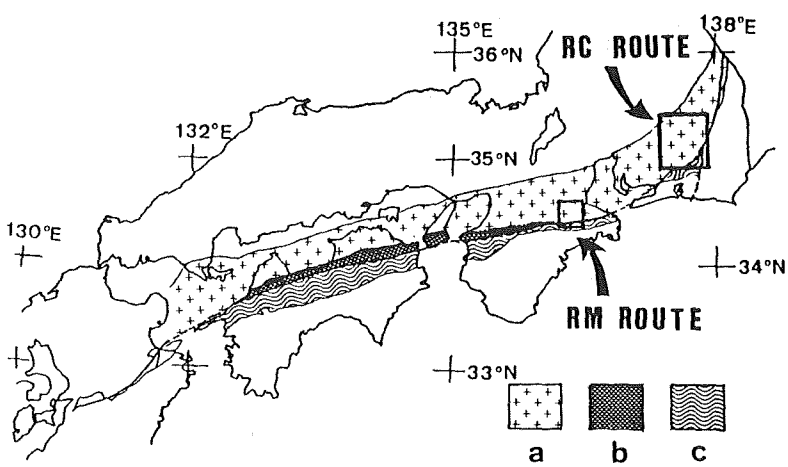

Fig.1 Locality of the two sampling routes; RM route and RC route.

a: the Ryoke belt

b: Izumi Group

c: the Sanbagawa belt

Fig.2 Experimental procedures

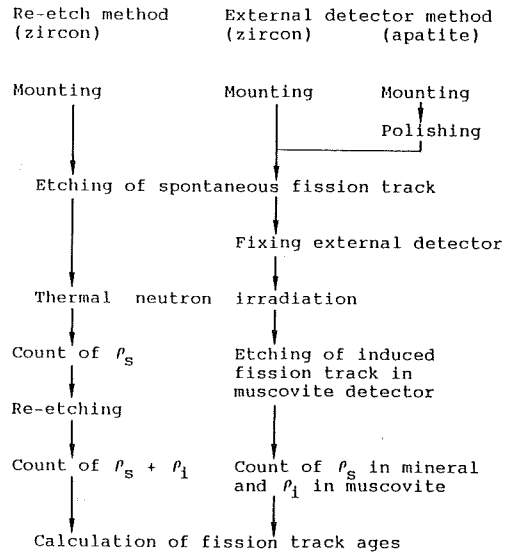

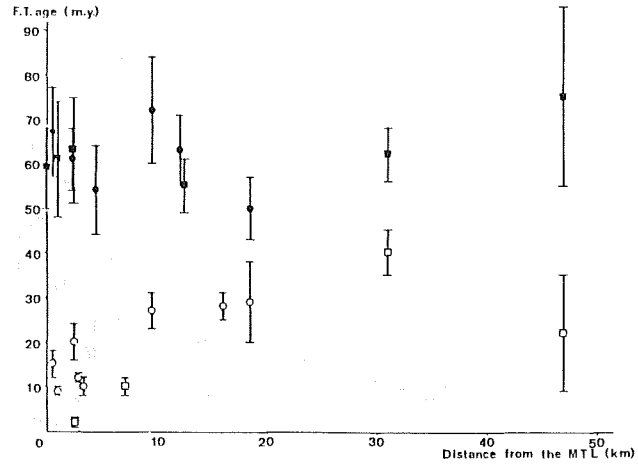

Fig.3 Fission track ages as a function of distance from the MTL.

● : fission track zircon age from RM route.

■ : fission track zircon age from RC route.

○ : fission track apatite age from RM route.

□ : fission track apatite age from RC route.

Table 1

Fission track ages calculated from totoal number of fission tracks (Naeser et al., 1979)

Sample code	Mineral	ρs	ρi	Φ	T	s	N	U
RM-01	zircon	3.35×10^6 (550)	2.05×10^6 (585)	4.84×10^{14} (2815.5)	47.1	2.9	7	157
03	"	3.11 " (996)	1.35 " (751)	"	66.3	3.4	12	103
04	"	3.24 " (1609)	1.36 " (777)	"	68.6	3.3	11	104
05	"	4.90 " (609)	2.57 " (509)	"	54.9	3.5	7	196
07	"	3.03 " (656)	1.44 " (498)	"	60.6	3.8	9	110
09	"	4.09 " (863)	1.79 " (609)	"	65.8	3.7	10	137
RC-01	"	5.89 " (359)	2.92 " (414)	"	58.1	4.3	6	223
02	"	3.36 " (559)	1.57 " (429)	"	61.6	4.1	11	120
03	"	4.10 " (692)	1.96 " (673)	"	60.2	3.5	10	150
05	"	4.60 " (602)	2.48 " (583)	"	53.4	3.3	9	190
07	"	4.07 " (1749)	1.93 " (1401)	"	60.7	2.5	17	148
08	"	5.94 " (705)	2.48 " (464)	"	69.0	4.3	8	190
RM-01	apatite	2.41×10^5 (123)	1.76×10^6 (1249)	6.45×10^{15} (2265)	26.3	2.5	10	10.6
02	"	2.87 " (336)	1.95 " (2394)	"	28.2	1.7	12	11.8
04	"	2.11 " (330)	1.51 " (2466)	"	26.8	1.7	12	9.1
06	"	7.10×10^4 (130)	1.70 " (3195)	"	8.01	.74	18	10.3
07	"	9.84×10^5 (427)	9.96 " (4570)	6.59×10^{15} (2184)	19.4	1.1	16	58.9
09	"	3.26 " (207)	4.51 " (4155)	"	14.2	1.1	15	26.7
10	"	1.92 " (517)	3.42 " (10474)	"	11.0	0.5	36	20.2
11	"	1.82 " (126)	3.89 " (2753)	"	9.17	.86	12	23.0
RC-03	"	6.44×10^3 (10)	6.45×10^5 (1132)	"	1.96	.62	13	3.8
04	"	1.38×10^5 (310)	2.92×10^6 (6626)	"	9.27	.57	18	17.3
07	"	2.84 " (672)	1.38 " (3429)	"	40.3	1.9	18	8.2
08	"	5.67×10^4 (88)	5.77×10^5 (1062)	"	19.3	2.2	11	3.4

ρs: spontaneous fission track density calculated from total number of tracks and total counted area (tracks/cm²)

ρi: induced fission track density calculated from total number of tracks and total counted area (tracks/cm²)

Φ : thermal neutron dose (neutrons/cm²)

Numbers in parenthes in the row of ρs, ρi and Φ shows the number of tracks counted to determine the track density or thermal neutron dose.

T : fission track ages calculated from ρs and ρi (Ma)

s : standard error of the calculated age (Ma)

N : number of counted grains

U : uranium concentration (ppm)

Considering the closure temperature of 175°C for zircon and 105°C for apatite (after Harrison and McDougall 1980), almost constant cooling rates of 2.5 - 3.0°C/km were calculated in the area more than 8 km apart from the MTL from 60 Ma to the present. This fact can be explained by the uplift and erosion in the area. The mean uplift rate is estimated to be about 0.09 mm/yr.

The cooling rates calculated from the apatite ages are significantly large in the area within 8 km of the MTL. In order to interpret this fact, two alternative models are possible:

i) There have been some differential uplifts between the regions within 8 km of the MTL and more than 8 km apart from the MTL.

ii) The thermal gradient in the vertical direction has been larger than the general value near the MTL. In this case, the heat source of the large thermal gradient is considered to be the shear heating of the MTL at 2 -20 Ma.

References:

Harrison, T.M.and I.McDougall (1980) Geochim. Cosmochim. Acta, 44, 1985.
Naeser, C.W.(1978) U.S. Geol. Surv. Open-File Rep., 76.
Naeser, C.W., A.J.W.Gleadow and G.A.Wagner (1979) Nucl. Tracks, 3, 133.
Nishimura, S. (1981) Nucl. Tracks, 5, 157.

NOBLE GAS SYSTEMATICS IN LAVAS AND A DUNITE NODULE FROM RÉUNION AND GRANDE COMORE ISLANDS, INDIAN OCEAN

Ichiro KANEOKA*, Nobuo TAKAOKA**
and B.G.J. UPTON***

* Geophysical Institute, University of Tokyo, Bunkyo-ku, Tokyo 113, Japan
** Department of Earth Sciences, Yamagata University, Yamagata 900, Japan
*** Grant Inst. of Geology, Univ. of Edinburgh, Edinburgh EH9 3JW, U.K.

The noble gases would serve as a unique indicator to clarify the characteristics of the source material of a magma. From $^3He/^4He$ and $^{40}Ar/^{36}Ar$ ratios, we can infer the occurrence of several typical sources for noble gases and mixing processes between them (Kaneoka, 1983; Kaneoka and Takaoka, 1980; Kyser and Rison, 1982). MORB (Mid-Ocean ridge basalt) is characterized by relatively uniform $^3He/^4He$ ratios of $(1-1.4) \times 10^{-5}$ together with high $^{40}Ar/^{36}Ar$ ratios of more than 5,000 in many cases. Compared with the values for MORB, higher $^3He/^4He$ ratios are observed for samples from typical hot-spot areas such as Hawaii, Iceland and Yellowstone (eg.) Craig et al., 1978; Kaneoka and Takaoka, 1980; Kyser and Rison, 1982; Polyak et al., 1976). However, samples from some other hot-spot areas such as Tristan da Cunha and Gough show lower $^3He/^4He$ ratios than that of MORB (Kurz et al., 1982). Hence, even among hot-spots, there seem to exist at least two isotopically different sources. Typical high $^3He/^4He$ ratios seem to be accompanied by relatively low $^{40}Ar/^{36}Ar$ ratios for samples from hot-spot areas, which appears to suggest the occurrence of a plume-type source which may still contain relatively large amounts of primordial components in terms of noble gas isotopes (Kaneoka, 1983; Kaneoka and Takaoka, 1980; Kyser and Rison, 1982). Both Réunion and Grande Comore are located in the Indian Ocean and have been regarded as hot-spots (Morgan, 1972; Wilson, 1973). Present study on noble gas isotopes on olivine phenocrysts of lavas from these islands has revealed that the source materials for Réunion lavas are similar to those of Hawaii and Iceland, whereas those of Grande Comore show closer affinity to Tristan da Cunha and Gough.

Réunion is a typical volcanic island, located in the western Indian Ocean, about 700 km east of Madagascar. It is built by two volcanoes, the extinct Piton des Neiges in the northwest and the still active Piton de la Fournaise in the southeast (Upton, 1982). Grande Comore is one of the volcanic islands which are located between Madagascar and African continent. Since both islands are regarded to be located on hot-spots (Morgan, 1972; Wilson, 1973), noble gas data for volcanic rocks from these islands would give us important information on noble gas characteristics of hot-spots in the Indian Ocean. To get information of noble gases on lava flows, olivine phenocrysts of more than 1 mm in size were carefully hand-picked from each sample and analysed by mass spectrometry. Experimentally it has been established that such large phenocrysts contain magmatic noble gases (eg.) Kaneoka and Takaoka, 1980; Kurz et al., 1982; Kyser and Rison, 1982). These samples represent relatively old products from Piton des Neiges (Re 78, Re 331) and recent ones from Piton de la Fournaise (Re 114) and Kartala volcano (Grande Comore)(72/GC/14), respectively. Since olivine phenocrysts contain relatively small amounts of noble gases, we used samples of more than 3 g for each analysis. For comparison, noble gases in one dunite nodule from Piton de la Fournaise (Re 496(16)) were also analysed.

Noble gas analyses were made on a mass spectrometer with a resolving power of about 600 to separate ^3He and $HD + H_3$ at the Yamagata University.

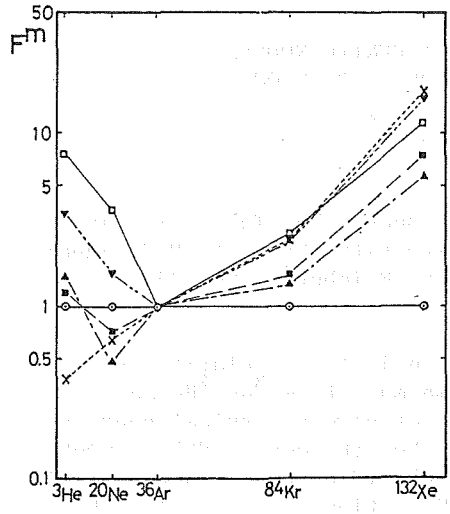

Fig. 1. Noble gas abundance patterns relative to ^{36}Ar for gases of Réunion and Grande Comore Island samples degassed at 1800°C. Except for ^3He, F^m is defined as $(^mX/^{36}Ar)_{sample}/(^mX/^{36}Ar)_{atmosphere}$, where ^mX indicates a noble gas isotope with the mass number m. For ^3He, F^m is defined as $(^3He/^{36}Ar)_{sample}/(^3He/^{36}Ar)_{planetary}$. Symbols : ⊙ = air (except for ^3He); ■ = Re 78 (olivine); ▲ = Re 114 (olivine); ▼ = Re 331 (olivine); □ = Re 496 (16)(dunite); x = 72/GC/14 (olivine).

Two temperature stepwise heating (700 or 750°C, 1800°C) was applied to remove secondary atmospheric components from a sample in the lower temperature fraction. Such experimental procedures are essentially the same as those reported before (Kaneoka and Takaoka, 1980).

All noble gas abundances together with isotopic ratios for lighter components (He, Ne, Ar) were measured. The elemental abundance patterns normalized to that of the atmospheric components are shown in Fig. 1 for the 1800°C fraction. For ^3He, however, $^3He/^{36}Ar$ is normalized to that of planetary component (0.00775).

As shown in Fig. 1, these samples are not always enriched in lighter noble gases such as Ne compared to ^{36}Ar, which are quite different from MORB (eg.) Dymond and Hogan, 1978). Compared with olivine of Loihi samples (Kaneoka et al., 1983), ^3He is relatively depleted except for a dunite nodule Re 496(16). However, all samples show relatively large enrichments of Xe compared to ^{36}Ar. Among present samples, the dunite nodule Re 496(16) shows larger enrichments in lighter noble gases compared with the other samples, suggesting the different mechanism for incorporating noble gases in this sample. The olivine phenocryst sample from Grande Comore 72/GC/14 seems to show systematical depletion of lighter noble gases to more degree than the heavier ones. This may reflect either the different characteristics of a noble gas source or secondary degassing process for this sample.

As shown in Fig. 1, the variation in the relative elemental ratios seems generally larger for lighter noble gases than the heavier ones. This probably reflects the larger mobility of lighter noble gases than those of heavier ones. Further, it implies that the elemental abundance patterns for lighter noble gases are more easily controlled by the secondary processes than the heavier ones. In this context, the relative enrichment of Xe compared with the atmosphere for all analysed samples would reflect the conditions of source materials and the processes where olivines were formed.

Our results indicate clear differences in the $^3He/^4He$ ratio between Réunion and Grande Comore. All analysed samples from Réunion show similar $^3He/^4He$ ratios of $(1.8 - 2.1) \times 10^{-5}$, which are definitely higher than that of MORB. By contrast olivine phenocrysts from a Grande Comore ankaramite show a distinctly lower $^3He/^4He$ ratio of 0.93×10^{-5}, which is still slightly lower than the averaged MORB value. Concerning $^3He/^4He$ ratios, similar results have been reported (Craig and Rison, 1982). Hence, coupled with present results, it is established that where $^3He/^4He$ ratios are concerned,

Réunion samples are similar to those of Hawaii and Iceland whereas Grande Comore samples are more like those of Tristan da Cunha and Gough. In this respect, it is interesting to note that $^{40}Ar/^{36}Ar$ ratios for these lava flows show still lower values than those of typical MORB values which generally exceed 5,000 (Dymond and Hogan, 1978). This situation is more clearly indicated in the $^{3}He/^{4}He$ vs. $^{40}Ar/^{36}Ar$ diagram (Fig. 2). From this diagram, we can definitely say that the source materials for lava flows of Réunion and Grande Comore are different on the basis of noble gas isotopes. For the Grande Comore ankaramite (72/GC/14), the $^{87}Sr/^{86}Sr$ ratio of 0.70393 ± 6 has been obtained (Notsu, personal communication). This value overlaps the lower value of the $^{87}Sr/^{86}Sr$ ratios reported for Réunion lava flows (Hedge et al., 1973). This implies that even if Sr isotopes show similar values, it would not always mean that those lavas were derived from similar source materials. Such differences probably reflect different chemical characters between noble gases and the other elements such as Sr together with the difference from radiogenic components due to different decay constants of parent radioactive elements.

As shown in Fig. 2, the three lava samples from Réunion show similar $^{3}He/^{4}He$ ratios with somewhat variable $^{40}Ar/^{36}Ar$ ratios. The variation in the $^{40}Ar/^{36}Ar$ ratio probably reflects the different degree of atmospheric contamination either in a magma reservoir or at a shallower depth. However, this case may be almost limited to sample Re 78. Samples Re 114 and Re 331 show rather similar values both for $^{3}He/^{4}He$ and $^{40}Ar/^{36}Ar$ ratios. Since

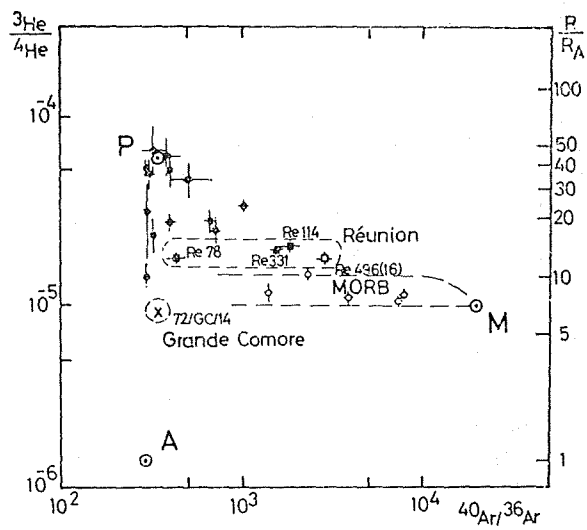

Fig. 2. The $^{3}He/^{4}He$ - $^{40}Ar/^{36}Ar$ diagram for samples from hot spot areas analysed by the authors (Kaneoka and Takaoka, 1980, 1984; Kaneoka et al., 1983) Samples include those reported here and those from Hawaii including Loihi, Iceland and Tahiti. P and M are tentatively assumed and A has definite values of the atmosphere as follows.

P : $^{3}He/^{4}He = 6 \times 10^{-5}$ (= 43 R_A), $^{40}Ar/^{36}Ar = 350$.
M : $^{3}He/^{4}He = 1 \times 10^{-5}$ (= 7.1 R_A), $^{40}Ar/^{36}Ar = 20{,}000$.
A : $^{3}He/^{4}He = 1.4 \times 10^{-6}$ (= R_A), $^{40}Ar/^{36}Ar = 295.5$.

Closed symbols indicate samples of olivine and clinopyroxene phenocrysts and open symbols those of ultramafic nodules.

these two samples represent quite different phases of magmatic activities both in space and time on Réunion, these coincidences in isotopic ratios may imply that these values represent typical values for magmatic sources beneath Réunion. Although we cannot preclude the possibility of some secondary atmospheric contamination the values are close to a mixing line between the assumed end members of P-type and M-type source materials (Kaneoka, 1983). In such a model, P-type source material is considered to represent that of a mantle plume and M-type that of MORB. Compared to Hawaii and Iceland, the variations in the observed $^{3}He/^{4}He$ ratios for the Réunion samples are much less, which may imply that the degree of mixing between the source materials is not so variable where noble gas isotopes are concerned. This may reflect relatively stable activity of the inferred mantle plume and/or the stable relationship between the mantle plume and the overlying M-type source materials.

In the present study, the dunite nodule Re 496(16) seems to be an exception. Although it shows a $^{3}He/^{4}He$ ratio similar to those of the lava flows, the $^{40}Ar/^{36}Ar$ ratio for this sample is higher than those of lava flows. As in the case for Loihi dunite nodules (Kaneoka et al., 1983), this nodule might have been derived from M-type source material originally and have been equilibrated with He in the sourrounding magma. The higher $^{20}Ne/^{36}Ar$ ratio in this sample may also support a different origin for the noble gases compared with the other samples from Réunion. However, petrogenetically and geologically there is a relatively close genetic relationship between the dunite and the oceanites (Upton and Wadsworth, 1972). Hence, this point must be clarified in a further work.

The noble gas data for the ankaramite from Kartala volcano, Grande Comore (72/GC/14) indicate different characteristics for the source material. The $^{3}He/^{4}He$ and $^{40}Ar/^{36}Ar$ ratios for this sample are similar to those observed for samples from island arc areas (Kaneoka and Takaoka, 1984). In the case of island arc materials, such values can be explained by the mixing among M-type, A-type and C-type source materials, where A-type and C-type source materials represent the atmospheric components and the crustal materials, respectively (Kaneoka and Takaoka, 1984). However, it is clear that Grande Comore is not located at a subduction area. Hence, apparent similarities in the $^{3}He/^{4}He$ and $^{40}Ar/^{36}Ar$ ratios may reflect either the old remains of such subducted materials beneath Grande Comore or other processes. As one of the possibilities in the latter case, the mixing between the mantle plume and the C-type material of old continental crustal material may be raised. Grande Comore Island is located between Africa and Madagascar which are conjectured to have been connected before separation by continental drift (Dietz and Holden, 1970). The relatively low $^{87}Sr/^{86}Sr$ ratio implies involvement of some M-type component.

Thus noble gas isotope studies have revealed that Réunion is grouped as a typical hot-spot area comparable with Hawaii and Iceland, whereas Grande Comore is a hot-spot of different type similar to Tristan da Cunha and Gough.

References

Craig, H. and Rison, W. (1982) EOS 63, 1144.

Craig, H., Lupton, J.E., Welhan, J.A. and Poreda, R. (1978) Geophys. Res. Lett., 5, 897.

Dietz, R.S. and Holden, J.C. (1970) J. Geophys. Res., 75, 4939.

Dymond, J. and Hogan, L. (1978) Earth Planet. Sci. Lett., 38, 117.

Hedge, C.E., Watkins, N.D., Hildreth, R.A. and Doering, W.P. (1973) Earth Planet. Sci. Lett., 21, 29.

Kaneoka, I. (1983) Nature, 302, 698.
Kaneoka, I. and Takaoka, N. (1980) Science, 208, 1366.
Kaneoka, I. and Takaoka, N. (1984) Isotope Geosci., in press.
Kaneoka, I., Takaoka, N. and Clague, D.A. (1983) Earth Planet. Sci. Lett., 66, 427.
Kurz, M.D., Jenkins, W.J. and Hart, S.R. (1982) Nature, 297, 43.
Kyser, T.K. and Rison, W. (1982) J. Geophys. Res., 87, 5611.
Morgan, W.J. (1972). Amer. Ass. Petrol. Geol. Bull., 56, 203.
Polyak, B.G., Kononov, V.I., Tolstikhin, I.N., Mamyrin, B.A. and Khabarin, L.V. (1976) Int. Assoc. Hydrol. Sci. Publ., 119, 15.
Upton, B.G.J. (1982) in The Oceans Basins and Margins (eds. E.M. Nairn & F.G. Stehli, Plenum Pub. Co.), 6, 585.
Upton, B.G.J. and Wadsworth, W.J. (1972) Contr. Mineral. Petrol. 35, 139.
Wilson, J.T. (1973) Tectonophysics, 19, 149.

MEAN IONOSPHERIC FIELD CORRECTION FOR MAGSAT DATA

Masahisa YANAGISAWA[1] and Masaru KONO[2]

1 Institute of Space and Astronautical Science, Komaba 4-6-1, Meguro-ku, Tokyo 153, Japan
2 Department of Applied Physics, Tokyo Institute of Technology, Ookayama 2-12-1, Meguro-ku, Tokyo 152, Japan

1. Introduction

The magnetic field observed by a near-earth satellite contains components due to sources both external (magnetospheric field) and internal (core field, induction field, crustal field, and ionospheric field) to the satellite orbit. If we wish to obtain the crustal magnetic anomalies from the satellite data, it is essential to identify and subtract field components of other origins. A good model of the main (core) field was already constructed from the analyses of the Magsat vector and scalar data (Langel et al., 1980). As this model, MGST(4/81), is expressed in terms of spherical harmonics up to the 13th degree and order, the internal magnetic field with wavelengths of about 3000 km or longer is represented by this model.

After the subtraction of the appropriate model field, there still remain induction, ionospheric, and magnetospheric fields, besides the anomaly field of crustal origin which we are seeking. As for the fields with origins external to the Magsat orbit, the main contributor is the equatorial ring current in the magnetosphere. The ring current field at ground level or at near-earth satellites can well be approximated by the first degree spherical harmonic $P_1(\cos\theta)$, where θ is the geomagnetic colatitude. This has already been shown by many authors by the expansion of the magnetic field data into zonal harmonics. The main part of the induction field is associated with the ring current and can also be approximated by the first term in spherical harmonic expansion. We show below that these two fields are also well defined for the Magsat data provided that the data for each half orbit is reasonably well distributed.

The most difficult problem in the satellite data reduction is to account for the field induced by currents flowing in the ionosphere. It is well known that a strong current system called Sq (solar daily quiet variation) current exists in the ionosphere centered at local noon meridian (e.g., Matsushita, 1967). The twilight sun-synchronous orbit of Magsat was originally selected to avoid the effect of Sq current system. However, it became clear that the effect of the ionospheric currents is by no means absent even at dawn or dusk meridians (Sugiura and Hagan, 1979). The most notable among such disturbance fields is the one which appears near dusk side equator, as discovered by Maeda et al. (1982).

In analysing satellite magnetic data, conventional methods for reducing these unwanted effects are to fit some numerical function to a continuous profile and subtract that. These are

called "path-by-path correction" in this article. Mayhew (1979) found large differences between magnetic profiles over North America obtained from closely spaced orbits of POGO satellite. He found that the path-to-path inconsistency was best accounted for by subtracting the best fitted quadratic function from each path. Meanwhile, Regan et al. (1981) showed that the subtraction of a four-term cosine series fitted to each complete half orbit improved the agreement of the data most effectively with those of adjacent or coincidental paths. They could certainly reduce inconsistencies among adjacent orbits. However, it was not at all clear why these corrections worked. The numerical functions fitted to the profiles were arbitrarily chosen and did not represent any physical reasoning nor an actual structure of the disturbance field.

It is the purpose of the present work to find a proper method of correction for the ionospheric field at dawn and dusk meridians, which yields meaningful magnetic anomaly maps from the Magsat data. We present here an approximation called the Mean Ionospheric Field Correction (MIFC), which takes into account a strong dependence of the disturbance field at the twilight meridians on the local dip latitude.

2. The Magnetospheric and Induction Fields

Investigator-B tapes distributed by Goddard Space Flight Center contain scalar and vector magnetic data at every 5 seconds, or at about 40 km intervals along the Magsat path. As the data with attitude errors larger than 20 arc seconds were discarded, the errors in the vector data are about 6 nT or less. First of all, the core field was subtracted from the data using the MGST(4/81) model which uses spherical harmonics of order up to 13. The next step is to apply the zonal harmonic expansion to

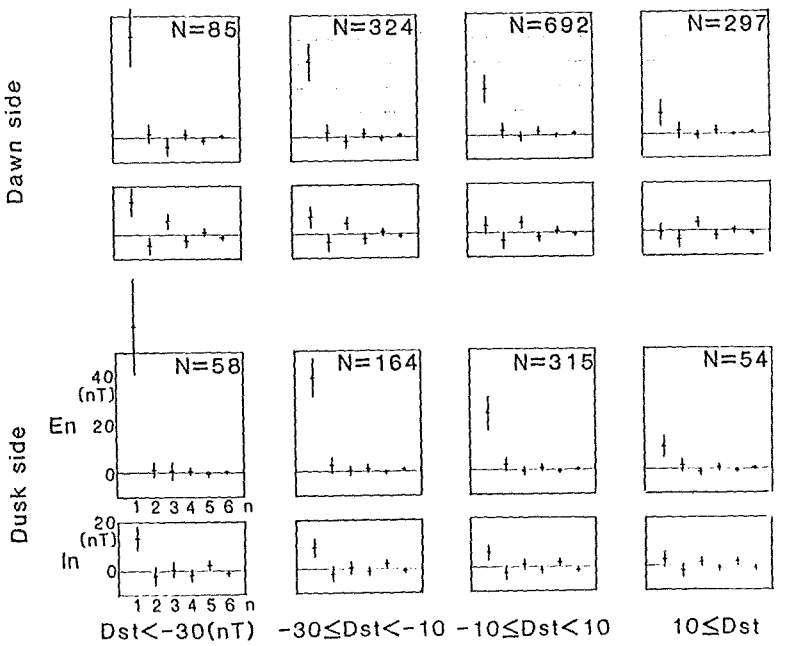

Fig. 1 Coefficients of harmonic expansion and their standard deviation of Magsat residual magnetic field. Upper panels for the dawn side data and lower panels for the dusk side data. Only E_1 and I_1 change significantly with magnetic disturbance monitored by Dst index.

extract the magnetospheric and induction field components. Based on error estimates obtained from synthetic data, the actual Magsat data were used if the paths contain 190 or more data points within the latitudinal range of -55° to $+55^{o}$. Another criterion was also employed to select the paths with a nearly uniform distribution of data.

Fig. 1 shows the mean values and the standard deviations of the internal (I_n) and external (E_n) coefficients of expansion determined for the selected individual Magsat paths. Data were divided into the dawn and dusk sides, as well as groups for different Dst ranges. There is a marked asymmetry in E_1 for the dawn and dusk sides. This is due to the field-aligned current which flows into the earth's polar ionosphere from sunward hemisphere and flows out from the nightside hemisphere (Suzuki and Fukushima, 1982; Suzuki et al., 1984). Another important point is that the values of E_1 and I_1 show a good correlation with Dst while other E_n and I_n do not. In particular, the averages of E_n's ($2 \leq n \leq 6$) are almost zero for both the dawn and dusk sides. On the other hand, the internal fields I_n are significantly different from zero for $2 \leq n \leq 6$; they do not show any noticeable correlation with E_1 but there is a marked difference between the dawn and dusk sides. These results can be interpreted as follows. The disturbance field external to Magsat can well be approximated by E_1 term in agreement with the former studies (e.g., Chapman and Price, 1930; Davis and Cain, 1973). It is noted that E_1 should be determined separately for dawn and dusk meridians to account for the dawn-dusk asymmetry. I_1 represents the induction field due to the current induced within the earth by the field of the equatorial ring current. It can therefore be concluded that the effects of the magnetospheric field and the induction field (due to the ring current) can be represented by the first degree zonal harmonics (external and internal) determined separately for the dawn or dusk meridians. I_2 to I_6 represent combined effects of the ionospheric currents and the currents induced within the earth by the time variations in the former.

3. The Ionospheric Field

Figs. 2a and 2b show the Z (vertical) component magnetic anomaly maps for the dawn and dusk sides respectively, which are constructed by subtracting the model field, MGST(4/81), and the E_1 and I_1 terms of the harmonic expansion for individual paths from the observed data. The mean satellite altitude is 420 km. According to the conclusion of the last section, almost all the magnetospheric field and the induction field should be removed by this procedure. However, a marked difference between two anomaly maps of different local times still exists. This discrepancy can be taken as the reflection of the structural difference of the ionospheric field at 0600 and 1800 local times.

It is clear that anomalies tend to elongate along the east-west direction, especially on the dusk side. In particular, the most prominent anomalies occur along the dip equator on the dusk side (Maeda et al., 1982). Such features are to be expected from the fact that the internal coefficients, I_n ($n \geq 2$), seem to be

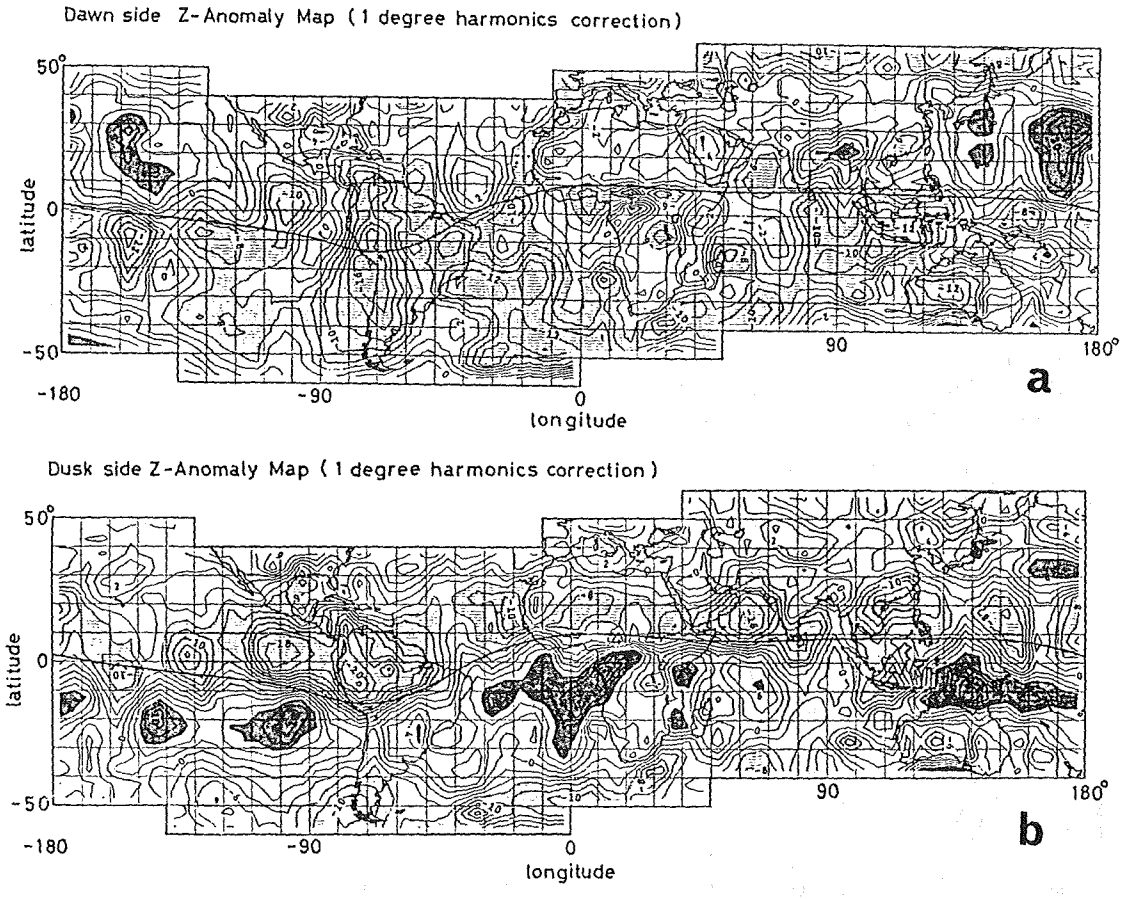

Fig. 2 Magnetic anomaly maps constructed separately from the (a) dawn or (b) dusk side Z(vertical)-component data. Main field and first-degree fields (E_1 and I_1) were subtracted. The mean altitude is 420 km, and the contor interval is 2 nT.

independent of the ring current activities represented by Dst index (Fig. 1). Both Figs. 1 and 2 suggest persistent structures in the ionospheric field at 0600 and 1800 local time meridians.

We need a method to reduce the effect of such disturbance fields. Consider that the crustal anomaly field is a function of position only while the ionospheric field depends on position and local time. The residual magnetic field obtained from the original data by subtracting the model field and fields due to E_1 and I_1 of equation may then be divided into two parts; i.e., crustal anomaly and ionospheric fields. If we average many residual magnetic profiles at the same local time over various longitudes and altitudes, fluctuations due to differences in longitudes and altitudes are averaged out and the resulting field should become "zonal". The contribution from crustal anomaly fields will then be negligible. This is because we already subtracted the model field expressed by spherical harmonics up to the 13th degree and order, and any zonal crustal field of long wavelengths, if existed, would have been included in the model field. This averaging, therefore, gives the ionospheric field for local times of 0600 and 1800 hours as a function of latitude. There are sufficient number of paths on both the dawn and dusk

sides which enable us to average out the crustal anomalies and fluctuations due to the satellite elevation.

The next step is to select a suitable latitude coordinate system for our use. Possible candidates are the geographic, geomagnetic or dip latitudes. From inspection of Fig. 3, it is clear that the ionospheric field depends mostly on the dip latitude. Maeda et al. (1982) showed that the equatorial dusk anomaly is highly correlated with the dip latitude but not with the geomagnetic latitude. Their results as well as our Fig. 2 show residual fields antisymmetric with respect to the dip equator, indicating the existence of ionospheric currents at the low latitude region which is parallel to the dip equator.

Fig. 3 shows the results of averaging magnetic profiles. In the figure, the mean value and its standard deviation are plotted by continuous and broken lines, respectively. Large differences exist between the dawn and dusk profiles for all the components (X, Y, Z) of the ionospheric field. The equatorial anomaly at

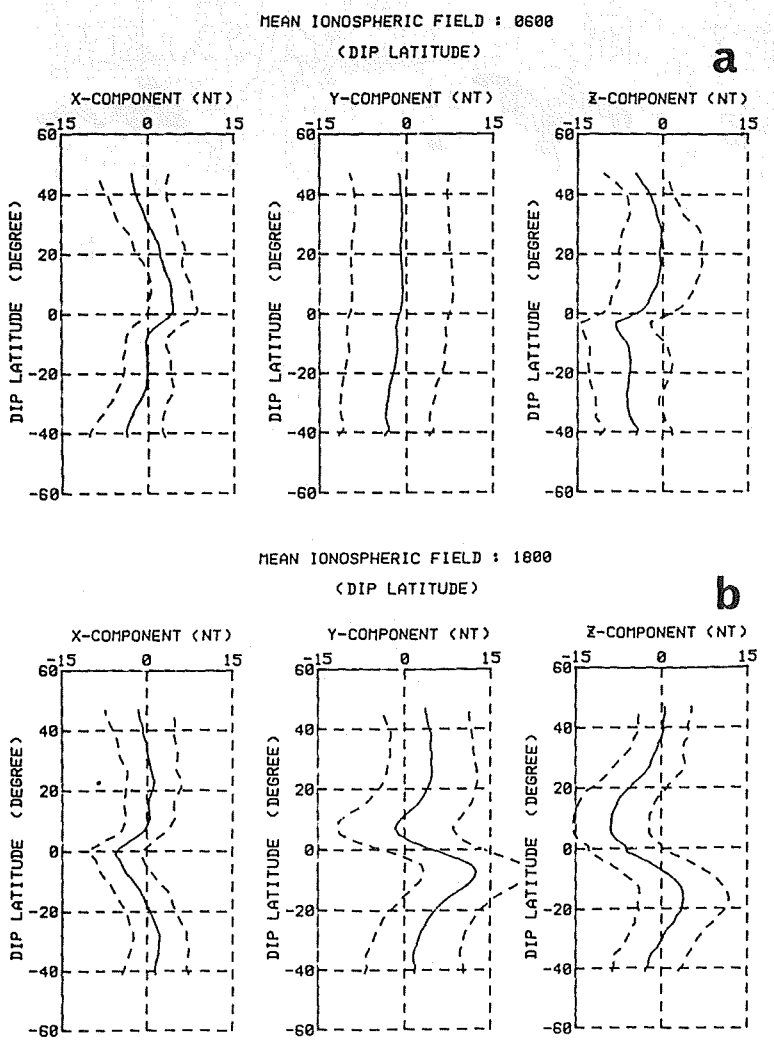

Fig. 3 The mean ionospheric field (MIF) for (a) 0600 and (b) 1800 local time meridians. The solid and broken lines indicate the mean value and ± one standard deviation, respectively. Horizontal components (X and Y) in this figure are in the direction of magnetic north and east defined by the model field, MGST(4/81).

the dusk side is most prominent (Maeda et al., 1982). However, there is little dependence of the averaged profiles upon the strength of the ring current expressed by the Dst index; shapes and amplitudes of the residual fields are quite similar for the periods of strong (Dst < -10 nT) and weak (Dst ≥ -10 nT) ring current. The profiles are also independent of the Kp index. Since both the Kp and Dst indices indicate the level of activity in the magnetosphere, our observations suggest that the ionospheric current system at twilight meridians are little influenced by the activity in the magnetosphere.

When we average the magnetic profiles separately for different altitude ranges, the averaged profiles show certain dependence on the satellite altitudes. Although the shape does not change much, the amplitude of anomalies increases (or sometimes decreases) with height. For instance, the amplitude of the equatorial anomaly in the dusk-Y component is about 10 nT for altitudes less than 400 km and about 4 nT for altitudes more than 450 km, indicating the proximity of the satellite orbit to the current system below. A similar decrease in the amplitude is observed in the dawn-X component. On the other hand, neither the dusk-Z nor dawn-Z component shows significant changes in the amplitude due to the difference in satellite altitudes. In the case of the dusk-X component, the altitude-amplitude relation seems to be inverted; the amplitude being larger for higher satellite altitudes.

4. Mean Ionospheric Field Correction

We have shown that the averaged ionospheric field depends mostly on dip latitude and to a lesser extent on the altitude of the satellite. Neglecting the effect of altitude, the mean of the profiles (Fig. 3) represent averages of the ionospheric field at 0600 or 1800 meridians as a function of dip latitude. We shall call this the Mean Ionospheric Field (MIF). In our approximation, the MIF is always present at respective local times while the field generated by crustal magnetization revolves with the earth's rotation. Although we did not go into the mechanism responsible for the ionospheric fields at twilight meridians, it is clear that the MIF is a good first order approximation for describing the effect of the disturbance fields at Magsat orbits. The subtraction of the MIF from the data will therefore reduce the fields caused by ionospheric currents and help isolate the crustal anomalies.

Fig. 4 shows the anomaly maps constructed from the data of Fig. 3 by subtracting the MIF as a function of dip latitude. The values are averaged in $5^{\circ}x5^{\circ}$ squares. As the standard deviation of the MIF is about 5 nT (Fig. 4), the accuracy of the averaged value would be about $5/\sqrt{40} = 0.8$ nT.

It must be pointed out that the MIF is <u>not</u> a direct expression of fields actually generated by the ionospheric current system. The MIF cannot account for the part of the ionospheric field which exists both at 0600 and 1800 local times. Such a field is included in the field model, because it is "zonal" and because its source is under the satellite orbit. We have, at present, no information about this common ionospheric field. The

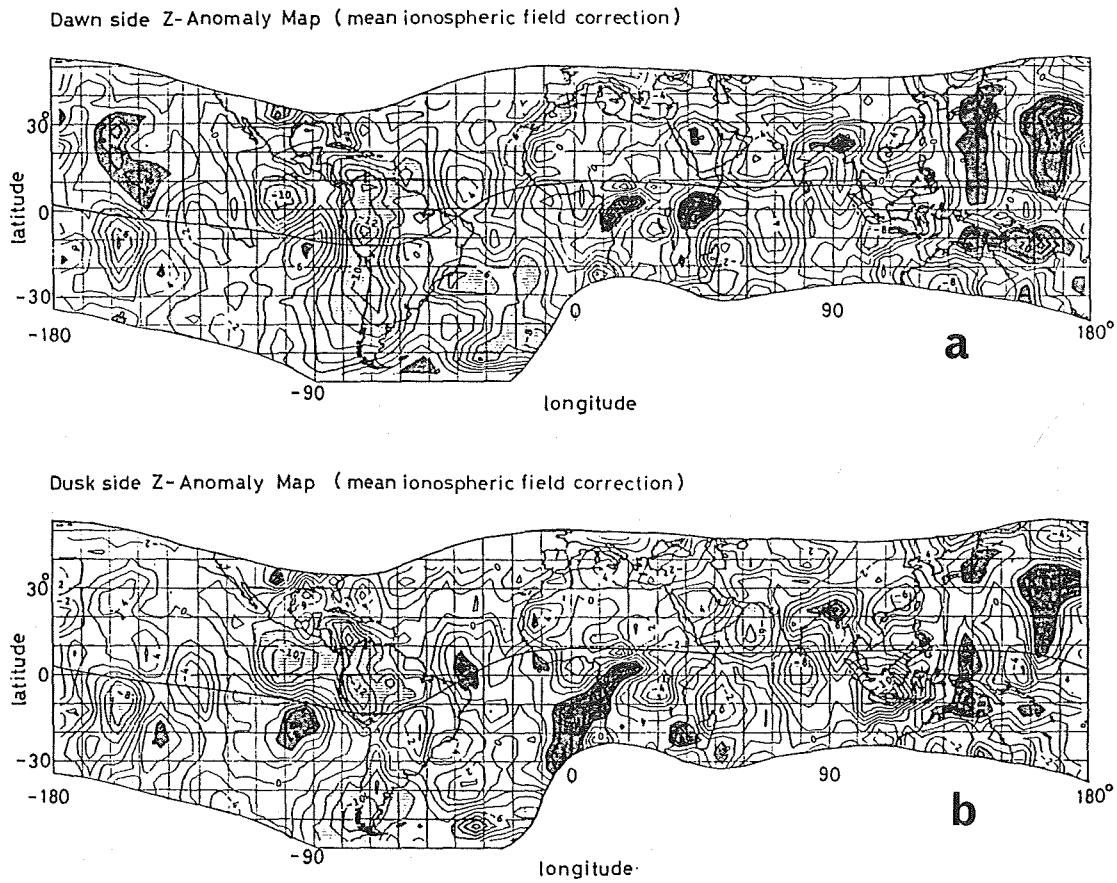

Fig. 4 Vertical component magnetic anomaly maps by MIFC for the (a) dawn and (b) dusk side data. The mean altitude is 420 km, and the contor interval is 2 nT.

MIF also includes contributions from the induction currents in the earth's interior, which are generated by the time variation (as seen from the earth) of the ionospheric currents.

Conventional path-by-path correction filters out the crustal anomalies whose wavelength is longer than about 1900 km along the satellite paths (Sailor et al., 1982). The anomalies obtained by such a method often elongate along the east-west direction. Using the MIFC, we can obtain anomalies whose wavelength is longer than 1900 km, though the subtraction of the model field removes the wavelength longer than 3000 km. On the other hand, this method needs many satellite paths to average out the elevation effect and day-to-day variations in the magnetospheric and ionospheric fields which are well reduced in the path-by-path correction. We used $5^{\circ}x5^{\circ}$ instead of $2^{\circ}x2^{\circ}$ squares which are generaly used for constructing anomaly maps from satellite data. To display the shorter wavelength anomalies by means of the MIFC, we need more data than those obtained by Magsat.

5. Conclusions

After the subtraction of the model field, a spherical

harmonic expansion of the Magsat magnetic field data revealed the disturbance field structures. The magnetospheric field and the induction field due to its variation are well approximated by the first degree zonal harmonic, separately for the dawn and dusk sides. This result agrees with the previous analyses based on the ground data and satellite scalar data. Averaging of the data at the same dip latitude, after the main field as well as the magnetospheric and induction fields are subtracted, gives the mean ionosheric field (MIF) at 0600 and 1800 local times. The MIF is independent of geomagnetic disturbances but depends on satellite altitude, and to a lesser extent, on longitude. Neglecting the dependence of the ionospheric field on longitude and altitude, we can obtain crustal anomalies by subtracting the MIF. Averaging the data in $5^{\circ}x5^{\circ}$ squares was necessary to reduce the path-to-path discrepancies to a satisafactory level.

The correlation of the anomalies obtained independently from the dawn and dusk side data is high, indicating that they are free from the contaminations due to the magnetospheric, induction, and ionospheric fields. The standard deviation of the anomalies is larger than those derived by path-by-path corrections. It can be concluded that the MIFC retains the long wavelength crustal anomalies which are highly reduced by other corrections.

In concluding, we note the following. If we had a number of Magsat-like satellites flying in polar sun-synchronous orbits at different local times, or if Magsat was not sun-synchronous but had a sufficiently long life time so that profiles can be obtained for different local time meridians, we could have generated MIF for the entire time zones. Such a study may be realized by the future generation of magnetic survey satellites.

References

Chapman, S. and A.T. Price, Phil. Trans. Roy. Soc. Lond., A229, 427-460, 1930.

Davis, W.M., and J.C. Cain, EOS Trans. AGU, 54, 242, 1973.

Langel, R.A., R.H. Estes, G.D.Mead, E.B. Fabiano, and E.R. Lancaster, Geophys. Res. Lett., 7, 793-796, 1980.

Maeda, H., T. Iyemori, T. Araki, and T. Kamei, Geophys. Res. Lett., 9, 337-340, 1982.

Matsushita, S., Physics of geomagnetic Phenomena, edited by S. Matsushita and W.H. Campbell, pp. 301-424, 1967.

Mayhew, M.A., J. Geophys., 45, 119-128, 1979.

Regan, R.D., D.W. Handschumacher, and M. Sugiura, J. Geophys. Res., 86, 9567-9573, 1981.

Sugiura, M., and M.P. Hagan, Geophys. Res. Lett., 6, 397-400, 1979.

Suzuki, A., and N. Fukushima, Geophys. Res. Lett., 9, 345-347, 1982.

Suzuki, A., N. Fukushima, and M. Yanagisawa, J. Geophys. Res., in press, 1985.

(in press in Journal of Geophysical Research, Magsat Issue)

THE INVERSE PROBLEM OF INSTANTANEOUS PLATE KINEMATICS BY USING VLBI NETWORK

Kosuke HEKI

Kashima Space Communication Center, Radio Research Laboratories, 893-1, Hirai, Kashima-machi
IBARAKI 314

Introduction

In order to determine the present parameters of the relative motions of the lithospheric plates, geophysical/geological data such as ocean magnetic anomalies, transform fault azimuths and earthquake slip vectors have been used (Minster et al., 1974; Minster & Jordan, 1978). Ocean magnetic anomaly data provide information on the speeds of the sea floor spreading at mid-oceanic ridges and transform fault azimiths and earthquake slip vectors provide information on the directions of the relative plate motions at plate boundaries. Minster et al. (1974) combined these rate data and directional data and then estimated the rotation pole positions and the rotation rates for individual plates by using the least squares fitting.

Although these data sets have been equally used to obtain the "instantaneous" plate motion parameters, time spans represented by these data sets are not equivalent. Among these data sets, earthquake slip vector data are thought to represent the plate motion in the time interval of, say the last ten or twenty years. However, the spreading rate data and transform fault azimuth data represent the averages of the plate movements during much longer time interval. For example, Minster & Jordan (1978) average the time interval of the last three million years to obtain the present spreading rates. Transform faults are also a kind of "geological" structure which have been developed during the geological time and their azimuths are considered to represent the average plate motion direction in such time spans.

Recent developments of various techniques enabled the very precise geodetical measurements between remote stations located on different plates. Centimeter accuracy of the measurement of the distance among such points yields the potential of clarifying the relative movement of these points which originates from the plate motion. Among other things, very long baseline interferometry (VLBI) has been suggested to be the most promising technique for geodynamics (e.g., Coates et al., 1975). In 1984, Radio Research Laboratories (RRL) succeeded in measuring the distances between Kashima station and American stations with an accuracy of a couple of centimeters. During the next five years, annual or semiannual experimemts in the VLBI network which consists of several American, Pacific, European and Japanese stations are programed. This project will greatly contribute to reveal the truely instantaneous plate kinematics.

In this short article, I propose the changing rates of the baseline lengths among points of various plates as a possible substitute for the geophysical/geological data conventionally used to determine instantaneous plate motions. I also present algorithms of

the forward problem and the inverse problem between the changing rates of inter-plate baseline lengths and plate tectonic parameters.

Forward problem

As the first step, let us consider how large the changing rate of the inter-plate baseline length is. Now, two VLBI stations A and B are assumed to be located on two different plates I and J, respectively. I denote the positions of the two stations by the geocentric Cartesian coordinates as A (x_a, y_a, z_a) and B (x_b, y_b, z_b). Then the length of the baseline (i.e., the distance) between A and B should be expressed as

$$D_{BA}^2 = (x_a - x_b)^2 + (y_a - y_b)^2 + (z_a - z_b)^2. \qquad (1)$$

The changing rate of the baseline length is obtained as its time derivative, that is,

$$\dot{D}_{BA} = (1/D_{BA}) \{(x_a - x_b)(\dot{x}_a - \dot{x}_b) + (y_a - y_b)(\dot{y}_a - \dot{y}_b) + (z_a - z_b)(\dot{z}_a - \dot{z}_b)\}, \qquad (2)$$

where dots represent time derivatives.

In order to obtain the relationship between the changing rate and the plate tectonic parameters, it is more convenient to express (x_a, y_a, z_a) and (x_b, y_b, z_b) by their latitudes and longitudes. Let θ_a/ϕ_a be the latitude/longitude of the station A and θ_b/ϕ_b those of the station B, then the three components are written as

$$\begin{matrix} x_a \\ y_a \\ z_a \end{matrix} = \begin{matrix} R\cos\theta_a\cos\phi_a \\ R\cos\theta_a\sin\phi_a \\ R\sin\theta_a \end{matrix} \qquad \begin{matrix} x_b \\ y_b \\ z_b \end{matrix} = \begin{matrix} R\cos\theta_b\cos\phi_b \\ R\cos\theta_b\sin\phi_b \\ R\sin\theta_b \end{matrix}, \qquad (3)$$

where R denotes the earth's radius (for the sake of simplicity, earth is treated as a sphere). It is widely known that the instantaneous motion of a rigid plate lying on a spherical surface can be completely and uniquely described in terms of the rotation about an Euler pole, which makes the velocity field of m plates written by specifying the m instantaneous angular velocity vectors. Then the instantaneous velocity vector of the stations A/B belonging to the plates I/J are given as the outer products of the angular velocity vectors of the plates and the position vectors of the stations. Now if we suppose the rotation pole of the plates I and J at latitudes of θ_i, θ_j and longitudes of ϕ_i, ϕ_j, with the rotation rates of ω_i and ω_j, then the velocity vector of the stations A and B, that is, $(\dot{x}_a, \dot{y}_a, \dot{z}_a)$ and $(\dot{x}_b, \dot{y}_b, \dot{z}_b)$ are expressed as follows;

$$\begin{matrix} \dot{x}_a \\ \dot{y}_a \\ \dot{z}_a \end{matrix} = \begin{matrix} R\,\omega_i(\sin\theta_a\cos\theta_i\sin\phi_i - \cos\theta_a\sin\phi_a\sin\phi_i) \\ R\,\omega_i(\cos\theta_a\cos\phi_a\sin\theta_i - \sin\theta_a\cos\theta_i\cos\phi_i) \\ R\,\omega_i\cos\theta_a\cos\theta_i\sin(\phi_a - \phi_i) \end{matrix} \qquad (4a)$$

$$\begin{matrix} \dot{x}_b \\ \dot{y}_b \\ \dot{z}_b \end{matrix} = \begin{matrix} R\,\omega_j(\sin\theta_b\cos\theta_j\sin\phi_j - \cos\theta_b\sin\phi_b\sin\phi_j) \\ R\,\omega_j(\cos\theta_b\cos\phi_b\sin\theta_j - \sin\theta_b\cos\theta_j\cos\phi_j) \\ R\,\omega_j\cos\theta_b\cos\theta_j\sin(\phi_b - \phi_j) \end{matrix} \quad (4b)$$

By connecting equations (2), (3) and (4), the changing rate of the baseline length can be written as a function of the geographic coordinates of the stations and the plate motion parameters, i.e., the rotation pole positions (latitudes and longitudes) and the rotation rates of the plates I and J, that is,

$$\dot{D}_{BA} = (R^2/D_{BA})\ [\cos\theta_a\cos\theta_b\sin(\phi_a-\phi_b)(\omega_i\sin\theta_i-\omega_j\sin\theta_j) - \cos\theta_a\sin\theta_b\{\omega_i\cos\theta_i\sin(\phi_a-\phi_i) - \omega_j\cos\theta_j\sin(\phi_a-\phi_j)\} + \sin\theta_a\cos\theta_b\{\omega_i\cos\theta_i\sin(\phi_b-\phi_i) - \omega_j\cos\theta_j\sin(\phi_b-\phi_j)\}]\ . \quad (5)$$

This equation gives a solution to the forward problem: given the parameters of instantaneous plate motions, we can calculate the changing rate of the inter-plate baseline length between any stations.

Inverse problem

Now let us consider the inverse problem of instantaneous plate kinematics: given a number of observations of the changing rates of the inter-plate baseline lengths, what is the best representation of instantaneous plate motions? This problem is analogous to the inverse problem described in Minster et al. (1974) and I treat it in a similar fashion.

Suppose the observations of the changing rates of the lengths were obtained for n inter-plate baselines, then these values constitute a data vector $\vec{d}^0$ made of n components. Similarly, the 3m-3 independent components of a plate motion model can be serially arranged to form a model vector $\vec{m}$:

$$\vec{m} = (\theta_1, \phi_1, \omega_1, \ldots\ldots, \theta_{m-1}, \phi_{m-1}, \omega_{m-1}), \quad (6)$$

where an arbitrary reference frame was chosen so that the m-th plate is fixed because only 3m - 3 components are independent for a relative plate motion model.

For any model vector $\vec{m}$ we can compute the data vector $\vec{d}(\vec{m})$ using equation (5). If the data were error free and the rigid plate model was correct, the model we seek would satisfy the equation

$$\vec{d}(\vec{m}) = \vec{d}^0. \quad (7)$$

However, the observations are not perfectly compatible and are contaminated with errors. If we suppose Gaussian distributions for the changing rate observations of the individual baselines, we will obtain the best model representation by maximizing a likelihood function proportional to

$$\exp\left\{-\sum_{i=1}^{n}\frac{[d_i^0-d_i(\vec{m})]^2}{2\sigma_i^2}\right\}, \tag{8}$$

where d_i^0 is the i-th component of $\vec{d}^0$, $d_i(\vec{m})$ is the value of the i-th data function evaluated at $\vec{m}$ and σ_i^2 $(i=1,\ldots,n)$ is the variance of the i-th rate datum. Maximization is attained by minimizing the following function

$$F = \sum_{i=1}^{n}\frac{[d_i^0-d_i(\vec{m})]^2}{2\sigma_i^2}. \tag{9}$$

After all, the problem is reduced to the non-linear least squares fitting and the best fitting model can be computed by an iterative refinement of the parameters using the Gauss-Newton method. Standard software of least squares fitting such as the Statistical Analysis by Least Squares fitting (SALS; Nakagawa and Oyanagi, 1982) is applicable for such problems by giving the elements of the Jacobian matrix.

The (i, j) elememt of the Jacobian matrix is given as the derivative of the i-th datum with respect to the j-th parameter. In the present case, they are given as the partial derivatives of the changing rate data with respect to the plate tectonic parameters such as the latitudes/longitudes of the rotation poles and the rotation rates. From equation (5), we obtain

$$\begin{aligned}\partial\dot{D}_{BA}/\partial\theta_k=(\delta_{ik}-\delta_{jk})R^2\,\omega_k\{&\cos\theta_a\cos\theta_b\sin(\phi_a-\phi_b)\\&+\cos\theta_a\sin\theta_b\sin\theta_k\sin(\phi_a-\phi_k)\\&-\sin\theta_a\cos\theta_b\sin\theta_k\sin(\phi_b-\phi_k)\}/D_{BA}\end{aligned} \tag{10a}$$

$$\begin{aligned}\partial\dot{D}_{BA}/\partial\phi_k=(\delta_{ik}-\delta_{jk})R^2\,\omega_k\{&\cos\theta_a\sin\theta_b\cos\theta_k\cos(\phi_a-\phi_k)\\&-\sin\theta_a\cos\theta_b\cos\theta_k\cos(\phi_b-\phi_k)\}/D_{BA}\end{aligned} \tag{10b}$$

$$\begin{aligned}\partial\dot{D}_{BA}/\partial\omega_k=(\delta_{ik}-\delta_{jk})R^2\{&\cos\theta_a\cos\theta_b\sin(\phi_a-\phi_b)\sin\theta_k\\&-\cos\theta_a\sin\theta_b\cos\theta_k\sin(\phi_a-\phi_k)\\&+\sin\theta_a\cos\theta_b\cos\theta_k\sin(\phi_b-\phi_k)\}/D_{BA},\end{aligned} \tag{10c}$$

where δ_{ik} and δ_{jk} are Kronecker deltas.

Actual inversion computation from dummy data was done by using standard software for least squares fitting, SALS, and the parameters were observed to converge to the expected values without any troubles.

Discussion and summary

In order to merely determine plate tectonic parameters, we need only minimum number of relative motion data. However, when we have more than the miminum amount of data, it becomes possible to examine the self-consistency of the data under the assumptions of plate tectonics such as the rigidity of the plates and constant area of the

earth. Many researchers such as Chase (1972), Minster et al. (1974), Minster & Jordan (1978) succeeded in obtaining such plate tectonic parameters which are well consistent with all the relative motion data representing the last several millions of years. However, there is no guarantee that the plates are behaving as rigid bodies in the context of instantaneous movements. Now, our major concern is how the plates are behaving today, in other words, wheather the theories of plate tectonics are applicable or not for such a short time span as a few years.

Several possibilities of the instantaneous plate kinematics can be imagined. One plausible possibility is that the plates are moving in a similar fashion to the already known time-averaged relative plate motion. In this case, model parameters will converge to the vicinities of the currently available plate tectonic parameters such as RM-2 of Minster & Jordan (1978). Another possibility is that the parameters converge to certain values which are significantly different from RM-2. In this case, plates are behaving as rigid bodies but their rotation rates and rotation axes are envisaged to be different from time-averaged ones. There is also a possibility that the parameters do not converge at all. In this case, the model assumptions of "plate tectonics" are considered to be wrong.

Now the world-wide VLBI network is not so sufficient as to establish the present day relative kinematics for all the known plates. Nevertheless, in a near future, it seems possible to examine the plate tectonic theories over the several plates where multiple VLBI stations are already available. The future development of the "mobile" VLBI stations may enable the measurements over the truely world-wide network covering all the known plates and reveal the instantaneous kinematics of these plates.

References

Chase, C. G., (1972) Geophys. J. R. astr. Soc., 29, 117-122.

Coates, R. J., T. A. Clark, C. C. Counselman, I. I. Shapiro, H. F. Hinteregger, A. E. Rogers & A. R. Whitney, (1975) Tectonophys., 29, 9-18.

Minster, J. B. & T. H. Jordan, (1978) J. Geophys. Res., 83, 5331-5354.

Minster, J. B., T. H. Jordan, P. Molnar and E. Haines, (1974) Geophys. J. R. astr. Soc., 36, 541-576.

Nakagawa, T. & Y. Oyanagi, (1982) Experimemtal Data Analysis with Least Squares --- Program SALS, Univ. of Tokyo Press, Tokyo. (in Japanese)

AUTHOR INDEX

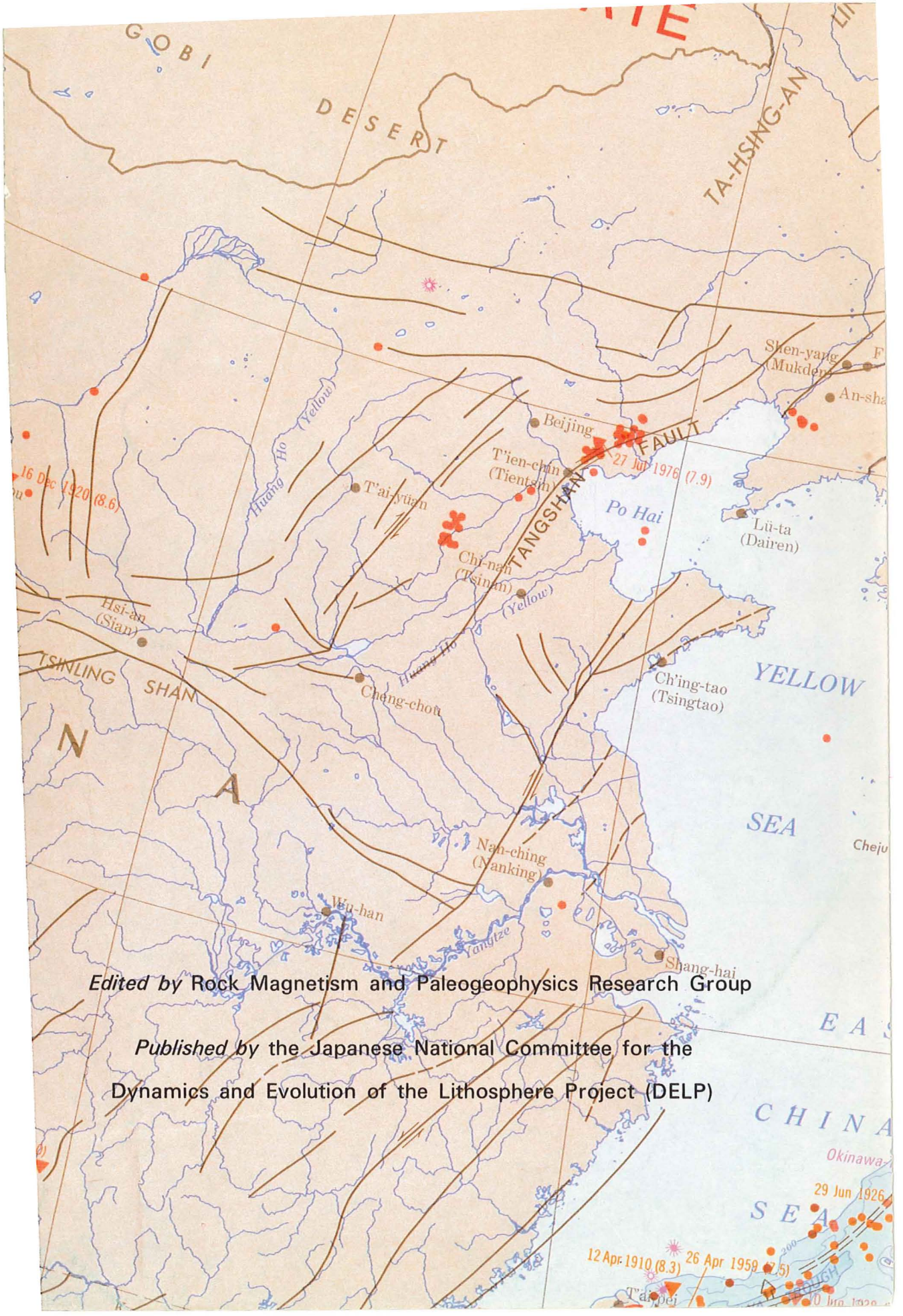

Edited by Rock Magnetism and Paleogeophysics Research Group

Published by the Japanese National Committee for the Dynamics and Evolution of the Lithosphere Project (DELP)